VOLUME 36 AUGUST 1958 NUMBER 8

Canadian Journal of Physics

Editor: H. E. DUCKWORTH

Associate Editors:

L. G. ELLIOTT, *Atomic Energy of Canada, Ltd., Chalk River*
J. S. FOSTER, *McGill University*
G. HERZBERG, *National Research Council of Canada*
L. LEPRINCE-RINGUET, *Ecole Polytechnique, Paris*
B. W. SARGENT, *Queen's University*
G. M. VOLKOFF, *University of British Columbia*
W. H. WATSON, *University of Toronto*
G. A. WOONTON, *McGill University*

Published by THE NATIONAL RESEARCH COUNCIL

OTTAWA CANADA

CANADIAN JOURNAL OF PHYSICS

(*Formerly Section A, Canadian Journal of Research*)

Under the authority of the Chairman of the Committee of the Privy Council on Scientific and Industrial Research, the National Research Council issues THE CANADIAN JOURNAL OF PHYSICS and five other journals devoted to the publication, in English or French, of the results of original scientific research. Matters of general policy concerning these journals are the responsibility of a joint Editorial Board consisting of: members representing the National Research Council of Canada; the Editors of the Journals; and members representing the Royal Society of Canada and four other scientific societies.

EDITORIAL BOARD

Representatives of the National Research Council

A. Gauthier, *University of Montreal*
R. B. Miller, *University of Alberta*
H. G. Thode, *McMaster University*
D. L. Thomson, *McGill University*

Editors of the Journals

D. L. Bailey, *University of Toronto*
T. W. M. Cameron, *Macdonald College*
H. E. Duckworth, *McMaster University*
K. A. C. Elliott, *Montreal Neurological Institute*
Léo Marion, *National Research Council*
R. G. E. Murray, *University of Western Ontario*

Representatives of Societies

D. L. Bailey, *University of Toronto*
Royal Society of Canada
T. W. M. Cameron, *Macdonald College*
Royal Society of Canada
H. E. Duckworth, *McMaster University*
Royal Society of Canada
Canadian Association of Physicists
K. A. C. Elliott, *Montreal Neurological Institute*
Canadian Physiological Society
P. R. Gendron, *University of Ottawa*
Chemical Institute of Canada
R. G. E. Murray, *University of Western Ontario*
Canadian Society of Microbiologists
T. Thorvaldson, *University of Saskatchewan*
Royal Society of Canada

Ex officio

Léo Marion (Editor-in-Chief), *National Research Council*
J. B. Marshall (Administration and Awards), *National Research Council*

Manuscripts for publication should be submitted to Dr. H. E. Duckworth, Editor, Canadian Journal of Physics, Hamilton College, McMaster University, Hamilton, Ontario.

(For instructions on preparation of copy, see **Notes to Contributors** (inside back cover).)

Proof, correspondence concerning proof, and orders for reprints should be sent to the Manager, Editorial Office (Research Journals), Division of Administration and Awards, National Research Council, Ottawa 2, Canada.

Subscriptions, renewals, requests for single or back numbers, and all remittances should be sent to Division of Administration and Awards, National Research Council, Ottawa 2, Canada. Remittances should be made payable to the Receiver General of Canada, credit National Research Council.

The journals published, frequency of publication, and prices are:

Canadian Journal of Biochemistry and Physiology	Monthly	$3.00 a year
Canadian Journal of Botany	Bimonthly	$4.00 a year
Canadian Journal of Chemistry	Monthly	$5.00 a year
Canadian Journal of Microbiology	Bimonthly	$3.00 a year
Canadian Journal of Physics	Monthly	$4.00 a year
Canadian Journal of Zoology	Bimonthly	$3.00 a year

The price of regular single numbers of all journals is 75 cents.

Canadian Journal of Physics

Issued by THE NATIONAL RESEARCH COUNCIL OF CANADA

VOLUME 36 AUGUST 1958 NUMBER 8

THE THERMAL NEUTRON CAPTURE CROSS SECTION AND THE RESONANCE ABSORPTION INTEGRAL OF Th^{230} (IONIUM)[1]

M. J. CABELL[2]

ABSTRACT

The thermal neutron capture cross section and the resonance capture integral of Th^{230} have been determined by an activation method. Assumptions are made that the thermal capture cross section and the resonance capture integral of Co^{59} are 36.5 barns and 48.6 barns respectively, that the half-life of Th^{230} is 8.00×10^4 years, and that Th^{230} behaves as a 1/v absorber in the subcadmium region. Based on these assumptions values of $\sigma_{2200} = 21.4 \pm 0.3$ barns and of 937 ± 32 barns for the resonance absorption integral (from 0.5 ev to ∞) have been obtained for Th^{230}.

The half-life of Th^{231} has been determined as 25.52 ± 0.01 hours.

INTRODUCTION

Hughes and Harvey (1955) quote 27 ± 2 barns for the thermal neutron capture cross section of Th^{230} as determined by the pile oscillator method and 35 ± 10 barns for its capture cross section for pile neutrons as measured by an activation method, but no experimental details are available for these measurements. Jaffey and Hyde (1952) give two widely different values (61 barns and 28 barns) for the thermal neutron capture cross section but the experimental uncertainties for each result are so large that neither can be preferred to the other. No measurements have been reported in the literature for either the resonance absorption integral of Th^{230} or the dependence of its absorption cross section on neutron energy. This paper describes activation measurements which have been made to determine the thermal neutron capture cross section more precisely; the resonance absorption integral has also been determined.

The following nuclear reactions are involved:

[1]Manuscript received March 3, 1958.

Contribution from the Research Chemistry Branch, Atomic Energy of Canada Limited, Chalk River, Ontario.

Issued as A.E.C.L. No. 592.

[2]Permanent address: Atomic Energy Research Establishment, Harwell, Berkshire, England.

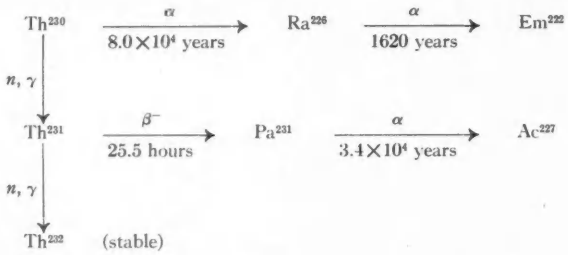

The experiments involved the irradiation in the NRX reactor of submicrogram amounts of Th^{230} (*a*) unshielded and (*b*) shielded with 0.025 in. cadmium. Cobalt monitors were attached to measure both the thermal and the epicadmium fluxes. After irradiation the thorium was purified by ion exchange and mounted on thin films for counting. Determinations of the absolute β-disintegration and absolute α-disintegration rates of each source gave measurements of its Th^{231} and Th^{230} content respectively. From these data and the known fluxes the effective capture cross section of Th^{230} for pile neutrons, its thermal capture cross section, and its resonance absorption integral were calculated.

The method used is similar to that reported by Cabell, Eastwood, and Campion (1958) and possesses the advantage that chemical yields from the purification process, which vary with each experiment, need not be known.

EXPERIMENTAL METHODS

(*a*) *Starting Material*

Approximately 25 μg of Th^{230} in 20 ml of solution was available as a concentrate from a Canadian pitchblende residue. The solution also contained macroquantities of rare earths and about 65 μg of Th^{232}. The thorium was purified in good yield and virtually free from all impurities by thenoyltrifluoroacetone extraction (Barnes and Potratz 1954) and ion exchange (see section on chemical purification) and was finally obtained in 5 ml of 5 *M* hydrochloric acid. This solution was used as a stock for all irradiations. Aliquots taken from it and examined by α-pulse analysis showed that less than 0.1% of the α-particles emitted had energies differing from the α-particle energy of Th^{230}.

(*b*) *Irradiations*

Fifty-microliter aliquots (approximately 0.2 μg Th^{230}) of the stock solution were pipetted into small silica ampoules. Some of these were sealed directly but those to be irradiated under cadmium, and three others, were taken to dryness and were then sealed except for a capillary vent. Cobalt monitors, approximately 10 mg in weight, were made from 0.005 in. cobalt wire and weighed to within $\pm$0.02 mg. These were wrapped helically around the sample ampoules which were then packed into super-pure iron irradiation capsules some of which were tightly lined with 0.025 in. cadmium. Reactor grade powdered

graphite was packed tightly into any remaining space and the capsules were then sealed.

Except for one group in which three irradiations were carried out, the samples were irradiated in pairs one after the other (one cadmium shielded, the other unshielded) for 5400 ± 2 seconds each in the same position in an empty fuel rod position of the NRX reactor during periods of constant pile power (constant to better than $\pm 0.5\%$).

(*c*) *Chemical Purification*

Cation and anion exchange chromatography were used to purify the irradiated thorium.

Each cation column consisted of 1.00 g (dry weight) of 200–400 mesh Dowex 50 (hydrogen form) contained in a tube 10 cm long and 6 mm in diameter sealed onto a reservoir 10 cm long and 3 cm in diameter. Both column and reservoir were jacketed at 60°. Before loading, the columns were prepared by washing with water.

Each anion column contained 0.25 g of 200–400 mesh Dowex 1 (chloride form) in a tube 6 cm long and 6 mm in diameter sealed onto a reservoir 5 cm long and 1.5 cm in diameter. The anion columns, which were operated at room temperature, were washed with 5 ml of 10 *M* hydrochloric acid before loading.

The irradiated thorium sample was dissolved in 5 ml of 4 *M* nitric acid and the solution was warmed to 80° before it was fed to a cation exchange column without application of pressure. When the feed had passed, 25 ml of hot 6 *M* nitric acid was poured into the reservoir and allowed to elute the column over a period of 1.5 hours. The effluent, which contained rare-earth impurities, was rejected. The resin was transferred to a conical flask by slurrying with 20 ml of hot 0.2 *M* ammonium oxalate solution and the thorium was extracted from it by boiling for 5 minutes. The resin was then filtered off and rejected.

The filtered oxalate solution was transferred to a centrifuge tube and 6 drops of a ferric nitrate solution (10 mg iron per ml) were added. The iron, which carries the thorium, was precipitated by adding excess ammonia and heating by immersion of the tube for 5 minutes in boiling water. The precipitate was collected by centrifuging, dissolved in concentrated nitric acid, and the solution was made alkaline once more. This precipitation–solution cycle was then repeated twice. The precipitate was washed with very dilute ammonia and then with water to remove any remaining ammonium nitrate.

The precipitate was next dissolved in 2 ml of 10 *M* hydrochloric acid and fed to an anion exchange column at the rate of 0.2 ml/min to remove the iron carrier. After the feed had passed, the column was eluted with 1 ml of 10 *M* hydrochloric acid and the total eluate was collected in a small beaker and evaporated to dryness. Two milliliters of concentrated nitric acid was added and the solution was again evaporated to dryness. Finally the residue, which was invisible to the naked eye, was dissolved in 1 ml of 3 *M* nitric acid and the resulting solution was used for making sources for counting. The total time taken for each purification was about three hours.

(*d*) *Absolute Disintegration-Rate Determinations*

Preliminary experiments were carried out to determine whether there were losses in counting Th^{230} α-particles or Th^{231} β-particles in a 4π counter owing to absorption of particles in the source mount.

In the first experiment a series of gold-coated VYNS films of known thickness were prepared and an aliquot of the stock Th^{230} solution was evaporated to dryness on a film 44 $\mu g/cm^2$ thick. This was α-counted in a 4π counter and then another film was made to adhere to the back of the source before counting again. Additional films were then added, with counting after each addition, until a final total thickness of 209 $\mu g/cm^2$ had been built up. Over this range, 44 to 209 $\mu g/cm^2$, no change in α-disintegration rate was observed which was outside the statistical error of each count, i.e., $\pm 0.3\%$.

In a second and similar experiment in which the Th^{231} β-particles from a neutron-irradiated sample of Th^{230} were counted, no change in β-disintegration rate outside the statistical error of each count ($\pm 0.2\%$) was detected over a source mount thickness which was varied from 80 to 264 $\mu g/cm^2$. Since for cross section measurements film thicknesses about 50 $\mu g/cm^2$ were used it was concluded that loss of β-particles or α-particles due to absorption in these films was so small that it could be neglected.

When a batch of irradiated Th^{230} had been purified, three or four aliquots (sufficient to give between 300 and 1000 β-particle counts/second each but whose volume did not need to be known) were mounted on thin films and each was counted for β-particles in a 4π counter. The progress of β-decay was then followed for at least seventeen days by which time the Th^{231} content had decayed to a negligibly small amount and the (apparent) residual β-particle count was only a small fraction of the background count. The (apparent) residual β-particle count, which was due to the α-activity of the Th^{230} in the sample, was then subtracted from the β-activities determined previously to follow the decay of the Th^{231} component of the source. These corrected results showed no departure from exponential decay when plotted graphically and confirmed the purity of the product. From the corrected initial β-particle count, the absolute β-disintegration rate which the Th^{231} in the source would have had at the time of the end of the irradiation was calculated using 25.52 hours (this investigation) for the half-life of Th^{231}.

After β-particle counting had been completed each source was α-particle counted in the same counter at a lower applied potential which was in the middle of the α-particle counting plateau. The results for each film were then expressed as the ratio $R_{\beta,\alpha}$ where

$$(1) \qquad R_{\beta,\alpha} = \frac{\text{absolute } \beta\text{-disintegration rate of the } Th^{231} \text{ in the source at the end of the irradiation}}{\text{absolute } \alpha\text{-disintegration rate of the } Th^{230} \text{ in the source}}.$$

Standard deviations for the three or four separate determinations of $R_{\beta,\alpha}$ for any one irradiation were always less than 2%. The results for unshielded samples are distinguished by the subscript 1, i.e. $(R_{\beta,\alpha})_1$, and those for shielded samples by the subscript 2.

(*e*) *Measurements with Cobalt Monitors*

The determination of $(nv_0)_t$ and $(nv)_{e\text{-}c}$ from the observed activity of cobalt monitors has already been described by Cabell, Eastwood, and Campion (1958). $(nv_0)_t$ is the "thermal" flux where n is the density of all neutrons below 0.5 ev (the cutoff energy for 0.025 in. cadmium), v_0 is the standard velocity, namely 2200 m/sec, and the subscript t denotes "thermal" with this spectrum definition. The quantity $(nv)_{e\text{-}c}$ is the epicadmium flux per unit interval of ln E. Throughout this paper a value of 5.28 years has been used for the half-life of Co^{60} and the thermal capture cross section and resonance capture integral of Co^{59} have been taken as 36.5 ± 1.0 barns (an average of the absorption and activation results) and 48.6 barns respectively (Hughes and Harvey 1955).

Although $(nv_0)_t$ and $(nv)_{e\text{-}c}$ were constant during each irradiation, $(nv_0)_t$ varied between 6.83 and 6.99×10^{13} and $(nv_0)_t/(nv)_{e\text{-}c}$ between 29.9 and 38.3 between separate irradiations.

(*f*) *Half-life of* Th^{231}

Results from the decay for four half-lives of 18 separate sources of Th^{231} prepared from five different irradiations and purifications were subjected to analysis by the method of least squares. The half-lives obtained are listed in Table I. The results gave an unweighted average of 25.52 ± 0.01 hours where the error quoted is the probable error of the mean. A similar treatment of five sources for decay for six half-lives gave $T_{1/2} = 25.59\pm0.05$ hours. These results agree well with those obtained recently by Jaffey, Jerome, and Warshaw

TABLE I

DETERMINATION OF THE HALF-LIFE OF Th^{231}

Irradiation	$T_{1/2}$ (hours)
1	25.57
	25.44
	25.51
2	25.43
	25.51
	25.43
	25.52
3	25.56
	25.47
	25.58
	25.51
4	25.59
	25.42
	25.58
5	25.66
	25.45
	25.56
	25.51
	Average 25.52 ± 0.01 hours, where the error is the probable error of the mean

(1951) and by Knight and Macklin (1949). The former obtained the figure 25.64 ± 0.1 hours as an average of two determinations and the latter 25.51 ± 0.23 hours as a weighted average of five results.

RESULTS

We define an effective capture cross section for pile neutrons, σ_{eff}, by the expression:

$$\sigma_{eff} = (R_{\beta,\alpha})_1 \times \lambda_1 / (nv_0)_t (1 - e^{-\lambda t_1}), \tag{2}$$

where $(R_{\beta,\alpha})_1$ has been defined by equation (1) and t_1 hours is the time of the irradiation. λ and λ_1 are the decay constants of Th^{231} (0.02716 hours^{-1}) and Th^{230} respectively. Unfortunately λ_1 is not known with a precision comparable with that of the other factors in equation (2). To avoid introducing a large uncertainty at an early stage the results were expressed as the ratio σ_{eff}/λ_1 and are listed as such in column 4 of Table II. Since the groups of experiments were conducted over a period of time during which several fuel rod changes had been made it is not to be expected that σ_{eff}/λ_1 will be constant.

TABLE II

THE EFFECTIVE AND THERMAL CAPTURE CROSS SECTIONS OF Th^{230}

Group	Experiment	Physical state of sample irradiated	$(\sigma_{eff}/\lambda_1) \times 10^{10}$	$(\sigma_{eff,Cd}/\lambda_1) \times 10^{10}$	$(\sigma_{2200}/\lambda_1) \times 10^{11}$
A	1	Solid		1.079 ± 0.025	
	2	Solid	1.871 ± 0.014		7.93 ± 0.28
B	3	Solid		1.086 ± 0.006	
	4	Liquid	1.878 ± 0.011		7.92 ± 0.12
	5	Solid	1.836 ± 0.012		7.50 ± 0.13
C	6	Liquid		0.991 ± 0.017	
	7	Solid	1.758 ± 0.012		7.67 ± 0.25
D	8	Solid		0.985 ± 0.007	
	9	Solid	1.772 ± 0.009		7.87 ± 0.12
				Weighted average	7.78 ± 0.09

Values of $\sigma_{eff,Cd}/\lambda_1$ are also listed in Table II. The quantity $\sigma_{eff,Cd}$, "the effective cross section under cadmium," is defined by the relationship:

$$\sigma_{eff,Cd} = (R_{\beta,\alpha})_2 \times \lambda_1 / (nv_0)_t (1 - e^{-\lambda t_2}). \tag{3}$$

By the definition used for calculating $(nv_0)_t$ from the monitor activities it will be seen that σ_{2200} m/sec for an absorber that, like cobalt, follows the 1/v law, is simply $\sigma_{eff} - \sigma_{eff,Cd}$. The values of $(\sigma_{eff} - \sigma_{eff,Cd})/\lambda_1$ are therefore listed in column 6 of Table II as $(\sigma_{2200}$ m/sec$)/\lambda_1$.

The errors in σ_{eff}/λ_1 and $\sigma_{eff,Cd}/\lambda_1$ which are given in Table II arise from two sources: an uncertainty in $(nv_0)_t$ which was always 0.4% and an uncertainty in $R_{\beta,\alpha}$ for which the standard deviation of the three or four determinations has been taken (this varied between 0.3% and 2.0%). When an

average was obtained for σ_{2200}/λ_1 each result was weighted proportionally to the reciprocal of the square of its error.

For calculating an absolute value of σ_{2200} a value for the half-life of Th^{230} must be assumed. The most precise value available, $8.23\pm0.25\times10^4$ years, was obtained by Curie (1930) but a more recent determination by Hyde (1949) has given $8.0\pm0.3\times10^4$ years. For want of better precision a value of 8.00×10^4 years has been assumed and σ_{2200} is expressed relative to this. Thus

$$\sigma_{2200} = (7.78\pm0.09\times10^{-11})\times(2.747\times10^{-13})\times10^{24} = 21.4\pm0.3 \text{ barns.}$$

The resonance capture integral is related to the cadmium ratio (R_{Cd}) by the expression:

$$\int_{0.5}^{\infty}\sigma_c\,dE/E = \frac{(nv_0)_t}{(nv)_{e\text{-}e}}\frac{\sigma_{2200}}{(R_{Cd}-1)}. \tag{4}$$

Table III lists the values of R_{Cd} and

$$\left(\int_{0.5}^{\infty}\sigma_c\,dE/E\right)/\sigma_{2200}$$

obtained.

TABLE III

THE RESONANCE CAPTURE INTEGRAL OF Th^{230}

Group	Experiments	R_{Cd}	$\left(\int_{0.5}^{\infty}\sigma_c\,dE/E\right)/\sigma_{2200}$
A	1 and 2	1.735 ± 0.041	42.9 ± 2.4
B	3 and 4	1.723 ± 0.009	41.0 ± 0.7
	3 and 5	1.692 ± 0.009	43.2 ± 0.7
C	6 and 7	1.774 ± 0.034	49.5 ± 2.3
D	8 and 9	1.799 ± 0.013	47.6 ± 0.9
		Weighted average	43.8 ± 1.4

Since $R_{Cd} = (R_{\beta,\alpha})_1/(R_{\beta,\alpha})_2$ for equal irradiation times, errors in R_{Cd} arise from both $(R_{\beta,\alpha})_1$ and $(R_{\beta,\alpha})_2$. Errors in $(R_{Cd}-1)$ were even larger and varied between 1.3% and 5.5%. The value of $(nv)_{e\text{-}e}$ was known with a precision of $\pm1\%$. Using the weighted average,

$$\int_{0.5}^{\infty}\sigma_c\,dE/E = (43.8\pm1.4)\times(21.4\pm0.3) = 937\pm32 \text{ barns.}$$

CONCLUSIONS

The thermal capture cross section obtained in this work, 21.4 barns, is considerably lower than any figure reported previously. It is clear that the results of Jaffey and Hyde (1952), i.e., 61 barns and 28 barns, are much too high since these authors did not take into account any contributions due to epithermal neutrons and, with such a large resonance integral, their effect cannot be ignored. It is not possible to say why the new figure differs from the

values quoted by Hughes and Harvey (1955) since no experimental data are available for their results.

Both the thermal capture cross section and the resonance absorption integral obtained in this work are subject to correction when a more precise value has been obtained for the half-life of Th^{230}. With such a large resonance absorption integral it is also possible that a large resonance absorption peak is situated near the thermal region. If this is so, the tail of this peak may extend below 0.5 ev, making the assumption that Th^{230} behaves as a 1/v absorber in the subcadmium region invalid; a correction, probably not more than a few per cent, would then have to be applied.

ACKNOWLEDGMENTS

The author is indebted to Dr. T. A. Eastwood of the Research Chemistry Branch for suggesting the problem and for many helpful discussions, and to Dr. J. M. Kennedy of the Theoretical Physics Division, Atomic Energy of Canada Limited, for his co-operation in the calculation of the half-life of Th^{231}. The gift of the pitchblende concentrate, which was extracted by Dr. A. P. Baerg from a rare-earth residue donated by the Eldorado Mining and Refining Co. Ltd., is gratefully acknowledged.

REFERENCES

BARNES, J. W. and POTRATZ, M. A. 1954. The determination of ionium in coral, Los Alamos Report LA-1721.

CABELL, M. J., EASTWOOD, T. A., and CAMPION, P. J. 1958. The thermal neutron capture cross section and the resonance absorption integral of U^{236}. J. Nuclear Energy (in press).

HUGHES, D. J. and HARVEY, J. A. 1955. Neutron cross sections, Brookhaven National Laboratory Report BNL-325 (U.S. Government Printing Office, Washington, D.C.).

JAFFEY, A. H., JEROME, L., and WARSHAW, S. 1951. Phys. Rev. **82**, 498.

JAFFEY, A. H. and HYDE, E. K. 1952. Thermal neutron capture cross section of Th^{230} by measurement of *UY*, Argonne National Laboratory Report T.I.D. 5223.

KNIGHT, G. B. and MACKLIN, R. L. 1949. Phys. Rev. **75**, 34.

NUCLEAR ORIENTATION EXPERIMENTS WITH Pr^{142} AND Yb^{175} NUCLEI[1]

J. M. DANIELS, J. L. G. LAMARCHE,[2] AND M. A. R. LE BLANC

ABSTRACT

Pr^{142} has been oriented as an impurity in cerium magnesium nitrate, and the anisotropy of the 1.57 Mev γ-ray was measured as a function of temperature in the range 0.003° K to 1.0° K, both in zero external field and in a field of 320 gauss parallel to the trigonal crystal axis. The results are not consistent with what has been published about the spin Hamiltonian of Pr^{+++} in this lattice. The magnetic moment of Pr^{142} is very small, and it was not possible to see any saturation of the anisotropy at low temperatures. Values for the magnetic moment of Pr^{142} were found for two different assumed decay schemes, these are 0.11 nuclear magnetons for the spin assignments $2 \xrightarrow{0} 2 \xrightarrow{2} 0$, and 0.15 nuclear magnetons for the spin assignments $2 \xrightarrow{1} 2 \xrightarrow{2} 0$. Similar experiments were carried out on Yb^{175}. Measurements were made in a variety of external magnetic fields up to 700 oersted, and at temperatures as low as 0.003° K. No anisotropy was observed for the 396 kev γ-ray, nor for the 282 kev γ-ray. The most likely explanation for this result is that the lifetime of the γ-emitting state is about 10^{-10} seconds. The relation between the results of this experiment and others on the same isotope (Phil. Mag. **2**, 1079 (1952)) is discussed.

1. INTRODUCTION

The magnetic hyperfine structure method of orienting nuclei has been established by Bleaney *et al.* (1954) and has already proved useful in establishing details of nuclear decay schemes, and in evaluating nuclear magnetic moments (e.g. Grace and Halban 1952). As part of a program to exploit the potentialities of such experiments, we have oriented Pr^{142} by this method, and have observed and measured an anisotropy in the emission of the 1.57 Mev γ-ray which occurs in the decay of this nucleus. A value of the magnetic moment of the Pr^{142} nucleus has been deduced from these measurements.

We have also performed experiments to orient Yb^{175} as an impurity in cerium magnesium nitrate. When these investigations were started, it was discovered that a group at Oxford were preparing to align this isotope. At that time, very little was known about the effect of interactions on the angular distribution of gamma rays from an assembly of aligned nuclei, except that such effects could be very large (Grace *et al.* 1954). In addition, only one isotope, Co^{60}, had been aligned in more than one crystalline environment (Bleaney *et al.* 1954; Ambler *et al.* 1953). Since the Oxford group planned to orient Yb^{175} in the ethylsulphate lattice, and we planned to align it in the double nitrate lattice, it was thought that these investigations might complement each other and yield information about the effects of interactions. The results of the investigations at Oxford have already been published (Grace *et al.* 1957), and are indeed very different from ours.

[1]Manuscript received April 18, 1958.
Contribution from the Department of Physics, University of British Columbia, Vancouver, B.C.
[2]Now at the University of Ottawa.

PART I—PRASEODYMIUM 142

2. EXPERIMENTAL

The experimental technique which we used is essentially that described in detail by Bleaney *et al.* (1954) (*q.v.*). A solution of a few milligrams of praseodymium nitrate in heavy water was irradiated in the B.E.P.O. pile at Harwell to an activity of some 8 millicuries. It was then brought to Vancouver by C.P.A.'s transpolar flight, and the active solution was poured into a saturated solution of about 20 g of cerium magnesium nitrate. Single crystals were then grown from this solution in a vacuum desiccator. Despite the short half-life of Pr^{142} (19 hours), it was possible within 2 days to obtain some 5 or 6 g of large, well-formed single crystals with a counting rate of about 200/second in the counting apparatus described below. These crystals, which are plates of trigonal symmetry, were mounted with parallel crystallographic orientation in a demagnetization cryostat, and cooled by adiabatic demagnetization. Temperatures of 3×10^{-3} °K can be, and were, attained by the adiabatic demagnetization of this salt. After demagnetization, the magnet was removed, and two scintillation counters were placed in position round the specimen. During the period when the crystals warmed up from the low temperature attained on demagnetization to the helium bath temperature of 1.25° K, from 10 to 20 minutes according to the conditions prevailing during an experiment, the counting rate was measured in the two counters, and the temperature of the crystals was measured using a mutual inductance and a ballistic galvanometer, as described by Bleaney *et al.* (1954). The counters were thallium-activated sodium iodide crystals $1\frac{1}{2}$ in. diam.$\times$1 in. long, pre-packaged by the Harshaw Chemical Co. In some of the experiments the cell containing the crystal was mounted directly onto the face of the photomultiplier tube (R.C.A. 6342), in others it was coupled to this tube by a lucite light pipe 6 in.$\times1\frac{1}{2}$ in. No significant loss of resolution was noticed with this latter arrangement. One scintillation crystal was placed on the trigonal axis of the radioactive crystals, about 10 cm from the source, and the other was placed at a similar distance in a direction at right angles to this axis. The pulses from each photomultiplier were first amplified, then fed into a discriminator which passed only those pulses of energy greater than 1 Mev, and finally into a scaler. There were two such identical channels, and the pulses from each photomultiplier were counted on a separate scaler. After the active crystals had warmed to 1.25° K, the counting rate was observed for a while to test the stability of the counters, and for normalization purposes. In some of the experiments, an external magnetic field of a few hundred gauss was applied to the radioactive crystals. This was produced by two water-cooled air-core coils in a quasi-Helmholtz arrangement. When these coils were used, the scintillation crystals were coupled to the photomultipliers by the light pipes, and the photomultipliers were shielded with one layer of mu metal and two layers of annealed soft iron. A bucking coil was wound round the soft iron shield of one of the photomultipliers.

We can define an anisotropy parameter ϵ by the relation $\epsilon = (I_\perp - I_\parallel)/I_\perp$, where $I_\parallel$ and $I_\perp$ are the normalized counting rates in directions parallel and

perpendicular respectively to the trigonal axis of the crystals. Values of ϵ for the same temperature, but from different demagnetizations, were averaged to improve statistics.

The absolute temperature of the radioactive crystals was obtained from magnetic susceptibility measurements, using the relationship given by Daniels and Robinson (1953). The Curie-Weiss Δ for our specimen was determined by comparing the measured value of the magnetic temperature T^* after demagnetization with the value calculated from the initial magnetic field and the initial temperature. Its value was 2.6 millidegrees, which is a reasonable value according to Daniels and Robinson (1953).

The results of the measurements are shown in Figs. 1 and 2, in which ϵ is plotted as a function of $1/T$; Fig. 1 is for the case where no external magnetic

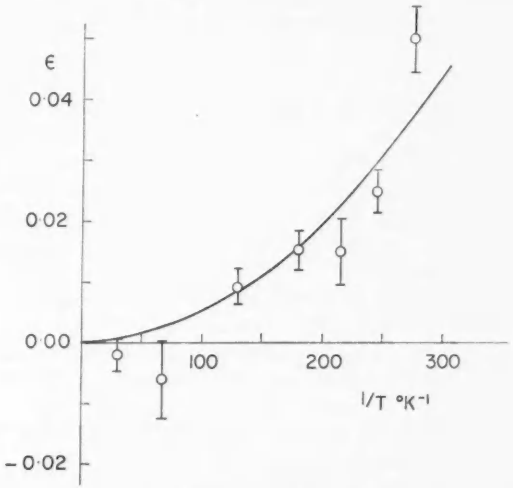

FIG. 1. Anisotropy of the 1.57 Mev γ-ray of Pr^{142}. No external magnetic field.

field is applied, Fig. 2 is for the case where an external magnetic field of 320 oersted is applied parallel to the trigonal axis of the crystals. In each figure the solid curve is the curve of the form $\epsilon = a/T^2$ which best fits the data. For zero external magnetic field $a = 4.95\times10^{-7}$ °K^{-2}, for an external field of 320 oersted $a = 18.7\times10^{-7}$ °K^{-2}.

3. DISCUSSION

The double nitrates $M_2Mg_3(NO_3)_{12}.24H_2O$, where M is one of La, Ce, or Pr, are isomorphous and form mixed crystals in all proportions. The paramagnetic resonance spectrum of the stable isotope, Pr^{141}, as an impurity in lanthanum magnesium nitrate, has been observed by Cooke and Duffus (1955), who assigned to this ion the spin Hamiltonian:

$$\mathcal{H} = g_{\parallel}\beta H_z S_z + A S_z I_z + \Delta_x S_x + \Delta_y S_y, \tag{1}$$

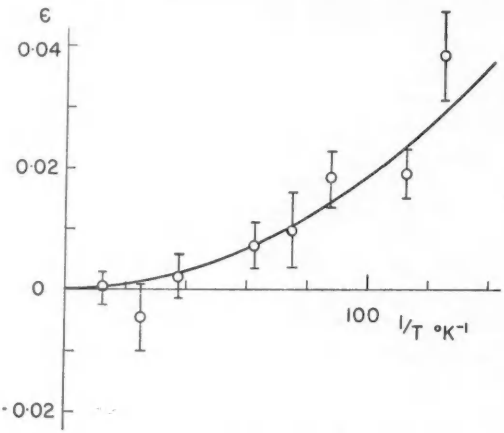

FIG. 2. Anisotropy of the 1.57 Mev γ-ray of Pr^{142}. An external magnetic field of 320 gauss applied along the trigonal axis.

where

$$\begin{aligned} g_{\parallel} &= 1.55, \\ A &= 0.077\ \text{cm}^{-1}, \\ \Delta &= \text{Average}\ \sqrt{\Delta_x^2+\Delta_y^2} \simeq 0.04\ \text{cm}^{-1}, \\ S &= \tfrac{1}{2}, \\ I &= 5/2, \end{aligned}$$

and the z-axis is the trigonal axis of the crystals. The Pr^{+++} ion has an even number of electrons, and hence the energy levels need not be doublets (Kramers' theorem). However the symmetry of the double nitrate crystal is such that the ground state is an accidental doublet. Strains and other distortions can cause a splitting of this doublet, and it has been suggested that this is the origin of the Δ-term. There is no unique value of Δ, a different value being appropriate for each ion, but an "average" value of Δ can be assigned. Δ is probably structure-sensitive. The most general spin Hamiltonian with trigonal symmetry has terms $g_{\perp}\beta(H_xS_x+H_yS_y)$ and $B(S_xP_x+S_yI_y)$ in addition to those in equation (1). To the accuracy of published measurements, both $g_{\perp}$ and B are zero. In the case where $S = \frac{1}{2}$, $g_{\perp} = B = 0$, and $\Delta = 0$, magnetic interactions between the ions do not affect the angular distribution of γ-rays (Daniels 1957). In this case also, an external magnetic field applied along the z-axis has no effect on the angular distribution (Daniels 1957). For "high" temperatures (in this experiment, $T > 0.005°$ K) the γ-ray anisotropy $\epsilon \propto 1/T^2$. The angular distribution of γ-rays can be represented by an operator $(1/4\pi+\Gamma')$, and the angular distribution at any temperature is given by

$$I(\theta, \phi) = \frac{1}{4\pi}+\frac{1}{2k^2T^2}\frac{\text{Spur}\ (\Gamma'\mathscr{H}^2)}{\text{Spur}\ (1)}+\ldots \tag{2}$$

(see Daniels (1957), in which some of the symmetry properties of Γ' are also

given). Substitution into (2) of the Hamiltonian (1) shows that the Δ-term does not affect the $1/T^2$ term in the angular distribution. It is thus difficult to understand the reason for the difference between the values found for ϵ with and without an external magnetic field. Many misgivings have been voiced that the spin Hamiltonian obtained from resonance experiments in a large magnetic field does not adequately express the state of an ion in zero magnetic field. This may be particularly so for praseodymium, which has no Kramers degeneracy. Under the circumstances we choose to use the values of ϵ in an external magnetic field to determine the magnetic moment of Pr^{142}. This is because:

(*a*) The spin Hamiltonian (1) was determined in a large external magnetic field, and is probably more applicable to the case where there is an external field than to the case where there is none.

(*b*) The measurements in this case were made at higher temperatures. The temperatures are more reliable, and the series expansion in powers of $1/T$ (2) is more likely to be applicable.

(*c*) The warming up times were longer and hence temperature inhomogeneities are not so likely.

(*d*) If the assumed spin Hamiltonian is inadequate, and for some reason magnetic interactions play a part in determining the anisotropy, an external field of 320 oersted should be sufficient to nullify these interaction effects, since the internal field in this salt is about 30 oersted.

The possibility was considered that bremsstrahlung from the 2.166 Mev β-ray could be counted as γ-rays and reduce the observed anisotropy. Calculations based on formulae in Siegbahn (1955) showed that this effect is negligible. The threshold of the discriminator was set at 1 Mev to get a good counting rate. In this case one must consider the reduction of anisotropy due to scattered γ-rays. Such a calculation was made by Bleaney *et al.* (1954) for the case of Co^{60} in an apparatus which is essentially similar to ours. It was found there that this correction is quite negligible for values of ϵ as low as 0.04, and we have therefore ignored it. It is very unlikely that the lifetime of the γ-emitting state is greater than about 10^{-13} seconds, hence loss of anisotropy due to precession in the crystalline fields can be discounted.

The decay scheme of 19.2h Pr^{142} has been studied by various workers, including Gideon *et al.* (1949), Jensen *et al.* (1950), Bartholomew and Kinsey (1953), Polm *et al.* (1954), and Sterk *et al.* (1955). The decay scheme suggested by Polm *et al.* (1954) is shown in Fig. 3. The arguments for this decay scheme are, briefly, as follows. Nd^{142} is an even–even nucleus; its ground state therefore is 0+. The 2.166 Mev β-ray has log $ft = 7.8$, and the first special shape appropriate to a beta transition with $\Delta I = 2$, yes; the spin and parity of Pr^{142} are thus 2−. The other beta transition has log $ft = 7.1$ and allowed shape; it is therefore suggested that it is first forbidden with $\Delta I = 0$ or ± 1, yes. Since the first excited states of nearly all even–even nuclei so far measured have spin and parity 2+, the excited state of Nd^{142} in this scheme is assigned spin and parity 2+, and the γ-ray is assumed to be $E2$.

Since the spin Hamiltonian (2) indicates that at 0° K all the nuclei are

oriented parallel to the trigonal crystal axis, it is possible in principle to distinguish between certain possible spin assignments in the decay scheme.

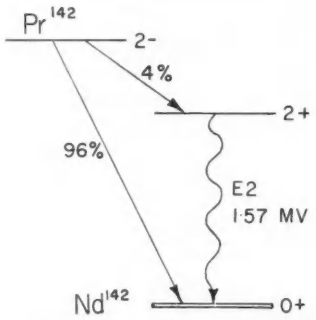

FIG. 3. Decay scheme of Pr^{142}.

For example, the limiting value of ϵ at low temperatures is $+1$ if the 0.586 Mev β–ν pair carries off no angular momentum; $+1/3$ if the β–ν pair carries off one unit of angular momentum, the other assignments being as in Fig. 3. However, we could not attain temperatures low enough to see any saturation of the γ-ray anisotropy. The observed positive sign of ϵ indicates that the γ-ray is quadrupole.

Substitution of (1) into (2) yields the formulae, $\epsilon = 3A^2/16k^2T^2$ if the β–ν carries off no angular momentum, and $\epsilon = 3A^2/32k^2T^2$ if the β–ν carries off one unit of angular momentum. Since the field at the praseodymium nucleus is due to the $4f$ electron shell, independent of the isotope, this field is $H = A_{141}I_{141}/\mu_{141} = A_{142}I_{142}/\mu_{142}$. These values are known for the stable isotope Pr^{141}, and it is a simple matter to substitute into these formulae to find μ_{142}. The result is: $\mu_{142} = 0.11$ nuclear magnetons if the β–ν carries off no angular momentum, or $\mu_{142} = 0.15$ nuclear magnetons if the β–ν carries off one unit of angular momentum.

PART II—YTTERBIUM 175

4. EXPERIMENTAL

The starting material for these investigations was Yb_2O_3, separated by the ion exchange method, and supplied to us by Dr. F. H. Spedding of the Ames Institute. One milligram was irradiated in the NRX pile at Chalk River, to an activity of about 5 mc. On receipt of the irradiated sample, the quartz capsule was crushed under about 20 cc of water contained in a platinum crucible. A special jig was used for this operation. About three drops of concentrated sulphuric acid were added, and the whole was evaporated to dryness, first on a sand bath and afterwards under a heat lamp. The residue was then dissolved in about 20 or 30 cc of water and added to about 10 g of cerium magnesium nitrate. Crystals were grown from this solution in a vacuum desiccator.

These double nitrates of the rare earths exist only for the rare earths from La to Gd, and ytterbium magnesium nitrate does not exist as such. However, some ytterbium does go into the crystal lattice. After a crystal was removed from the solution, it was washed with distilled water to remove any solution from its surface, and dried with filter paper, to preclude the possibility that the activity is due to a layer of dried off solution on the surface. The crystals were generally clear enough for the observer to see that they contained no large inclusions of solution. On one occasion, a sample of Yb_2O_3 became contaminated in the irradiation, and the solution from which the crystals were grown emitted a gamma ray of about 700 kev energy, yet this gamma ray was completely absent from the crystals grown from this solution. In this way we are sure that the ytterbium does go into the crystal lattice; it is most reasonable to assume that it goes into a rare-earth position, although there is no direct evidence for this. The specific activity of the crystals was about 1/30 that of the solution.

During the irradiation of natural ytterbium, three isotopes are formed, 4.2 day Yb^{175}, 32.4 day Yb^{169}, and 6.7 day Lu^{177}. However, about 10 times as much Yb^{175} as Yb^{169} or Lu^{177} is produced (Cork *et al.* 1950), and the 396 kev γ-ray of Yb^{175} has a greater energy than any other from any of the three isotopes. Yb^{169} has a γ-ray of 300 kev, but this is less intense than the 282 kev γ-ray of Yb^{175}. The technique used to orient the ytterbium was exactly the same as that used to orient praseodymium, described in Part I of this paper. Measurements were made on both the 396 kev γ-ray and also on the 282 kev γ-ray; for the former a bottom cut discriminator was used, set to pass the photo-peak of the 396 kev γ-ray; for the latter a single channel kicksorter was used, set to pass only the photo-peak of this γ-ray. These measurements were made with zero external magnetic field, with fields of 260, 380, 510, and 700 oersted parallel to the trigonal crystalline axis, and with fields of 58, 100, and 160 oersted perpendicular to this axis. In no case was any significant anisotropy of γ-radiation observed at any temperature. The results are shown in Fig. 4.

5. DISCUSSION

The principal features of the decay scheme of Yb^{175} are shown in Fig. 5. This decay scheme has been studied by a variety of investigators (de Waard (1955), Åkerlind *et al.* (1955), Marty (1955), Mize *et al.* (1955*a*, *b*), Cork *et al.* (1956)) and has been analyzed theoretically by Chase and Wilets (1956). We shall therefore assume that the decay scheme is established correctly. From measurements of the anisotropy of γ-rays from Yb^{175} oriented in ytterbium ethylsulphate, Grace *et al.* (1957) deduced a value for the magnetic moment of Yb^{175}; it is 0.15 ± 0.04 nuclear magnetons; the sign is not known. The 396 kev γ-ray and the 282 kev γ-ray are both M2 with a small admixture of E1. The experiments so far carried out do not give consistent values for the mixing ratios of these γ-rays (see Grace *et al.* 1957).

No one has observed paramagnetic resonance in Yb^{+++} in the double nitrate lattice, hence the spin Hamiltonian is not known. We have made an estimate of the constants in the spin Hamiltonian by the following method. We assume

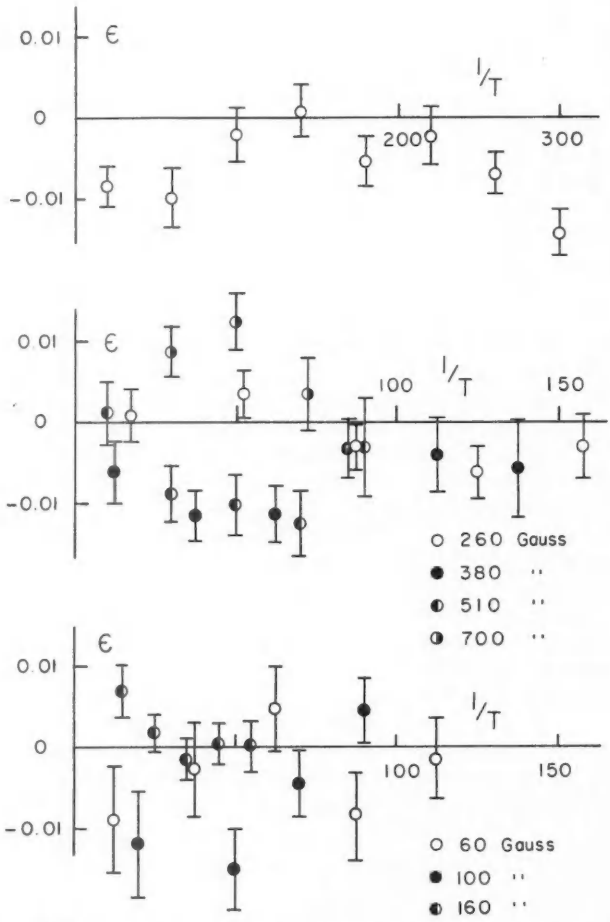

FIG. 4*a*. Anisotropy of the 396 kev γ-ray of Yb^{175}. Upper graph—no external magnetic field. Middle graph—external magnetic fields applied along the trigonal axis. Lower graph—external magnetic fields applied perpendicular to the trigonal axis.

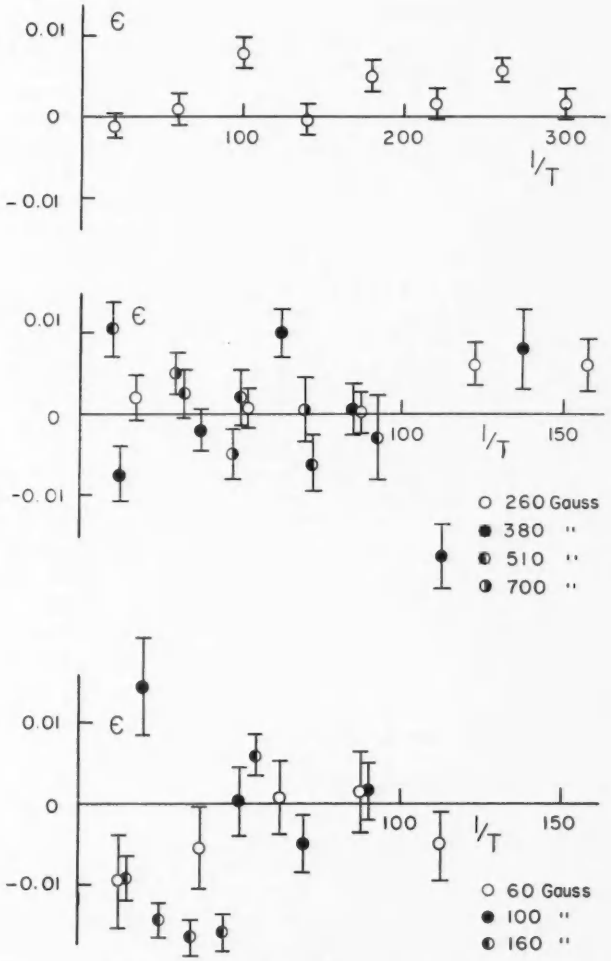

FIG. 4*b*. Anisotropy of the 282 kev γ-ray of Yb^{175}. Upper graph—no external magnetic field. Middle graph—external magnetic fields applied along the trigonal axis. Lower graph—external magnetic fields applied perpendicular to the trigonal axis.

that the crystalline field acting on the ytterbium ion is the same as that acting on the cerium ion; the coefficients for the expansion of this field in a

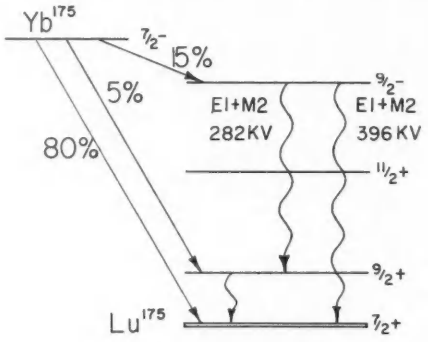

FIG. 5. Decay scheme of Yb^{175}.

series of spherical harmonics are given by Judd (1955*a*). We assume that the formula given by Elliott and Stevens (1953*a*) for the radius of the 4*f* shell,

$$\overline{r^n} \propto (Z-55)^{-n/4},$$

is applicable. Using these values of crystal field parameters and ionic radii, we can work out an energy matrix for the ytterbium ion using the method and formulae given by Stevens (1952), Elliott and Stevens (1952, 1953*a*, *b*), and Judd (1955*a*, *b*). The results of these calculations are as follows: whereas the free Yb^{+++} ion has $J = 7/2$ and an eight-fold degenerate ground state, in the double nitrate environment, this degenerate level is split into 4 doublets whose energies are -2.26, $+39.4$, $+0.4$, and -37.5 cm^{-1}. The state with energy $-2.26\,cm^{-1}$ is the doublet spanned by $|J_z = 3/2\rangle$ and $|J_z = -3/2\rangle$, which lies lowest in the ethylsulphate. The lowest energy level is the one at -37.5 cm^{-1}. This is spanned by the wave function

$$0.794|7/2\rangle - 0.424|1/2\rangle - 0.435|-5/2\rangle$$

and

$$-0.794|-7/2\rangle - 0.424|-1/2\rangle + 0.435|5/2\rangle.$$

Assuming a spin Hamiltonian of the form

$$g_{\parallel}\beta H_z S_z + g_{\perp}\beta(H_x S_x + H_y S_y) + AS_z I_z + B(S_x I_x + S_y I_y),$$

we find $g_{\parallel} = 4.2$, $g_{\perp} = 2.9$. The extent of the hyperfine structure is given by AI and BI. Assuming that the magnetic moment of Yb^{175} is 0.15 nuclear magnetons, $AI = 0.024°$ K and $BI = 0.017°$ K. It is true that it is rather optimistic to expect such a calculation to give a result which is quantitatively correct, but unfortunately no better estimate of the properties of the ytterbium ion in this lattice exists. On the basis of these estimates, we should expect to observe nuclear orientation under the conditions of our experiments.

In view of the established fact that sizeable anisotropies of both the 396 kev γ-ray and the 282 kev γ-ray have been observed from oriented Yb^{175} nuclei (Grace *et al.* 1957), the absence of an anisotropy in zero external field in our experiment can be explained by one or more of the following hypotheses:

(i) The ytterbium ion does not enter the lattice in a rare-earth position.

(ii) The spin Hamiltonian is isotropic, i.e., $g_{\parallel} = g_{\perp}$ and $A = B$.

(iii) Magnetic interactions in the double nitrate crystal destroy the alignment of the ytterbium nuclei.

(iv) The γ-emitting state is long-lived and precession of the excited Lu^{175} nucleus in the internal atomic fields destroys the alignment before the emission of the γ-ray.

As for hypothesis (ii), the application of an external magnetic field in any direction should cause an anisotropy of γ-emission to appear (Gorter 1948; Rose 1949; Ambler *et al.* 1953). Since this does not occur, the possibility of the other hypotheses must also be considered.

Hypothesis (iii) is certainly applicable in this case. The theory of the effect of interactions has been given by Daniels (1957), and an order of magnitude calculation based on the formulae given there shows that the magnetic interference can be much greater than the forces which tend to orient the nuclei. Naively, the internal field at a rare-earth site is about 30 oersted; this will produce a splitting of the ground state of about 0.01° K, whereas the forces which tend to produce spatial orientation are of the order of magnitude of $(A-B)I$, or about 0.007° K. However, the application of an external field larger than the internal field of 30 oersted should cause an anisotropy to appear, and this is not so.

Hypothesis (iv) is quite sufficient to explain our results, and also to explain the difference between our results and those obtained at Oxford. In the spin Hamiltonian for the Yb^{+++} ion in the ethylsulphate, $g_{\perp} = 0 = B$. Under these circumstances, the angular distribution of γ-rays is not affected by precession of the γ-emitting nucleus. This is easily seen, for the angular distribution of γ-rays is given by an expression of the form

$$\sum_r g_r \langle \psi_r | \Gamma | \psi_r \rangle,$$

where g_r is a statistical distribution (e.g., Boltzmann) factor, ψ_r is a wavefunction of the ion containing the γ-emitting nucleus, and Γ is an operator which represents the angular distribution of γ-rays (see e.g., Daniels 1957). Because of the axial symmetry of the ion and its environments in a representation with S_z diagonal only the diagonal elements of Γ appear in the result. If there is precession for a time t before the emission of the γ-ray, $|\psi_r\rangle$ must be replaced by $\exp[-i\mathcal{H}t/\hbar]|\psi_r\rangle$. This is equivalent to replacing Γ by $\exp[i\mathcal{H}t/\hbar]\,\Gamma\exp[-i\mathcal{H}t/\hbar]$. Now the spin Hamiltonian $\mathcal{H}$ for ytterbium ethylsulphate is diagonal in this representation and hence the diagonal elements of $\exp[i\mathcal{H}t/\hbar]\,\Gamma\exp[-i\mathcal{H}t/\hbar]$ are independent of t. Thus the angular distribution of γ-radiation in ytterbium ethylsulphate is not affected by precession. This is not so for the more general spin Hamiltonian which presumably applies to the double nitrate. It is difficult to estimate the lifetime necessary to wipe

out all the anisotropy which should be there. If we take as a rough criterion that the lifetime should be about as long as it would take for the excited Lu^{175} nucleus to precess in the atomic magnetic field, the result is about 10^{-10} seconds. Chase and Wilets (1956) have explained that for both γ-rays, the E1 transition is strongly inhibited, and the lifetime should be about that appropriate to an M2 transition. Weisskopf's formula for the lifetime of a 400 kev M2 emitting state gives 10^{-8} seconds; since the transition in Yb^{175} is a collective transition, not a single nucleon transition, a lifetime of 10^{-10} seconds is more likely. A question arises whether the spin Hamiltonian of the ytterbium ion should be used during the precession, since after the γ-emission the electronic configuration should be that of lutecium, which is not magnetic. This depends principally on the lifetimes of the $4f$ states. These are probably about 10^{-6} to 10^{-8} seconds, typical lifetimes for optical transitions, and in the absence of further information the use of the ytterbium spin Hamiltonian is justifiable. Thus, it appears that hypothesis (iv) is adequate to explain our results.

6. CONCLUSIONS

(i) *Praseodymium 142*

An anisotropy of γ-emission from oriented Pr^{142} has been observed and measured. Although the anisotropy is not completely understandable in terms of the published spin Hamiltonian Pr^{+++}, it seemed plausible to assign a value to the magnetic moment of this nucleus. The value assigned is 0.11 nuclear magnetons if the cascade β-ray carries away no angular momentum, and 0.15 nuclear magnetons if the β-ray carries away one unit of angular momentum.

(ii) *Ytterbium 175*

No anisotropy was observed for either γ-ray of ytterbium 175 in cerium magnesium nitrate. Although the possibility must always be kept in mind that ytterbium does not replace cerium in cerium magnesium nitrate, it seems that the most likely reason for not observing any γ-ray anisotropy is that the γ-emitting state has a lifetime of about 10^{-10} seconds. The observation of anisotropies from this same nucleus in ytterbium ethylsulphate is quite consistent with this hypothesis, since the internal fields in this salt are such that precession would not affect the angular distribution of γ-rays. The estimate of 10^{-10} seconds for the lifetime of the γ-emitting state is consistent with all the other evidence about this nucleus.

ACKNOWLEDGMENTS

This work was supported by a grant-in-aid from the National Research Council of Canada, to whom grateful acknowledgment is made. One of us (M.A.R.L.) wishes to thank the National Research Council for the award of a Studentship.

REFERENCES

ÅKERLIND, L., HARTMANN, B., and WIEDLING, T. 1955. Phil. Mag. **46**, 448.
AMBLER, E., GRACE, M. A., HALBAN, H., KURTI, N., DURAND, H., JOHNSON, C. E., and LEMMER, H. R. 1953. Phil. Mag. **44**, 216.

BARTHOLOMEW, G. A. and KINSEY, B. B. 1953. Can. J. Phys. **31**, 1025.
BLEANEY, B., DANIELS, J. M., GRACE, M. A., HALBAN, H., KURTI, N., ROBINSON, F. N. H., and SIMON, F. E. 1954. Proc. Roy. Soc. A, **221**, 170.
CHASE, D. M., and WILETS, L. 1956. Phys. Rev. **101**, 1038.
COOKE, A. H. and DUFFUS, H. J. 1955. Proc. Roy. Soc. (London), A, **229**, 407.
CORK, J. M., KELLER, H. B., RUTLEDGE, W. C., and STODDARD, A. E. 1950. Phys. Rev. **78**, 95.
CORK, J. M., BRICE, M. K., MARTIN, R. W., SCHMID, L. G., and HALMER, G. R. 1956. Phys. Rev. **101**, 1042.
DANIELS, J. M. 1957. Can. J. Phys. **35**, 1133.
ELLIOTT, R. J. and STEVENS, K. W. H. 1952. Proc. Roy. Soc. A, **215**, 437.
——— 1953*a*. Proc. Roy. Soc. A, **218**, 553.
——— 1953*b*. Proc. Roy. Soc. A, **219**, 387.
GIDEON, D. N., MILLER, W. C., and WALDMAN, B. 1949. Phys. Rev. **75**, 329.
GRACE, M. A. and HALBAN, H. 1952. Physica, **18**, 1227.
GRACE, M. A., JOHNSON, C. E., KURTI, N., LEMMER, H. R., and ROBINSON, F. N. H. 1954. Phil. Mag. **45**, 1192.
GRACE, M. A., JOHNSON, C. E., SCURLOCK, R. G., and TAYLOR, R. T. 1957. Phil. Mag. **2**, 1079.
GORTER, C. J. 1948. Physica, **14**, 504.
JENSEN, E. N., LASLETT, L. JACKSON, and ZAFFARANO, D. J. 1950. Phys. Rev. **80**, 862.
JUDD, B. R. 1955*a*. Proc. Roy. Soc. A, **226**, 458.
——— 1955*b*. Proc. Roy. Soc. A, **227**, 552.
MARTY, N. 1955. Compt. Rend. **240**, 963.
MIZE, J. P., BUNKER, M. E., and STERNER, J. W. 1955*a*. Phys. Rev. **99**, 671.
——— 1955*b*. Phys. Rev. **100**, 1398.
POLM, A. V., LEWIS, W. E., TALBOY, J. H. Jr., and JENSEN, E. N. 1954. Phys. Rev. **95**, 1523.
ROSE, M. E. 1949. Phys. Rev. **75**, 213.
SIEGBAHN, K. 1955. β- and γ-ray spectroscopy (North Holland Publishing Co., Amsterdam) pp. 13 and 653.
STERK, W. J., NIESSBAUM, R. H., and CERFONTAIN, H. 1955. Physica, **21**, 541.
STEVENS, K. W. H. 1952. Proc. Phys. Soc. A, **65**, 209.
DE WAARD, H. 1955. Phil. Mag. **46**, 445.

THE ELECTRICAL CONDUCTIVITY OF MANGANESE ARSENIDE AND ANTIMONIDE[1]

GASTON FISCHER AND W. B. PEARSON

ABSTRACT

New measurements of the electrical resistivity of MnAs and MnSb are reported as part of a program of relating the electronic and crystal structure of compounds to their electrical properties. Modern experimental methods have been used in an attempt to obtain better samples and to avoid the formation of cracks which greatly influence the measured resistivity. The electrical resistivity of MnAs in the paramagnetic range where it is fairly independent of temperature is about 5×10^{-4} ohm cm. In the ferromagnetic range it is about 2×10^{-4} ohm cm at 0° C with a temperature coefficient of 5×10^{-3} per ° C.

INTRODUCTION

Manganese arsenide, antimonide, and bismuthide each have the hexagonal nickel arsenide type of structure. The substances are interesting for the transitions which they undergo (Table I). As part of a program designed to gain more understanding of the relationship between electronic and crystal structure on the one hand and electrical properties on the other hand, we

TABLE I*

TRANSITIONS IN MNAS, MNSB, MNBI

MnAs	25°–50° C	With hysteresis. Ferromagnetic ↔ paramagnetic. First order transition
	~130° C	A second order transition appears to occur in this region
MnSb	313° C	Ferromagnetic ↔ paramagnetic. Normal second order transition
MnBi	340°–360° C	Ferromagnetic ↔ paramagnetic. First order transition resulting from some Mn atoms changing their sites in the crystal structure

*Cf. Guillaud 1951; Bates 1934; Willis and Rooksby 1954; Bacon and Street 1955; Roberts 1956.

have made careful measurements of the electrical conductivity of MnAs and MnSb. Although this property has been measured previously (Guillaud 1951; Bates 1934) the details of the measurements of MnAs, particularly, are open to some doubt owing to the micro- and macro-cracks which permeate samples after they have been cooled through the ferromagnetic transition at 25°–50° C, and furthermore, an absolute value of the resistivity has not so far been obtained. It was thought that some improvement over the earlier measurements could be obtained (1) by never allowing the samples of MnAs to cool through the transition at ~40° C before the measurements were made (this should avoid the formation of cracks in the specimen which were thought

[1]Manuscript received March 14, 1958.
Contribution from the Division of Pure Physics, National Research Council, Ottawa, Canada.
Issued as N.R.C. No. 4830.

to arise at the discontinuous anisotropic change of unit cell dimensions occurring at the transition); (2) by using, in the preparation of the sample, some of the methods now employed in the preparation and handling of semiconducting compounds. Although zone purification does not appear feasible, slow cooling and solidification of the melt from one end should lead to the formation of perfect stoichiometric crystals at least at the start of the process. Furthermore, by a suitable distribution of temperature gradients along the sealed silica tubes in which samples are prepared, it should be possible to prevent distillation of the volatile components from the surface of the sample.

We were also particularly interested in making measurements of samples of MnBi because the work of Roberts (1956) using neutron diffraction has established the nature of the change at 350° C which, as in MnAs, is a first order transition. Unfortunately, however, we have not succeeded in preparing samples of MnBi of sufficient quality for conductivity measurements.

EXPERIMENTAL METHODS

The principles outlined above were followed during the preparation of the samples in vertical or horizontal gradient furnaces. Pure hydrogen-treated electrolytic manganese was mixed with the required proportion of 99.9% As or 99.995% Sb and sealed in an evacuated silica tube. The mixture was slowly heated up to the melting point and then held some 25° C above this temperature for 1 hour. After a vigorous shaking it was solidified slowly and finally cooled either to 50° C or to room temperature over a period of 2 days.

Microscopical and X-ray examination showed the MnAs samples to be homogeneous but MnSb samples contained about 4 volume per cent of other phases, even after they were annealed at 800° C for several days. The samples were polycrystalline and strongly ferromagnetic at room temperature.

The electrical resistivity of the samples was measured by a potential method (Dauphinee and Mooser 1955). During measurement the specimens were kept under one atmosphere pressure of helium to prevent loss of As or Sb by evaporation.

ELECTRICAL RESISTIVITY

(*a*) MnAs

The temperature dependence of the electrical resistivity of two samples (A and B) of MnAs which had never been cooled through the transition at ~40° C is shown in Fig. 1 ((*a*) and (*b*)). However, even when the polycrystalline samples were heated and cooled a number of times without passing through the transition temperature, it appeared that microcracks were formed since the specimens became softer and there were small changes in resistivity. This behavior probably resulted from the strongly anisotropic thermal expansion of the material (cf. Willis and Rooksby 1954) and its inability to be plastically deformed. On the other hand one sample (C) prepared in the vertical furnace remained very strong and showed no tendency to crumble after cooling to room temperature. This sample also was the only one to show a marked change of slope in the resistivity temperature curve

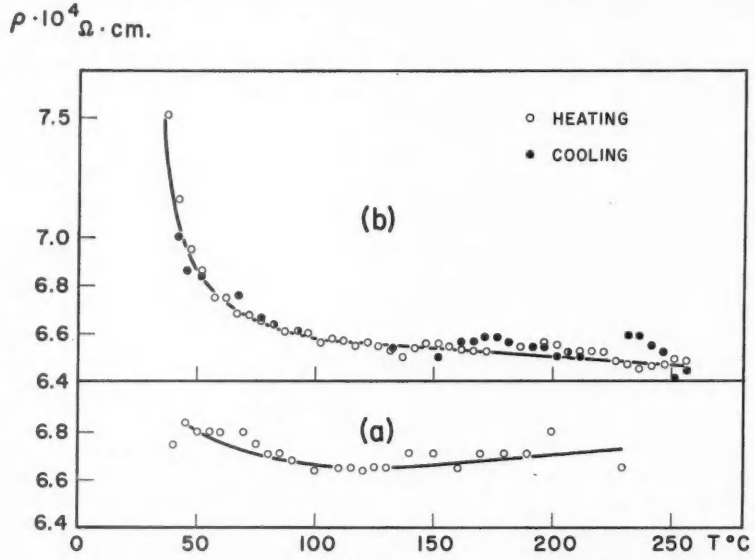

FIG. 1. Electrical resistivity of MnAs as a function of temperature. (*a*) Measurements obtained during the first heating cycle of a sample (A) which was never cooled below 40° C. The sample was prepared horizontally and the last portion to crystallize was measured. (*b*) Measurements obtained after several heating cycles: the resistivity starts to rise near the transition temperature. The sample (B) was taken from the same ingot used in (*a*) but the first portion to crystallize was measured in this case.

(Fig. 1 (*c*)) in the region of 130° C where the presence of a further "transition" had been suggested by lattice spacing variation and other evidence (cf. Guillaud 1951; Willis and Rooksby 1954).

The electrical resistivity of samples A and B ($\sim 6.6 \times 10^{-4}$ ohm cm at 130° C) was not much larger than that of sample C ($\sim 4.8 \times 10^{-4}$ ohm cm at 130° C) at temperatures where the samples could be compared; however, when samples A and B were eventually cooled through the transition at ~40° C their resistivity increased greatly, being then about a hundred times larger than that of specimen C. Such behavior is entirely consistent with the nature of the transition which is described in the following paper (Basinski and Pearson), since the effect on the resistivity of the fragmentation which occurs will depend on the relative grain sizes and orientations in the samples.

In the paramagnetic range above 50° C the reasonable agreement of the resistivity of samples which had not been cooled through the transition with that of the sample which did not crumble on passing through the transition establishes the electrical resistivity of MnAs as about 5×10^{-4} ohm cm and as being relatively independent of temperature. In the ferromagnetic range we believe that sample C, which remained mechanically strong and did not crumble, gives the true electrical resistivity of polycrystalline MnAs. Between

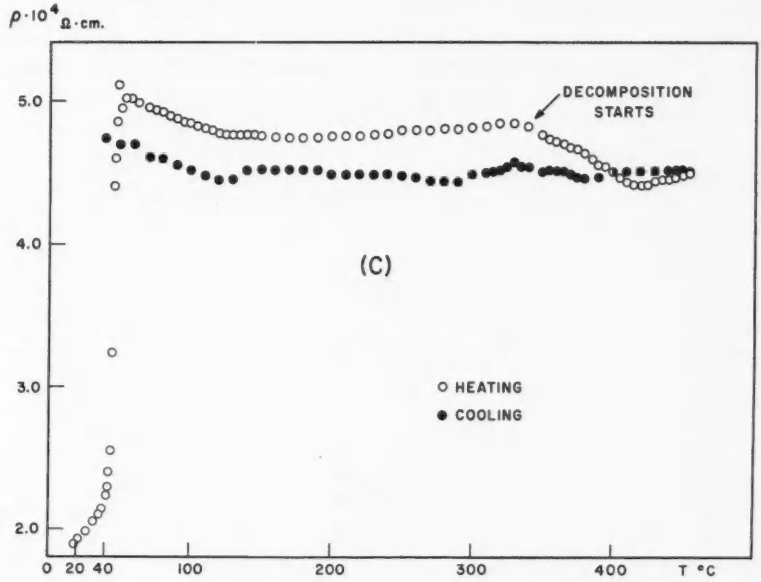

FIG. 1(*c*). Electrical resistivity of MnAs as a function of temperature. This sample (C) was prepared vertically and it remained strong and did not crumble on cooling through the transition at about 40° C.

−120° C and 20° C its resistivity varied linearly with temperature with a coefficient of $+5\times10^{-3}$ per °C, the resistivity at 0° C being 1.7×10^{-4} ohm cm.

Finally we must add that at the time when these measurements were made, we were not aware of the mechanism of the transformation at 40° C. It was rather that the peculiar variability of the electrical resistivity which we encountered led us to make the detailed study of the transformation mechanism reported in the following paper (Basinski and Pearson).

(*b*) MnSb

The variation of the electrical resistivity of two samples of MnSb during various heating cycles is shown in Fig. 2, and similar behavior has been observed in three other samples examined. In particular the behavior in the region of the Curie point is very variable. Nevertheless the measurements in the ferromagnetic range establish the temperature coefficient of resistivity (assumed to be constant) as about 3×10^{-3} per °C and indicate a resistivity of the order of 2×10^{-3} ohm cm for MnSb at room temperature.

DISCUSSION

The value of the electrical resistivity of MnAs in the paramagnetic range suggests that the substance is metallic and we therefore think that there is

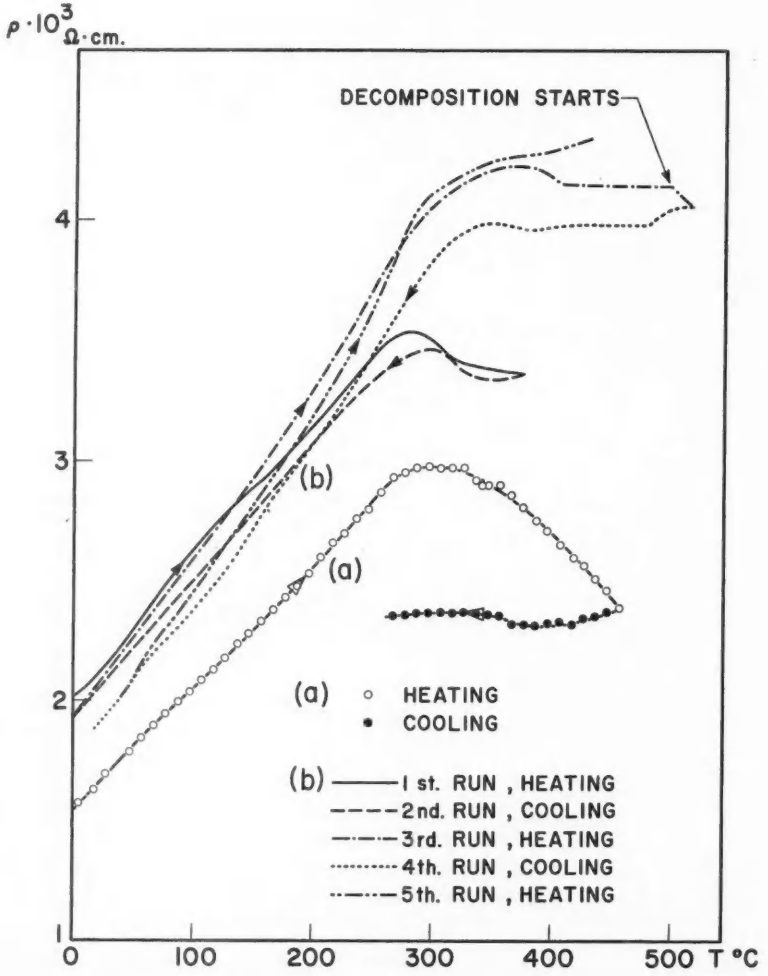

FIG. 2 Electrical resistivity of MnSb as a function of temperature. (*a*) Measurements made on a sample during the first heating and cooling cycle. The heating curve can be considered typical of MnSb. (*b*) Measurements made on another sample of MnSb during successive heating and cooling cycles, showing typical variations of resistivity encountered.

direct interaction between the *d* electrons of the manganese atoms since, in the absence of such interactions, we would have expected MnAs to show semiconducting properties. However, the discussion of Pearson (1957) shows that the value of the axial ratio of the unit cell of MnAs, $c/a = 1.53$, is close to a critical region of values where a change from metallic to semiconducting

properties occurs in substances with the nickel arsenide structure. The interactions between the manganese atoms would not therefore be expected to be well developed, and this is supported by the electrical resistivity of MnAs of about 5×10^{-4} ohm cm at 50° C, which is high for a good metal. The unpaired electrons on the manganese atoms should thus be regarded as mainly localized and a large contribution to the electrical resistivity from spin-disorder scattering may occur in the paramagnetic range (cf. Mott and Stevens 1957; Coles 1958). Reduced $\rho_{(T)}$ curves for MnAs and MnSb are compared in Fig. 3 with those of other substances in which spin-disorder scattering is held to make a large contribution to the electrical resistivity. The dis-

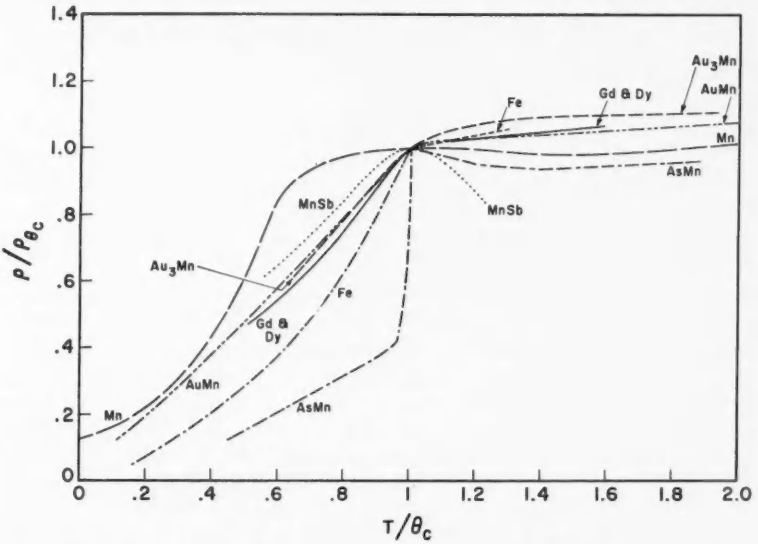

FIG. 3. Reduced resistivity versus reduced temperature for several ferromagnetic and antiferromagnetic substances. θ_c is the transformation temperature as determined by electrical measurements; it may differ appreciably from the results of magnetic or structural observations as in the cases of Dy and Mn. The data pertaining to the graph are:

	θ_c in °K	ρ_c in Ω cm	Reference
Fe	1033	—	Mott and Stevens (1957)
Mn	65	140×10^{-6}	White and Woods (1957)
Gd	289	—	Gerritsen (1956)
Dy	170	120×10^{-6}	Gerritsen (1956)
AuMn	500	75×10^{-6}	Gerritsen (1956)
Au_3Mn	150	45×10^{-6}	Gerritsen (1956)
AsMn	321	505×10^{-6}	Present work
MnSb	580	295×10^{-6}	Present work

continuous increase in resistivity at the transition in MnAs which accompanies a similar increase in axial ratio indicates, as expected, a decrease in the charge carrier concentration. Because of the "critical" value of the axial ratio of this compound the carrier concentration should be sensitive to small changes

in the unit cell dimensions. In these circumstances the anomalous temperature dependence of the electrical resistivity above the transition at 40° C might also arise in part from an abnormal variation of charge carrier concentration and mobility with temperature.

ACKNOWLEDGMENT

It is a pleasure to acknowledge discussions with Dr. E. Mooser.

REFERENCES

BACON, G. E. and STREET, R. 1955. Nature, **175**, 518.
BATES, L. F. 1934. Phil. Mag. **17**, 783.
COLES, B. R. 1958. Phil. Mag. Supp. **7**, 40.
DAUPHINEE, T. M. and MOOSER, E. 1955. Rev. Sci. Instr. **26**, 660.
GERRITSEN, A. N. 1956. Handbuch der Physik, Vol. 19 (Springer-Verlag, Berlin), p. 137.
GUILLAUD, CHARLES. 1951. J. phys. radium, **12**, 223.
MOTT, N. F. and STEVENS, K. W. H. 1957. Phil. Mag. **2**, 1364.
PEARSON, W. B. 1957. Can. J. Phys. **35**, 886.
ROBERTS, B. W. 1956. Phys. Rev. **104**, 607.
WHITE, G. K. and WOODS, S. B. 1957. Can. J. Phys. **35**, 346.
WILLIS, B. T. M. and ROOKSBY, H. P. 1954. Proc. Phys. Soc. B **67**, 290.

THE NON-MARTENSITIC DIFFUSIONLESS TRANSITION IN MANGANESE ARSENIDE AT ABOUT 40° C[1]

Z. S. Basinski and W. B. Pearson

ABSTRACT

We have investigated the nature of the transition at about 40° C in manganese arsenide. It is already well known that the transition involves a discontinuous change of the length of the *a* axis of the hexagonal unit cell, and that there is no change of crystal structure. The transition is accompanied by a loss of ferromagnetism of MnAs on proceeding to higher temperature. We find that the transformation takes place by a novel diffusionless non-martensitic mechanism. It appears that plastic deformation of MnAs is impossible and so, instead of the change following the martensitic pattern, the strain energy of the transformation is minimized by a fragmentation of the crystal grains into pencil-like subgrains whose direction lies parallel to the *c* axis of the crystals.

INTRODUCTION

Manganese arsenide has an interesting transition which occurs with hysteresis just above room temperature (between 25° and 50° C). Both high and low temperature phases have the nickel arsenide type of structure; however, the discontinuous changes of lattice spacing along the *a* axis (Guillaud 1951; Willis and Rooksby 1954) and of the electrical resistivity (Guillaud 1951; Fischer and Pearson 1958) indicate a first order transition. The low temperature phase is ferromagnetic, but the ferromagnetism disappears at the transition point (Bates 1934; Guillaud 1951). The positive coefficient of susceptibility which is found between the transformation point and a temperature of about 130° C has been interpreted by Guillaud as evidence of antiferromagnetism in this temperature interval, particularly as a ferromagnetic–antiferromagnetic change would be of the first order. However, a recent neutron diffraction study by Bacon and Street (1955) revealed no evidence of antiferromagnetism in the high temperature phase.

Let us note that MnBi also undergoes a first order transition with rather similar characteristics at about 350° C. Roberts (1956) in a neutron diffraction study found that the Mn atoms were definitely in a paramagnetic state above the transition temperature. At the transition a movement of some 10% of the Mn atoms takes place randomly from the 0, 0, 0; $\frac{1}{2}$, $\frac{1}{2}$, $\frac{1}{2}$ sites in the nickel arsenide structure stable at low temperatures to the trigonal bipyramidal holes at $\frac{1}{3}$, $\frac{2}{3}$, $\frac{3}{4}$; $\frac{2}{3}$, $\frac{1}{3}$, $\frac{3}{4}$. Himmel and Jack (1956) found that the high-temperature MnBi phase could be retained by quenching and that it was also ferromagnetic at room temperature, the Curie point being at about 200° C. Although there is an apparent similarity of the transitions in MnAs and MnBi it appears improbable that the mechanism of the change would be the same in each case, since we would not expect a normal diffusion-controlled reaction to

[1]Manuscript received March 14, 1958.
Contribution from the Division of Pure Physics, National Research Council, Ottawa, Canada.
Issued as N.R.C. No. 4787.

occur in MnAs at temperatures as low as 40° C. Indeed, in MnBi we know that a diffusion-controlled reaction can occur at an appreciable rate only at temperatures *above* 170° C, because not until this temperature is reached on heating up from room temperature, does the quenched metastable MnBi phase revert to the stable low-temperature phase. It thus appeared likely to us that the transition of MnAs would be a diffusionless type. All known diffusionless transformations involving an appreciable change of the unit cell dimensions are of the martensitic type, i.e., the strain energy is minimized during the change by fitting the parent and daughter phases coherently along a "habit" plane which either remains macroscopically unrotated and undisturbed (Wechsler, Lieberman, and Read 1953), or undergoes only a small dilatation (Bowles and MacKenzie 1954) during the transformation. To accomplish this, the strain responsible for the change of the lattice is generally homogeneous only over very small regions; macroscopically the adjacent segments are either separated by fine slip, or undergo different deformations with the result that the daughter phase consists of fine lamellae of twins. As, however, MnAs is extremely brittle, showing no traces of plastic deformation, and as there are no known mechanical twins occurring in the material, it might not be expected to be able to undergo a normal *martensitic* type of diffusionless transition.

We have therefore decided to study the transformation in more detail to try to find out the mechanism of the change.

EXPERIMENTAL INVESTIGATION

In the first place we have attempted to retain the high-temperature paramagnetic phase by rapid quenching, but the ferromagnetic phase was always obtained when small samples were quenched into iced water, acetone-cooled with liquid nitrogen, or liquid nitrogen. In order to guard against the possibility that the metastable phase itself becomes ferromagnetic at low temperatures, the samples were also transferred into iced water after the initial quenching and then tested immediately, but the same results were found.

A polished sample of MnAs was examined microscopically during the transformation on heating. No martensitic platelets could be seen, but instead irregular cracks appeared randomly over the surface. The time taken for a crack to form was too short to be observed visually. During the reverse transformation the cracks were observed to close up but they still remained visible. No new cracks were seen to form in further cycling through the transformation temperature. Fig. 1 shows a portion of the surface of the specimen after several transformation cycles.

The change of magnetic properties during the transformation was used to study the nature of the change within the areas bounded by the surface cracks. The sample was covered with a colloidal solution of magnetite and microscopical observations were made under dark field illumination. During the transformation on heating, the small areas bounded by the cracks individually became suddenly darker as the particles of colloid lifted from the surface when the grains became paramagnetic. These observations indicated

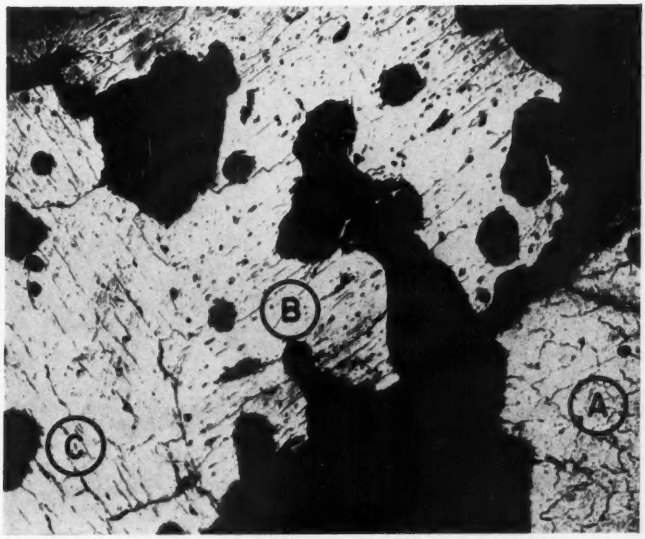

FIG. 1. Polished surface of MnAs after several transformations. Areas *A*, *B*, and *C* are the regions investigated by the back-reflection Laue technique.

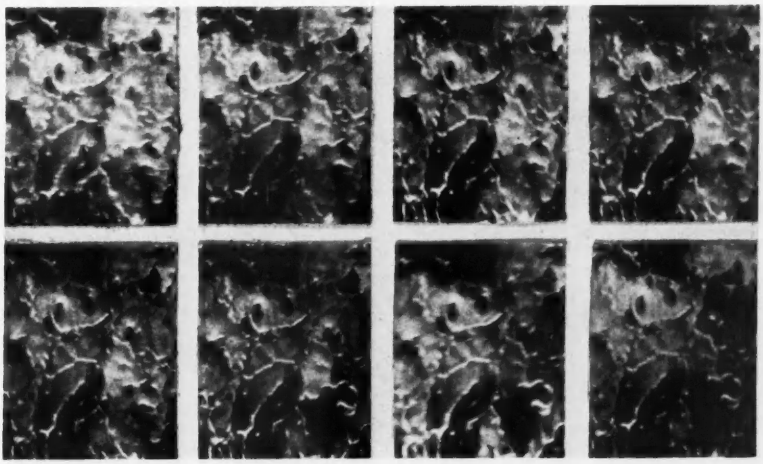

FIG. 2. Successive frames of the cine film of the transformation. Interval between the pictures 1/16 sec: ×100 approximately.

that the transformation of a grain and the opening of the cracks surrounding it were simultaneous.

As already noted, the changes also occurred sufficiently rapidly to appear instantaneous on visual observation. This was confirmed by cinematography at 48 frames per second which showed that areas had transformed completely between successive frames. The contrast on prints of these films was unfortunately not sufficiently high to allow reproduction. It was found, however, that a slight tilting of the grains occurred during the transformation and that the change could be shown under critical oblique illumination conditions (cf. Lomer and Pratt 1951–52). Fig. 2 shows the transformation proceeding on the surface of a specimen during 8 successive frames taken at 16 frames per second.

It was thus apparent that the rate of transformation of individual grains was very rapid, so making any diffusion-controlled mechanism very improbable. To check whether the possibility of a diffusion-controlled mechanism could be completely ruled out by the rate of change of single subgrains, we made further use of the change of magnetic properties to fix an upper limit on the time taken for a grain to transform. A specimen of MnAs was placed inside a coil in a magnetic field and the signals obtained during the transformation were, after amplification, observed on an oscilloscope screen. Each individual change took place in a time of about 50 microseconds, which was of the same order as the over-all resolving time of the apparatus. We can therefore place only a lower limit on the rate of transformation. It could conceivably be very much faster. However, this rate is sufficiently high to rule out completely a diffusion mechanism for the transformation.

Over most of the area of polished surfaces of samples of MnAs which had been transformed several times, the cracks formed an irregular network (e.g., see region *A*, Fig. 1). In some areas, however, they lay predominantly in one direction. An example of such an area is shown in region *B*, Fig. 1. The orientations of the areas marked *A*, *B*, *C*, in this figure, shown in the stereographic projection (Fig. 3), were determined by microbeam back-reflection Laue

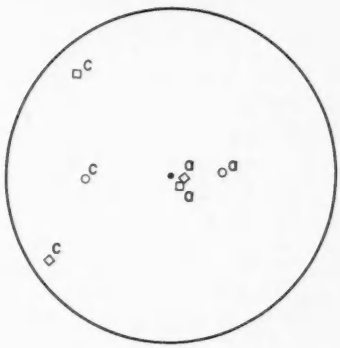

FIG. 3. Stereographic plot of the orientations of the three crystals marked *A*, *B*, and *C* in Fig. 1. ○—*A*, ◇—*B*, □—*C*.

photographs using a beam diameter of about 100 μ. In the areas B and C the c axis lay within 5° of the surface of the sample. In both cases also it was found that the direction of the c axis coincided with the directions of the cracks. The c axis of subgrains in the region A, however, was inclined at about 35° to the plane of the microsection. It would therefore appear that the cracks run parallel to the c axis in the original grains of MnAs, and the crystals fragment during the transformation into pencil-like subgrains.

This conclusion was confirmed by the microscopical observation of the transformation in regions where the subgrains were aligned with their c axis parallel to the specimen surface. In these areas the regions which transformed individually were long and narrow rather than having the irregular shape shown in Fig. 2.

The back-reflection Laue photographs generally showed asterism. This might correspond to a spread of orientations of the individual subgrains in the transformed material, since the beam diameter of about 100 μ was larger than the size of individual subgrains. For geometrical reasons such misorientations can only correspond to small rotations of the singly crystalline subgrains around the c axis. In order to test these conclusions the following observations were made from back-reflection Laue photographs.

(*a*) A specimen which was never cooled below 50° C showed perfectly sharp spots with no trace of asterism.

(*b*) After the specimen was cooled to room temperature each spot was found to have degenerated into several closely spaced spots.

(*c*) After several cycles through the transition the spots in both the high and the low temperature phases merged into continuous short (asterism) lines. In all cases the direction and amount of elongation corresponded to about 2° of rotation about the c axis. A Laue photograph taken looking down the c axis of subgrains in the area A of Fig. 1 showed almost no asterism, thus confirming this conclusion.

It is not surprising that such misorientations exist in the repeatedly transformed samples, since one could hardly expect that the pencil-like subgrains would strictly retain their original orientations under the conditions with which the transformation takes place.

DISCUSSION

The transition at ~40° C in MnAs which appears to be discontinuous, diffusionless, and non-martensitic is, as far as we are aware, unique. In so far as the expansion of the a axis of the unit cell* does not occur by the rather subtle mechanism required of a martensitic change, it might be called a "brute force transition." The change may be contrasted with those found in ferroelectrics which appear always to occur by a martensitic process.

In a martensitic transformation the strain energy is minimized by fitting the parent and daughter phases along an unrotated and undistorted habit plane, but the mechanism of the transformation also involves some plastic

*The c axis does not undergo any noticeable change during the transition. The a axis expands by about 1% on going to lower temperatures.

deformation of the product phase. We believe that MnAs does not transform by the martensitic mechanism because such plastic deformation is not possible. Instead, the strain energy of the transformation in MnAs is minimized by a fragmentation of the crystal grains into pencil-like subgrains. The expansion of the *a* axis in the transformation of MnAs produces dilatational stresses which are maximum across the planes parallel to the *c* direction. It is therefore not surprising that all of the cracks lie parallel to this direction. It is at present difficult to visualize the mechanism of transformation inside each "pencil." However, we presume that the strain produced during the transformation is absorbed elastically within each subgrain and that the boundary dividing the two phases travels along the "pencil" with a high velocity, which perhaps approaches the speed of sound.

Finally we may note that the discovery of a diffusionless non-martensitic transformation reduces *martensitic* transitions to a subclass among *diffusionless* transitions and the words should no longer be used synonymously.

ACKNOWLEDGMENT

We are grateful to Mr. Gaston Fischer for discussions and for providing the samples of manganese arsenide.

REFERENCES

BACON, G. E. and STREET, R. 1955. Nature, **175**, 518.
BATES, L. F. 1934. Phil. Mag. **17**, 783.
BOWLES, J. S. and MACKENZIE, J. K. 1954. Acta Met. **2**, 129, 138, 224.
FISCHER, G. and PEARSON, W. B. 1958. Can. J. Phys. This issue.
GUILLAUD, C. 1951. J. phys. radium, **12**, 223.
HIMMEL, L. and JACK, K. H. 1956. J. Metals, **8**, 1406.
LOMER, W. M. and PRATT, P. L. 1951–52. J. Inst. Metals, **80**, 409.
ROBERTS, B. W. 1956. Phys. Rev. **104**, 607.
WECHSLER, M. S., LIEBERMAN, D. S., and READ, T. A. 1953. J. Metals, **5**, 1503.
WILLIS, B. T. M. and ROOKSBY, H. P. 1954. Proc. Phys. Soc. (London), B **67**, 290.

FIELD-INDUCED ABSORPTION IN HYDROGEN[1]

M. F. CRAWFORD AND R. E. MACDONALD[2]

ABSTRACT

This paper reports an investigation of the fundamental rotation–vibration absorption induced in hydrogen by an electric field. The integrated absorption coefficients of the first four components of the Q branch have been measured for a range of field strengths at densities of 83.9 and 44.6 Amagat. The integrated absorption coefficient of the $S(1)$ line has been determined at the higher density for one high field strength. The relative intensities of the Q components are in good agreement with the predicted ratios. Accurate experimental values of the matrix element of the mean value of the polarizability, $(\alpha)_{01}$, and the matrix element of its anisotropy, $(\gamma)_{01}$ have been obtained. They are: $(\alpha)_{01} = 0.968\times10^{-25}$ cm^3, and $(\gamma)_{01} = 0.72\times10^{-25}$ cm^3 at 83.9 Amagat, and are only slightly dependent on density. The frequencies of the lines have been measured. Only $Q(1)$ and $S(1)$ show a measurable shift with density. The optical collision diameter has been determined and is very small, 0.26Å.

I. INTRODUCTION

The strength of an absorption line is proportional to the square of the change in the dipole moment associated with the corresponding transition. A homonuclear molecule such as hydrogen has no dipole moment and absorption corresponding to the fundamental rotation–vibration band does not occur. It is possible, however, to distort the charge distribution and the rotation–vibration lines can then be observed in absorption. This induced absorption is produced by collisions, and by the application of an external electric field as predicted by Condon (1932). The collision effect was first observed by Crawford, Welsh, and Locke (1949) and the field effect by Crawford and Dagg (1953).

The subject of this paper is the field effect and it occurs when an external electric field is applied to the molecules in the absorbing path. The electric field induces a dipole moment in the molecule, the magnitude of which is determined by the product of the polarizability and the field strength. Since the polarizability is a function of the internuclear separation and the orientation of the molecule the induced dipole will be modulated at the vibrational and rotational frequencies. Thus the rotation and rotation–vibration transitions can be observed in absorption. The amplitude of the modulated component of the dipole moment for a vibrational transition is proportional to the product of the rate of change of the polarizability with respect to the normal coordinate and to the field strength. Therefore, the selection rules are determined by the matrix elements of the polarizability, and consequently are the same as those governing the Raman effect.

The field effect is a new technique for determining molecular constants and for studying intermolecular interactions. Accurate values for the rates of

[1]Manuscript received April 2, 1958.
Contribution from the Department of Physics, University of Toronto, Toronto, Ontario.
[2]Present address: The Bell Telephone Laboratories, Murray Hill, N.J., U.S.A. Holder of Ontario Research Council Scholarships, 1954–1956.

change of the polarizability with vibrational motion and the anisotropy of the polarizability can be obtained directly from the experimentally determined line strengths. Inherent in this experiment is the possibility of readily determining these over a wide range of conditions. These so-called molecular constants are of considerable theoretical significance. For hydrogen many calculations of the polarizability and its rates of change are available. Intercomparison of the theoretical and experimental values is a means of assessing the adequacy of the wave functions used. Further, accurate values of the rates of change are desired for other problems, in particular for the theoretical calculation of the collision-induced absorption (van Kranendonk and Bird 1952). An optical collision diameter can also be evaluated from the integrated absorption coefficient and the integrated absorption, and is a function of the forces between molecules.

II. THEORY

The integrated absorption coefficient, B', for light with its electric vector in the direction ϵ relative to the direction of the applied field can be written

$$B' = \frac{8\pi^3 \nu N l}{hc} \left| \int \psi_n^* P_\epsilon \psi_{n'} \, d\tau \right|^2, \tag{1}$$

where

P_ϵ = $\alpha_\epsilon E_\epsilon$ = the component of the induced dipole moment in the direction of the light vector;
E_ϵ = the component of the applied electric field in the direction of the light vector;
α_ϵ = the polarizability of the molecule in the direction of the light vector;
n, n' = the totality of quantum numbers required to define the initial and the final state;
l = path length;
h = Planck's constant;
c = velocity of light;
ν = frequency of the transition (where ν can be expressed in cm^{-1} or sec^{-1}, and B' has the corresponding unit);
N = number of molecules per unit volume in the initial state.

Equation (1) was formulated by Condon (1932), but the matrix elements of the induced dipole moment of the transition for hydrogen were not explicitly evaluated.

The dipole moment, $P = \alpha E$, is a tensor relation. For a linear molecule the polarizability, α, can be expressed in terms of the polarizability parallel to the internuclear axis, $\alpha_\parallel$, and the polarizability perpendicular to the internuclear axis, $\alpha_\perp$. Thus the dipole moment can be written,

$$\begin{aligned} P_\parallel &= \alpha_\parallel E_\parallel, \\ P_\perp &= \alpha_\perp E_\perp. \end{aligned} \tag{2}$$

Fig. 1 shows a molecule in the orientation θ, ϕ, in the co-ordinate system in which the x axis is the direction of the applied field and the z axis the direc-

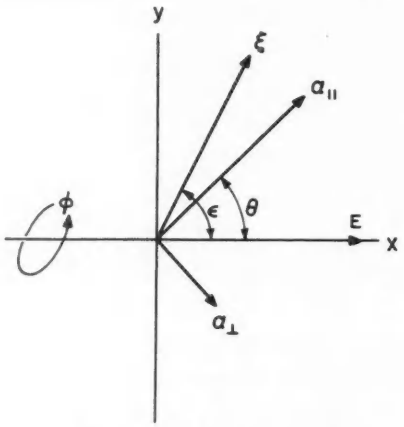

FIG. 1. Molecular co-ordinates.

tion of propagation of the radiation. The components of the dipole moment in the x and y directions are,

$$(3)\qquad \begin{aligned} P_x &= P_\parallel \cos\theta + P_\perp \sin\theta = E(\alpha_\parallel \cos^2\theta + \alpha_\perp \sin^2\theta), \\ P_y &= P_\parallel \sin\theta\cos\phi - P_\perp \cos\theta\cos\phi = E(\alpha_\parallel - \alpha_\perp)\sin\theta\cos\theta\cos\phi. \end{aligned}$$

From equations (3) and the wave function of the vibrating rotator the matrix elements in equation (1) for the ($v' = 1$, $v = 0$) vibrational transition can be written,

$$(4)\qquad \begin{aligned} \int \psi^*_{0Jm} P_\epsilon \psi_{1J'm'}\, d\tau = E\cos\epsilon \Big[&(\alpha_\parallel)_{01} \int Y^*_{(Jm)} \cos^2\theta\, Y_{(J'm')} \sin\theta\, d\theta\, d\phi \\ &+ (\alpha_\perp)_{01} \int Y^*_{(Jm)} \sin^2\theta\, Y_{(J'm')} \sin\theta\, d\theta\, d\phi \Big] \\ &+ E\sin\epsilon(\gamma)_{01} \int Y^*_{(Jm)} \cos\theta\cos\phi\sin\theta\, Y_{(J'm')} \sin\theta\, d\theta\, d\phi, \end{aligned}$$

where

$(\alpha_\parallel)_{01} = \int \psi_0^*\, \alpha_\parallel\, \psi_1\, d\tau_v$;
$(\alpha_\perp)_{01} = \int \psi_0^*\, \alpha_\perp\, \psi_1\, d\tau_v$;
$(\gamma)_{01} = (\alpha_\parallel)_{01} - (\alpha_\perp)_{01}$;
$Y_{(Jm)}$ = the normalized spherical harmonic eigenfunctions.

Values of the matrix elements of the Q branch ($\Delta J = 0$) and the S branch ($\Delta J = +2$) for plane polarized radiation with its electric vector parallel to the applied field, $\epsilon = 0$, are listed in Table I. Table I shows that $(\gamma)_{01}$, the matrix element of the anisotropy of the polarizability, is entirely responsible

for the absorption in the S branch and contributes to the absorption in all components of the Q branch except $Q(0)$.

TABLE I

SQUARES OF THE MATRIX ELEMENTS OF THE INDUCED MOMENTS

Transition ($v' = 1$, $v = 0$)

$J' \leftarrow J$	The sum over m and m' of the squares of the induced moments
	Q components
$0 \leftarrow 0$	$E^2(\alpha)_{01}^2$
$1 \leftarrow 1$	$E^2[3(\alpha)_{01}^2+(8/75)(\gamma)_{01}^2]$
$2 \leftarrow 2$	$E^2[5(\alpha)_{01}^2+(8/63)(\gamma)_{01}^2]$
$3 \leftarrow 3$	$E^2[7(\alpha)_{01}^2+(8/45)(\gamma)_{01}^2]$
	S components
$2 \leftarrow 0$	$E^2(\gamma)_{01}^2\times 4/45$
$3 \leftarrow 1$	$E^2(\gamma)_{01}^2\times 80/525$

The integrated absorption coefficient B', equation (1), is proportional to the number of absorbers in the initial level and to the square of the matrix element of the induced moment. Under the condition of thermal equilibrium the relative number of absorbers in the initial level is given by the product of the Boltzmann distribution factor $e^{-BJ(J+1)/kT}$ and the weighting factors introduced by the nuclear statistics and the degeneracy of the rotational levels. For hydrogen the odd rotational levels are weighted 3:1 relative to the even levels. Since the experimental results show that $(\gamma)_{01}^2$ is about one half of $(\alpha)_{01}^2$ its contributions to the squares of the induced moments of the Q branch are negligible. This means that the relative intensity of a Q component is proportional to the Boltzmann factor for its initial level times the $(2J+1)$ degeneracy of the rotational state times the nuclear weighting factor. These calculated intensities are listed in the last column of Table III.

III. EXPERIMENTAL

In the field effect the observable quantity is an absorption contour. The apparatus required for the measurement of this quantity consists of a source of infrared radiation, an absorption cell, a means of applying and accurately measuring the electric fields, and a high resolution spectrometer.

(a) *Optical System*

Radiation from a 750-watt projection bulb, operated from a Sorenson line regulator, traverses a monochromating system and a small band pass in the region of 2.4 μ is defined by the entrance aperture of the absorption cell. The absorption cell contains a parallel plate condenser which also serves as a light guide. The hydrogen obtained from commercial cylinders is admitted to the pressure cell through a needle valve and brass block. The pressure is read from a Bourden type gauge calibrated against a dead weight tester.

The dipole moment induced in a hydrogen molecule has its major component in the direction of the applied field. An accurate evaluation of the

absorption coefficient therefore requires a determination of the degree of polarization of the radiation. This is effected by introducing a Wollaston double image prism between the exit aperture of the pressure cell and the entrance slit of the spectrometer. This prism gives an angular separation of about 0.04 rad between the two images of the exit aperture polarized in perpendicular directions. One image or the other is focussed on the entrance slit of the spectrometer by a condensing lens.

The Littrow type spectrometer has a plane grating as the dispersing element. The grating, obtained from Bausch and Lomb, has 300 lines per mm, a blaze angle of 26° 45′, and a ruled area 204 mm wide and 130 mm high. The autocollimating mirror is a 13° off-axis paraboloid, 8 cm diameter, 100 cm focal length. The limiting aperture is set by the collimator.

For several reasons the signal intensity available at the detector is relatively low. The small half-widths of the observed transitions, of the order of 0.13 cm^{-1}, impose a restriction on the spectral slit widths that can be used if a reasonable peak absorption is to be recorded, and the signal at the detector is proportional to the product of the entrance and exit slit widths of the spectrometer. The available signal is further limited by the presence of the collision-induced absorption which is proportional to the square of the density, by the low efficiency of the light guide, and by the fact that the radiation is restricted to one plane of polarization. Accordingly, stringent requirements are placed on the electronic amplifying system.

(*b*) *Detector and Amplifying System*

A lead sulphide photoconductive cell is the detector. This cell has a sensitive area $\frac{1}{8}$ in. $\times \frac{3}{8}$ in. and a resistance of 0.6 meg at room temperature. When the cell is cooled with a mixture of dry ice and acetone the resistance reaches a terminal value of 20 meg in one half hour.

The block diagram, Fig. 2, portrays the main components of the amplifying system. Radiation incident on the detector is periodically interrupted by a

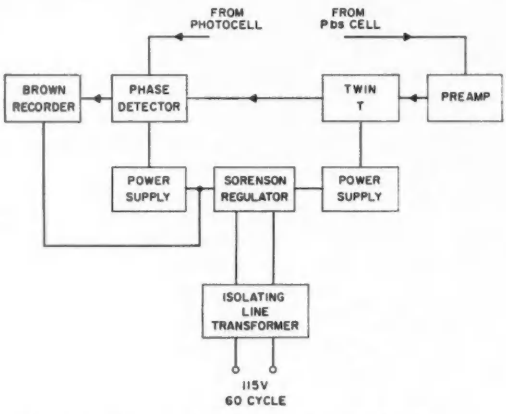

FIG. 2. Block diagram of the amplifying system.

mechanical chopper placed at the entrance slit of the spectrometer and the chopping frequency is 150 cycles/sec. A signal generated at the detector is applied in succession to a preamplifier, a twin T amplifier, and a phase detector. A reference signal from a photocell circuit, chopped at the same frequency as the wanted signal, is applied to the suppressor grids of the push–pull stage in the phase detector and ensures that out-of-phase noise voltages are rejected. The unidirectional output from the phase detector is filtered and the d-c. signal displayed on a 50-millivolt Brown "Elecktronik" recorder. The amplifying system with a gain of 50,000 gives a full scale deflection for the Johnson noise of the input resistance. The twin T band pass filter, tuned to 150 cycles/sec, is adjusted to a band width of approximately five cycles/sec to prevent overloading the phase detector with noise. The phase detector gives an effective band width variable from $\frac{1}{2}$ to $\frac{1}{6}$ cycle/sec and this is independent of variations in the chopping frequency. The electronically regulated power supplies are fed from a Sorenson line regulator which is powered by an isolating line transformer. The isolating line transformer is required because in this laboratory the 60 cycle a-c. neutral line is a very poor ground. The PbS cell when cooled is operated with a polarizing voltage of 30 v supplied by a shielded B battery.

(*c*) *Measurement of the Field*

The absorption cell is that used previously in the investigations of the collision-induced absorption (Crawford, Welsh, and Locke 1949). To establish the electric field within the absorption cell a source of high voltage is applied through a spark plug to one side of a parallel plate condenser. The other plate of the condenser is contacted through a spring clip to the steel wall of the pressure cell which is grounded externally to a water pipe.

The parallel plate condenser consists of two plane strips of glass 82.4 cm long, 1.2 cm wide, 0.3 cm thick, coated with silver and mounted in two Lucite spacers as shown in Fig. 3. The grooves in each spacer were milled simultaneously with two cutters, and are slightly wider than the thickness of the glass plates. The plates are held in the grooves by set screws bearing against

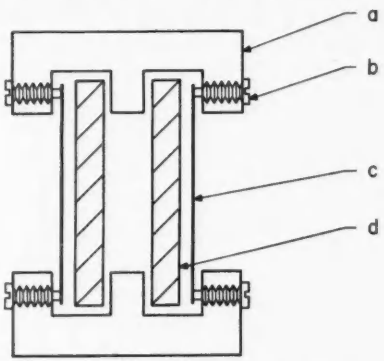

FIG. 3. Cross section of the condenser.

strips of brass shim stock inserted between the outer surfaces of the plates and the outer walls of the grooves. The plates were aligned by adjusting the set screws and their parallelism checked by measuring their separation with a travelling microscope at many positions along the top and bottom of the assembled unit. The mean deviation of the separation did not exceed 0.01 mm. The condenser with its highly reflecting plate also functions as a light guide.

Since the absorption coefficient is proportional to the square of the electric field strength, the field must be maintained constant and its strength measured accurately. The field was produced by a power supply obtained from Neutronic Associates. It is regulated to 0.1% and its output can be varied continuously in the range 5–30 kilovolts. The potential difference between the condenser plates was determined by connecting in parallel with the plates a voltage divider consisting of 14.99 ± 0.02 meg resistor in series with a 1000-ohm standard and measuring the voltage across the standard with a potentiometer.

(*d*) *Measurement of Integrated Absorption Coefficients*

For the field effect we define a nominal absorption coefficient $k(\nu)$ by the relation

$$I(\nu) = I_0(\nu)e^{-k(\nu)l}, \tag{5}$$

where

$I_0(\nu)$ = the signal in the absence of the electric field;
$I(\nu)$ = the signal when the field is applied;
l = the path length;
$I/I_0 = T(\nu)$ = the transmission.

The absorption is defined as

$$A = \int_{-\infty}^{\infty} (1 - T(\nu))d\nu. \tag{6}$$

The distribution of $I_0(\nu)$ with frequency is a function of the collision-induced absorption, the spectral distribution of the radiation source, and the response of the spectrometer. In Fig. 4 the dotted line represents the distribution of $I_0(\nu)$ over part of the hydrogen fundamental region. The dip in the absorption contour at 4155 cm^{-1} divides the Q branch of the collision-induced absorption into two parts and each has a half-width of $\sim$250 cm^{-1}. With the application of the electric field four lines appear which are not present in the zero field trace. These lines, labelled $Q(0)$, $Q(1)$, $Q(2)$, $Q(3)$, are components of the Q branch, $\Delta J = 0$, of the fundamental vibrational transition ($v' = 1 \leftarrow v = 0$); the initial value of J is designated by the number in parentheses. The field effect lines are exceedingly sharp and have a half-width which is mainly instrumental even at a pressure of 1500 p.s.i. By evaluating $\int k(\nu)ld\nu = \int \log_e(I_0/I)d\nu$ over the absorption contour of a line the nominal integrated absorption coefficient, B, is obtained. This nominal integrated absorption coefficient in general differs from the integrated absorption coefficient, B', unless the resolving limit of the spectrometer is appreciably less than the half-width of the transition probability. However, it will be shown that B' can be obtained from B.

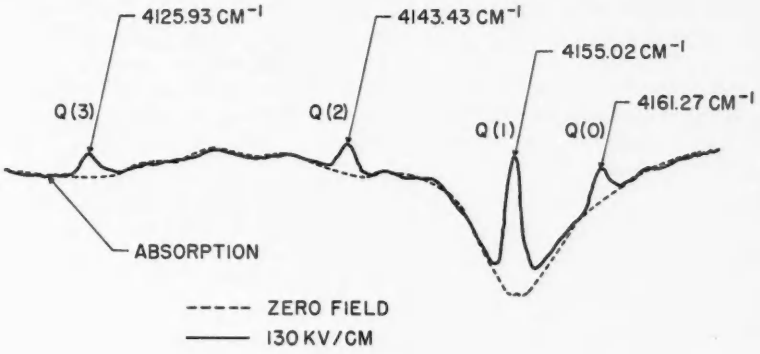

FIG. 4. The Q components of the fundamental vibrational band.

B was determined from a point-by-point scan of the absorption contour. The grating was set at a fixed angle in the vicinity of the absorption; the field was turned on and off several times to ensure a good average value for $\log_e(I_0/I)$. The grating was then rotated through a small angle and the procedure repeated. The total angle through which the grating turned in traversing a line was about 5×10^{-4} rad. Consequently, the angular separation between adjacent settings of the grating had to be measured to within 10^{-6} rad to obtain a precision of a few per cent in the integrated absorption coefficient. The driving mechanism of the grating did not permit a determination of the angular change with this precision.

The required precision was obtained by an interferometric method. The interferometer consists of two flats and one face of each is coated with a dielectric film of high reflectivity in the green region of the spectrum. One of the flats is mounted so that it moves with the grating while the other remains stationary. With a small separation between the coated surfaces, narrow localized fringes are visible when the interferometer is illuminated with collimated monochromatic light. The angular separation between adjacent settings of the grating was determined from the number of fringes that crossed a fiducial mark on one of the plates during the rotation of grating from one setting to the next. The angular change is given by (8), which is derived from

$$N\lambda = 2t\cos(r\pm\theta), \qquad \Delta t = d.\Delta\theta, \tag{7}$$

where

N = order of interference;
λ = wavelength;

t = separation between the inner faces of the flats at the fiducial mark;
r = angle of refraction measured at the air space between the two flats;
θ = angle between the inner faces of the flats;
$\Delta\theta$ = change in θ due to rotation of grating;
d = distance from the axis of rotation of the grating to the fiducial mark.

The angles r and θ were adjusted to approximately zero. For this condition a small change in θ due to rotation of the grating changed t, but had negligible effect on the cosine term. Therefore

$$\Delta\theta = \lambda.\Delta N/2d, \tag{8}$$

where ΔN is the number of fringes that crossed the fiducial mark. Angular rotations of 2×10^{-5} rad were measured by this method to within 2×10^{-7} rad.

IV. RESULTS

As shown by the discussions of Dennison (1928), Nielsen, Thornton, and Dale (1944), and by Kostkowski and Bass (1956) the nominal integrated absorption coefficient and the integrated coefficient are in general unequal but related. The relation involves the half-width of the transition probability under the experimental conditions, the resolution of the spectrometer, and the peak absorption. Under two conditions the nominal integrated absorption coefficient equals the integrated absorption coefficient. These are: (1) when the instrumental half-width is small compared to the half-width of the transition probability, (2) when the absorption is small enough so that only the linear term in the expansion of the exponential is required. Since the experimental conditions were not compatible with (1), the integrated absorption coefficients were obtained under condition (2) by extrapolating the nominal coefficients to small absorption.

(a) *Nominal Integrated Absorption Coefficients—Q Components*

The nominal integrated absorption coefficients were determined under various experimental conditions using plane polarized light and $\epsilon = 0$. Values of B for four field strengths are recorded in Table II for the $(1 \leftarrow 1)$ component

TABLE II

NOMINAL INTEGRATED ABSORPTION COEFFICIENTS—$Q(1)$ COMPONENT

Transition $(v' = 1, v = 0)$

$E^2\times10^{-4}$(e.s.u./cm)^2	B, cm^{-1} (measured)	$B/E^2\times10^7$, cm^{-1}/(e.s.u./cm)^2	B, cm.$^{-1}$ (calculated eq. (10))
6.35[a]	.271	42.7	.273
4.77	.229	47.8	.227
2.82	.151	53.6	.150
1.81	.102	56.5	.101

For *a*: absorption, $A = 0.248$ cm^{-1}; minimum transmission, $T_{min} = 62\%$.
Conditions: 1.98 mm spacer; density 83.9 Amagat; 27° C; 82.4 cm path length; 0.46 cm^{-1} slit width.

of the Q branch. Representative contours from which these nominal absorption coefficients were evaluated are shown in Fig. 5. Each B value is an average of at least two traces and each point on a contour, Fig. 5, is itself an average of a minimum of three measurements of $\log_e(I_0/I)$. An average deviation of about 1% for the smaller coefficients is a realistic measure of their precision.

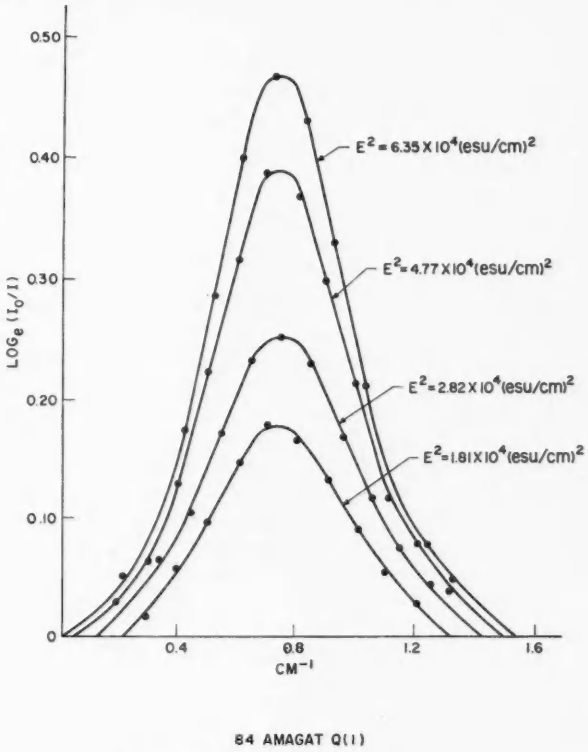

FIG. 5. Contours of the $Q(1)$ components.

Theoretically the integrated absorption coefficient, B', is proportional to the square of the field strength. It is evident from column 3 of Table II that the nominal integrated absorption coefficient departs progressively with increasing field strength from the predicted constant relationship. In Fig. 6 a plot of B vs. E^2 illustrates this deviation from linearity. It is anticipated from condition (2) that when the resolving limit is larger than the transition half-width of the component the departure from linearity will be a function of the integrated absorption coefficient. Therefore B can be represented by a power series in E^2,

$$B = a_0E^2+a_1E^4. \tag{9}$$

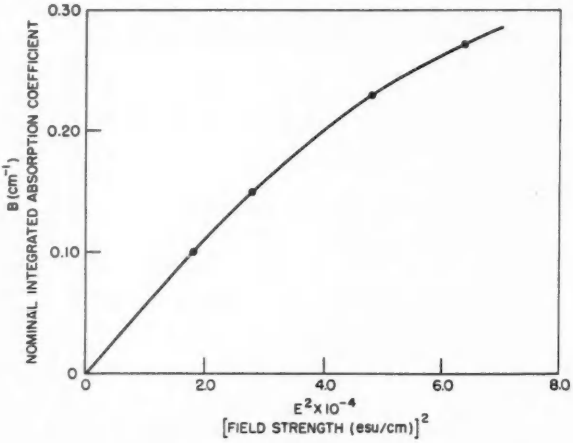

FIG. 6. Nominal absorption coefficient vs. field strength squared.

Because of the small deviations associated with the experimental results graphical methods are adequate to determine the constants. Fig. 7 is a plot of B/E^2 vs. E^2. This linear relation gives

$$a_0 = 61.5\times10^{-7}\ \text{cm}^{-1}/(\text{e.s.u./cm})^2, \tag{10}$$
$$a_1 = -2.85\times10^{-11}\ \text{cm}^{-1}/(\text{e.s.u./cm})^4.$$

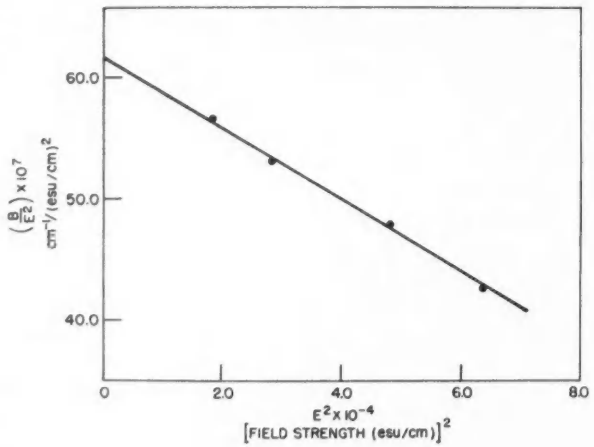

FIG. 7. B/E^2 vs. E^2.

Substitution of these values of a_0 and a_1 in equation (9) yields column 4 of Table II. Thus for the experimental conditions noted in Table II, the depen-

dence of the nominal integrated absorption coefficient on the field strength is well represented by the equation

$$B = 61.5\times10^{-7}\,E^2-2.85\times10^{-11}E^4. \tag{11}$$

The coefficient of the first term on the right hand side of equation (11) is the value of B', the integrated absorption coefficient, per unit field strength squared.

To appraise the accuracy of a_0, the slit width and the separation of the plates of the condenser were varied. The spectral slit width was increased from 0.46 to 0.86 cm^{-1} and the plate separation decreased from 1.98 to 1.37 mm. It was somewhat surprising to observe that with the application of the electric field an absorption was detected over the whole of the spectral range transmitted by the monochromator (0.2 μ). Further tests showed that the effect persisted and with about the same magnitude (6% absorption for 15 kilovolts), even beyond the region of the collision-induced absorption. This anomalous absorption was evident in nitrogen to about the same degree as in hydrogen and was just detectable in the case of helium gas. Returning to hydrogen, the dependence of the anomalous absorption on the field strength was found to be linear. With the Wollaston prism set to select only the component of the radiation with the electric vector perpendicular to the applied field, the absorption recorded was only about one third that of the parallel component for the same experimental conditions. The effect was not detectable when the larger spacer, 1.98 mm, was used, even though an equal field was applied. It appears that the field slightly decreases the reflectivity of the silvered condenser plates. A slight decrease in reflectivity has a greater effect on the signal when the narrower spacer and wider slit are used because a larger portion of the signal is then due to radiation multiply reflected in the light guide.

By measuring the absorption well outside the region of the $Q(1)$ line and applying this as a constant correction to the absorption recorded in the region of the $Q(1)$ line, the result obtained was

$$a_0 = 60.0\times10^{-7}\ cm^{-1}/(e.s.u./cm)^2. \tag{12}$$

The agreement between the values of a_0 in (10) and (12) is very good. There appears to be little evidence for a systematic error in the results associated with the slit width or the condenser plate separation.

Another value of a_0 was obtained from a series of measurements with the 1.98 mm spacer and the grating in a different geometrical arrangement. The value of a_0 obtained was 61.0×10^{-7} $cm^{-1}/(e.s.u./cm)^2$.

The nominal integrated absorption coefficient of the $Q(0)$ component was measured at two field strengths and that of the $Q(2)$ and of the $Q(3)$ at only one high field strength. Since the absorption in these components is small it was not necessary to make extensive measurements at a number of field strengths as required for the $Q(1)$ component. From the nominal integrated absorption coefficients of these three components their integrated absorption coefficients can be obtained by using the ratio of the coefficients of the powers

of E as determined in the analysis of the data for the $Q(1)$ component. Equation (9) can be rewritten

$$B = a_0E^2+(a_1/a_0^2)(a_0E^2)^2. \tag{13}$$

Since the absorption is small the second term on the right hand side of equation (13) is small and a_0E^2 can be approximated by B, giving

$$B = a_0E^2+(a_1/a_0^2)B^2, \tag{14}$$

where the ratio a_1/a_0^2 is obtained from the analysis of the $Q(1)$ data (10).

The adequacy of equation (14) was tested and proven by applying it to the nominal integrated absorption coefficients of the $Q(0)$ component obtained at the two field strengths. It was also used to determine the value of a_0 for the other two components.

The average value of a_0 with its average deviation for each of the four components of the Q branch is listed in Table III, column 2. The ratios of these experimental values are given in column 3 and the ratios of the theoretical values in column 4. The good agreement between columns 4 and 5 shows that the experimental measurements and their analysis give accurate values of the integrated absorption coefficients.

TABLE III

INTEGRATED ABSORPTION COEFFICIENTS—Q COMPONENTS

Transition ($v' = 1, v = 0$)

(83.9 Amagat; 27° C; 82.4 cm path)

		Ratio	
$J' \leftarrow J$	$a_0\times10^7$ cm^{-1}/(e.s.u./cm)^2	Experimental	Theoretical
$0 \leftarrow 0$	12.0 ±0.2	1.000	1.000
$1 \leftarrow 1$	61.0 ±0.3	5.08	5.11
$2 \leftarrow 2$	11.1 ±0.3	0.925	0.915
$3 \leftarrow 3$	8.15±0.2	0.679	0.705

(*b*) *Dependence of the Absorption Coefficient on Density*

B of the $Q(1)$ component was measured at a lower density, 44.6 Amagat, and its dependence on field strength was found to be

$$B = 31.3\times10^{-7}\,E^2-0.984\times10^{-11}\,E^4. \tag{15}$$

From equation (15) a_0 equals 31.3×10^{-7} cm^{-1}/(e.s.u./cm)^2. The ratio of a_0 to the density at a density of 44.6 Amagat is 0.702; at a density of 83.9 Amagat (Table III) the ratio is 0.727. This 4% difference in the ratios indicates that the rate of change of the polarizability increases slightly with increasing density. In view of the accuracy of the experiments, it is highly probable that this increase with density is real. It is qualitatively consistent with the observations of MacNaughton (1948) on the variation of Raman scattering per molecule with the density of the scattering medium, but the magnitude of the effect in hydrogen is too small relative to the experimental precision to warrant quantitative deductions.

A small correction should be applied to a_0 because the local fields at the absorbing molecule are slightly different than the static and radiation fields. This correction for hydrogen, neglecting fluctuations, reduces a_0 by less than 2% for the higher and 1% for the lower density (van Kranendonk 1957).

(*c*) *Anisotropic Absorption—S(1) Component*

The matrix element of the anisotropy of the polarizability, $(\gamma)_{01}$, can be determined more accurately from the S branch than from the Q branch. The contribution of $(\gamma)_{01}$ to the absorption is quite small in both branches, but it is the sole contributor in the S branch for any polarization. Most favorable measurements can be made on the $S(1)$ component because at room temperature it is the strongest. The absorption was first detected using a high field strength obtained with a small plate separation. Because the anomalous absorption observed with a small plate separation introduces a correction of the same order as the absorption due to $(\gamma)_{01}$, better accuracy was obtained with a large plate separation even though the absorption was smaller.

The absorption was measured with the light vector parallel to the applied field and six determinations of the integrated absorption coefficient were made at high field strengths. Since the peak absorption was only $2\frac{1}{2}$% the nominal integrated absorption coefficient equals the absorption coefficient. For a density of 83.9 Amagat, a path length of 82.4 cm, and a plate separation of 1.98 mm, the value obtained is

$$a_0 = 1.89 \pm 0.11 \times 10^{-7} \text{ cm}^{-1}/(\text{e.s.u./cm})^2. \tag{16}$$

(*d*) *Frequencies of the Absorption Lines*

The measurements by Crawford and Dagg (1953) on the components of the Q branch indicated a frequency shift, the magnitude of which was dependent upon the J value involved in the transition and the density. More accurate measurements of the frequencies were made in this investigation to test the dependence indicated by their preliminary results.

The components of the Q branch were measured by superposing an argon emission spectrum on the absorption spectrum and recording both on the same trace. Seven argon lines conveniently bracket the second order of the Q components and are suitable as secondary standards (Plyler, Blaine, and Tidwell 1955). The maximum separation between adjacent standards is 150Å in $N\lambda$ and interpolation within this interval is precise. The value of the refractive index required for converting wavelength to frequency was obtained from the formula proposed by Edlén (1953). The frequency of each Q component was determined from six scans and had an average deviation of 0.05 cm^{-1} and a maximum deviation of 0.1 cm^{-1}. Measurements were made at densities of 83.9 and 44.6 Amagat for the Q lines. The frequency of the $S(1)$ line was measured relative to neon standards, but the small absorption permitted measurements at the higher density only.

The results of our frequency determinations and the recent low density Raman effect measurements of Stoicheff (1957) are contained in Table IV.

Both the present static field and Raman frequencies quoted in Table IV

TABLE IV

COMPARISON OF FIELD EFFECT AND RAMAN EFFECT FREQUENCIES

Transition ($v' = 1, v = 0$)

(units cm^{-1})

Component $J' \leftarrow J$	Field effect		Raman effect[a]
	83.9 Amagat	44.6 Amagat	1.5 Amagat
$0 \leftarrow 0$	4161.20	4161.21	4161.13
$1 \leftarrow 1$	4155.02	4155.13	4155.20
$2 \leftarrow 2$	4143.43	4143.44	4143.39
$3 \leftarrow 3$	4125.93	4125.90	4125.83
$3 \leftarrow 1$	4712.80		4712.86 4713.08[b] 4713.01[c]

[a]Stoicheff (1957).
[b]Cumming (1952).
[c]Feldman (1955).

are accurate to 0.05 cm^{-1}. Intercomparison of the measured frequencies indicates a small, density-dependent shift of the $Q(1)$ component to lower frequency. The dependence of the shift on density is linear within the limits of error. The frequencies of the other three components of the Q branch are all greater than the corresponding Raman frequencies, but the shifts are less than the experimental errors and are not density-dependent. Only the $S(1)$ component of the S branch was measured in the static field experiment. A measured value of the frequency of the $S(1)$ component is not contained in the paper by Stoicheff, but from the listed molecular constants a value can be calculated. The frequency of this line has been measured in the Raman effect of the gas at low density by Cumming (1952) and by Feldman (1955). Their values are 4713.08 and 4713.01 cm^{-1}, respectively. Comparison of the three Raman effect values and the field effect value listed in Table IV shows that the $S(1)$ line at a density of 83.9 Amagat is shifted in the same direction as the $Q(1)$ component and by about the same amount. Thus the static field results establish that only the $Q(1)$ and $S(1)$ components show a density dependent frequency shift and even for these components it is very small.

Raman effect measurements in the gas at high density are not available for comparison, but Raman results for liquid and solid hydrogen (Allin, Feldman, and Welsh 1956) with an ortho/para ratio equal to the equilibrium ratio at room temperature show for the $Q(1)$ line a shift of about 11 cm^{-1} and in the same direction as that recorded for the gas in the field effect. But the shift is not linear with density up to the density of the liquid.

V. INTERPRETATION

(*a*) *Matrix Elements of the Polarizability*

The anisotropic and isotropic parts of the matrix elements of the polarizability can now be determined from the experimental data. Inserting the squares of the matrix elements listed in Table I and the appropriate values of a_0, equation (1) becomes for the $S(1)$ component

$$B/E^2 = \frac{8\pi^3\nu Nl}{hc}\frac{80(\gamma)_{01}^2}{525} = a_0 = 1.89\times10^{-7}\,\text{cm}^{-1}/(\text{e.s.u./cm})^2;$$

and for the $Q(1)$ component

$$B/E^2 = \frac{8\pi^3\nu Nl}{hc}\left[3(\alpha)_{01}^2+\frac{8}{75}(\gamma)_{01}^2\right] = a_0 = 61.0\times10^{-7}\,\text{cm}^{-1}/(\text{e.s.u./cm})^2,$$

where

N $= 49.7\times10^{19}/\text{cm}^3$,
l $= 82.4$ cm,
$\nu(S(1))$ $= 4713$ cm^{-1},
$\nu(Q(1))$ $= 4155$ cm^{-1}.

From these equations

$$(\gamma)_{01} = (0.72\pm.02)\times10^{-25}\,\text{cm}^3,$$

and

$$(\alpha)_{01} = (0.968\pm.01)\times10^{-25}\,\text{cm}^3.$$

These values are for the gas at a density of 84 Amagat. The density dependence discussed in Section IV(b) indicates that at zero density $(\alpha)_{01}$ is smaller, but by less than 2%.

The results of at least eight theoretical calculations are available for comparison with the experimental values of $(\alpha)_{01}$ and $(\gamma)_{01}$ and are summarized in a paper by Ishiguro, Arai, Kotani, and Mizushima (1952). Since their calculations are the most elaborate and take into consideration both the electrical and the mechanical anharmonicities our results are compared with their predictions in Table V. The experimental values of $(\alpha)_{01}$ and $(\gamma)_{01}$ are appreciably lower (30%) than the theoretical predictions although the theoretical and experimental ratios of $(\alpha_\parallel)_{01}/(\alpha_\perp)_{01}$ are in much better agreement. An accurate calculation of second order molecular constants such as the rates of change of the polarizability places stringent requirements on the theory, and the comparison in Table V shows that even for hydrogen the best calculation to date is not very satisfactory.

TABLE V

EXPERIMENTAL AND THEORETICAL VALUES OF THE MATRIX ELEMENTS
Transition ($v' = 1$, $v = 0$)

	Field effect	Theoretical[a]
$(\alpha)_{01}$	0.968×10^{-25} cm^3	1.39×10^{-25} cm^3
$(\gamma)_{01}$	0.719	0.901
$(\alpha_\parallel)_{01}$	1.45	1.99
$(\alpha_\perp)_{01}$	0.73	1.09
$(\alpha_\parallel)_{01}/(\alpha_\perp)_{01}$	1.99	1.83

[a]Ishiguro, Arai, Kotani, Mizushima (1952).

Our value of $(\alpha)_{01}$ can also be compared with the preliminary value reported by Crawford and Dagg (1953), and with the value obtained from the measure-

ments of the intensity ratio of Rayleigh to Raman scattering (Stansbury, Crawford, and Welsh 1953). The preliminary value is appreciably higher, $1.2(5)\times10^{-25}$ cm^3; the difference is due mainly to the inaccuracy of the method used in the earlier experiment to measure small angular rotations of the grating. The value of $(\alpha)_{01}$ derived from the intensity ratio experiment is 1.1×10^{-25} cm^3 compared to 0.968×10^{-25} cm^3. This agreement is satisfactory in view of the much larger error quoted for the scattering experiments.

(*b*) *Optical Collision Diameter*

The absorption lines of hydrogen even at 1435 p.s.i. are very narrow, symmetrical, and not shifted appreciably. The interaction between molecules is small and one is justified in applying the classical theory of impact broadening to derive an optical collision diameter. The following treatment is based on the paper by Dennison (1928).

With the transmission defined by

$$T_\nu = e^{-k_\nu l}, \tag{17}$$

Dennison shows that for a spectrometer of infinite resolution

$$k_\nu l = \frac{1.353\, B'N\sigma^2/\pi(\pi\beta m)^{1/2}}{(7.60N^2\sigma^4/4\pi\beta m)+(\nu-\nu_0)^2} = \frac{a^2}{b^2+x^2}, \tag{18}$$

where

σ = the optical collision diameter;
m = the mass of the molecule;
$\beta = 1/kT$;
B' = the integrated absorption coefficient;
N = the number of molecules per cm^3.

For a spectrometer of finite resolution the area under the absorption curve is

$$A = \int_{-\infty}^{\infty}(1-T\nu)d\nu, \tag{19}$$

independent of slit width. Using equations (17), (18), equation (19) can be written

$$A = \int_{-\infty}^{\infty}(1-e^{-a^2/(b^2+x^2)})dx. \tag{20}$$

σ is readily obtained by substituting the experimental values of B' and A in an expanded form of (20). For the higher density, $B' = a_0E^2 = 61.0\times6.35\times10^{-3} = 0.387$ cm^{-1}, $A = 0.248$ cm^{-1}, $T_{\min} = 62\%$ (Tables II, III), and $\sigma = 0.24\times10^{-8}$ cm. For the lower density (Section IV*b*), $B' = 31.3\times6.35\times10^{-3} = 0.199$ cm^{-1}, $A = 0.145$ cm^{-1}, $T_{\min} = 76\%$, and $\sigma = 0.27\times10^{-8}$ cm. This agreement is satisfactory, and 0.26×10^{-8} cm is taken as the optical collision diameter.

The value of σ can be checked by calculating minimum transmissions, $T_{\min}$, and comparing these with the measured values. When the resolving

limit of the grating is appreciably smaller than the spectral slit width a triangular distribution function is a good representation of the instrumental intensity distribution. For this condition

$$T_{\min} = \frac{2}{w^2}\int_0^w (w-x)e^{-k_\nu l}dx, \tag{21}$$

where

$x = (\nu-\nu_0)$;
ν_0 = frequency at the center of the line;
w = spectral slit width.

Using $\sigma = 0.26\times10^{-8}$ cm, values of $T_{\min}$ were calculated for a sequence of values of w. The slit widths 0.43 cm^{-1} and 0.40 cm^{-1} give transmissions in agreement with the measured values for the higher and lower densities, respectively. The spectral slit width determined from the measured widths of the entrance and exit slits was 0.46 cm^{-1}. The difference is the order of the error in the direct measurement of the slit width. Thus the observed contours give a consistent value of the optical collision diameter. For the experimental conditions listed in Table II the transition half-width obtained from equation (18) by substituting $\sigma = 0.26\times10^{-8}$ cm is

$$\Delta\nu_{1/2} = 2\left[\frac{7.60N^2\sigma^4}{4\pi\beta m}\right]^{1/2} = 0.13\ \text{cm}^{-1}.$$

The small value of the collision diameter, which is about one third the internuclear separation, is qualitatively consistent with the interaction energy between two hydrogen molecules and shows that only S-type scattering is effective in producing broadening.

REFERENCES

ALLIN, E. J., FELDMAN, T., and WELSH, H. L. 1956. J. Chem. Phys. **24**, 1116.
CONDON, E. U. 1932. Phys. Rev. **41**, 759.
CRAWFORD, M. F. and DAGG, I. R. 1953. Phys. Rev. **91**, 1569.
CRAWFORD, M. F., WELSH, H. L., and LOCKE, J. L. 1949. Phys. Rev. **75**, 1607.
CUMMING, C. 1952. Ph.D. Thesis, University of Toronto, Toronto, Ontario.
DENNISON, D. M. 1928. Phys. Rev. **31**, 503.
EDLÉN, B. 1953. J. Opt. Soc. Amer. **43**, 339.
FELDMAN, T. 1955. Ph.D. Thesis, University of Toronto, Toronto, Ontario.
ISHIGURO, E., ARAI, T., MIZUSHIMA, M., and KOTANI, M. 1952. Proc. Phys. Soc. (London), A, **65**, 178.
KOSTKOWSKI, H. J. and BASS, A. M. 1956. J. Opt. Soc. Amer. **46**,1060.
MACNAUGHTON, E. B. 1948. Ph.D. Thesis, University of Toronto, Toronto, Ontario.
NIELSEN, J. R., THORNTON, V., and DALE, E. B. 1944. Revs. Mod. Phys. **16**, 307.
PLYLER, E. K., BLAINE, L. R. and TIDWELL, E. D. 1955. J. Research NBS, **55**, 279.
STANSBURY, E. J., CRAWFORD, M. F., and WELSH, H. L. 1953. Can. J. Phys. **31**, 954.
STOICHEFF, B. P. 1957. Can. J. Phys. **35**, 730.
VAN KRANENDONK, J. 1957. Physica, **23**, 825.
VAN KRANENDONK, J. and BIRD, R. B. 1951. Physica, **17**, 953.

NUCLEAR LEVEL SPACINGS[1]

A. G. W. CAMERON

ABSTRACT

T. D. Newton's shell-dependent level spacing formula depends upon the densities of single-particle orbits near the Fermi level in the nucleon gas. It has been found that these densities can be computed by taking appropriate averages of the second differences between adjacent atomic masses, using the writer's semiempirical mass formula from which electrostatic and pairing energy terms have been omitted. With this procedure, observed nuclear level spacings have been fitted with a root mean square error factor of 1.74. This fit shows that the level spacings are proportional to $(2J+1)^{-1}$ to a good approximation. Since the average density of single-particle orbits depends on the nuclear excitation energy, and since its computation takes a long time even with an electronic computer, an approximation formula with five coefficients has been fitted to the computed orbit densities for each Z and N in the ranges $10 \leqslant Z \leqslant 109$ and $10 \leqslant N \leqslant 189$. These coefficients are tabulated.

1. INTRODUCTION

For many years it has been customary to represent nuclear level spacings by a formula of the type

$$D = c_1 \exp -c_2 E^{1/2}, \tag{1}$$

where D is the spacing of levels of a given spin and parity at excitation energy E, and c_1 and c_2 are constants which depend upon the nucleus. With empirically determined values of c_1 and c_2, this formula could be expected to give an order-of-magnitude estimate of level spacings in nuclei not too near closed shells of nucleons. Recently Newton (1956) has shown that a more elaborate formula of this type, derived for a Fermi gas model of the nucleus, can fit nuclear level spacings with a root mean square error factor of 3, provided one replaces the density of nucleon orbits at the Fermi level by the density of nucleon orbits in the shell model (Klinkenberg 1952).

Although Newton's achievement represents an enormous increase in accuracy over previous level-spacing formulas which do not depend on shell effects, nevertheless the remaining error factor of three is too large for the rather precise calculations required in nuclear astrophysics (Cameron 1957*a*). Therefore, the writer undertook the present investigation in an attempt to improve Newton's level-spacing formula following a hint from Newton that the density of nucleon orbits at the Fermi level might be better calculated using nuclear masses instead of Klinkenberg's shell-model energy spacings.

2. THE LEVEL-SPACING FORMULA

The derivation of the level-spacing formula from the Fermi gas model has been given in detail by Newton (1956). According to this derivation one can

[1]Manuscript received November 13, 1957.
Contribution from Atomic Energy of Canada Limited, Chalk River, Ontario.
Issued as A.E.C.L. No. 643.

write the density of levels with magnetic quantum number M at excitation energy U in a nucleus with Z protons and N neutrons as

$$P(UZNM) = (2\pi)^{-2}(f_1f_2f_3f_4)^{-1/2}\exp\frac{\pi^2}{3}Gt-\frac{3}{2}-\frac{M^2}{\bar{m}^2Gt}, \tag{2}$$

where

$$f_1 = G_Zt,$$
$$f_2 = G_Nt,$$
$$f_3 = \bar{m}^2Gt,$$
$$f_4 = \frac{\pi^2}{3}Gt^3-\frac{3}{2}t^2,$$
$$G = G_Z+G_N,$$

t is the nuclear temperature, G_Z is the density of proton orbits at the Fermi level, G_N is the density of neutron orbits at the Fermi level, and $\bar{m}^2$ is a weighted average of the squares of the magnetic quantum numbers of the nucleons at the Fermi level. The density of levels of spin J is

$$D^{-1}(UZNJ) = P(UZN, M = J)-P(UZN, M = J+1). \tag{3}$$

The nuclear temperature is

$$t = \frac{3}{\pi^2G}\left[\frac{3}{2}+\left(\frac{9}{4}+\frac{2\pi^2GU}{3}\right)^{1/2}\right]. \tag{4}$$

This fairly complicated expression has been used in these calculations rather than the simplified expression given by Newton (1956), in order that the level-spacing formula (2) will not approach zero at zero excitation energy, an unattractive feature of Newton's formula in many calculations. Although the derivation of the level-spacing formula does not hold for small values of U, the formula does go smoothly to a finite value at $U = 0$ when the nuclear temperature is given by equation (4).

Following Newton, the following two approximations are made:

$$\bar{m}^2 = \text{const. } A^{2/3}, \tag{5}$$

$$\exp\left[\frac{-J^2}{\bar{m}^2Gt}\right]-\exp\left[\frac{-(J+1)^2}{\bar{m}^2Gt}\right] = \frac{\text{const. } (2J+1)}{A^{2/3}Gt}. \tag{6}$$

The level-spacing formula can thus be written:

$$D(UZNJ) = \text{const. } (2J+1)^{-1}\left[G_ZG_NG^3A^2\left(\frac{\pi^2}{3}Gt-\frac{3}{2}\right)t^7\right]^{1/2}\exp-\frac{\pi^2}{3}Gt. \tag{7}$$

This formula has one adjustable constant, provided G_Z and G_N can be accurately determined. Newton used a second adjustable constant in his procedure for determining values of G_Z and G_N.

3. THE DENSITIES OF NUCLEON ORBITS

Consider a nuclear potential well containing a set of degenerate nucleon orbits. As one adds nucleons to these orbits, to a first approximation, the

nucleons all have the same binding energy. If we now destroy the degeneracy and introduce a spacing d between the energies of successive orbits, then to a first approximation the difference between the binding energies of successive nucleons will also be d. These differences between successive nucleon binding energies are equal to the second differences between the masses of the nuclei so formed. This simple model forms the basis of the work reported here.

The writer has recently published a revised form of the semiempirical atomic mass formula (Cameron 1957*b*), in which shell and pairing corrections have been determined by an empirical procedure. The mass formula contains volume and surface energies and Coulomb and Coulomb exchange energies. Not all these terms are desirable in the proposed task of determining nucleon orbit spacings from second differences of masses. In the process of forming excited nuclear states, nucleons are raised from occupied orbits to unoccupied ones, and the energy differences involved are not the same as the binding energy differences which result when additional particles are added to the nucleus. For this reason it was decided to drop the Coulomb and Coulomb exchange energy terms from the mass formula and also the pairing energy terms. When a proton is raised to an excited orbit the electrostatic energy of the nucleus is unchanged to a good approximation. The pairing energy is a collective phenomenon which has no direct relation to the spacing of nucleon orbits.

The modified mass excess formula can then be written as:

$$M'(Z, A) = 8.367A - 0.783Z + E_v + E_s + S(Z, N), \tag{8}$$

where

$$E_v = -17.0354\left[1 - 1.846\,\frac{(A-2Z)^2}{A^2}\right]A,$$

$$E_s = 25.8357\left[1 - 1.712\,\frac{(A-2Z)^2}{A^2}\right]\left[1 - \frac{0.62025}{A^{2/3}}\right]^2 A^{2/3},$$

and $S(Z, N)$ is a shell correction energy which was empirically determined. The above terms are expressed in Mev energy units. The shell and pairing energies were written as

$$S(Z, N) = S(Z) + S(N), \tag{9}$$

$$P(Z, N) = P(Z) + P(N). \tag{10}$$

$P(Z)$ and $P(N)$ are zero for odd values of Z or N, respectively. The quantities $S(Z)+P(Z)$ and $S(N)+P(N)$ have been tabulated (Cameron 1957*b*). The pairing corrections $P(Z)$ and $P(N)$ are given here in Table I.

Newton (1956) has shown that a fictitious excitation energy U must be used in the level-spacing formula. This fictitious energy is based on the energy the ground state would have in an odd–odd nucleus where there is no pairing energy. We therefore write

$$U = E + P(Z, N), \tag{11}$$

where E is the actual excitation energy and $P(Z, N)$ is the sum of appropriate negative energy terms in Table I.

TABLE I

PAIRING ENERGIES FOR NEUTRONS AND PROTONS
(If either nucleon number is odd, the pairing energy is zero for that nucleon)

Z or N	$P(Z)$	$P(N)$	Z or N	$P(Z)$	$P(N)$	Z or N	$P(Z)$	$P(N)$
10	−2.25	−2.70	74	−1.23	−1.20	138		−0.80
12	−2.10	−2.48	76	−0.85	−0.94	140		−0.68
14	−2.13	−2.17	78	−0.98	−1.00	142		−0.64
16	−1.54	−1.74	80	−0.72	−1.05	144		−0.58
18	−1.42	−1.75	82	−0.80	−0.54	146		−0.55
20	−1.51	−1.72	84	−0.77	−0.60	148		−0.57
22	−1.73	−1.63	86	−0.89	−0.75	150		−0.57
24	−1.44	−1.41	88	−0.92	−0.75	152		−0.55
26	−1.45	−1.29	90	−0.80	−0.85	154		−0.60
28	−1.37	−1.47	92	−0.81	−0.97	156		−0.58
30	−1.09	−1.32	94	−0.69	−1.02	158		−0.58
32	−1.36	−1.46	96	−0.70	−1.05	160		−0.61
34	−1.42	−1.44	98	−0.76	−1.06	162		−0.63
36	−1.33	−1.46	100	−0.73	−1.07	164		−0.65
38	−1.20	−1.52	102	−0.80	−1.06	166		−0.66
40	−1.00	−1.51	104	−0.74	−1.05	168		−0.65
42	−1.16	−1.47	106	−0.73	−1.02	170		−0.65
44	−1.28	−1.45	108	−0.72	−0.97	172		−0.64
46	−1.38	−1.28	110	−0.72	−0.91	174		−0.64
48	−1.38	−1.23	112	−0.72	−0.83	176		−0.63
50	−1.32	−1.27	114	−0.71	−0.74	178		−0.61
52	−1.04	−0.62	116	−0.69	−0.66	180		−0.59
54	−1.11	−0.76	118	−0.68	−0.61	182		−0.55
56	−1.13	−1.23	120	−0.66	−0.61	184		−0.39
58	−1.21	−1.22	122	−0.61	−0.90	186		−0.36
60	−1.43	−1.40	124	−0.42	−0.52	188		−0.40
62	−1.15	−1.36	126	−0.36	−0.81	190		−0.40
64	−0.99	−1.30	128	−0.41	−0.68	192		−0.40
66	−0.91	−1.29	130	−0.49	−0.72	194		−0.40
68	−0.92	−1.24	132		−0.77	196		−0.40
70	−1.00	−1.28	134		−0.68	198		−0.40
72	−1.11	−1.24	136		−0.67	200		−0.40

We now define the orbit separation energies as

$$d(Z) = [M'(Z, A) - 2M'(Z-1, A-1) + M'(Z-2, A-2)]_v. \tag{12}$$

$$d(N) = [M'(Z, A) - 2M'(Z, A-1) + M'(Z, A-2)]_v. \tag{13}$$

Here the bracket with subscript v indicates that the quantities must be evaluated near the valley of beta stability where the shell corrections were determined (these expressions vary slowly as one crosses the valley of beta stability).

When this procedure was first contemplated it was thought that the right hand sides of equations (12) and (13) would have to be multiplied by some constant factor of order unity in order to correct for the errors in orbit spacings introduced by a calculation in which one adds particles rather than excites existing particles. The necessity for such a multiplicative constant would have been demonstrated if the resulting level-spacing formula did not have the correct dependence on A. However, the excellent fit which has been obtained shows that no such constant is needed.

Orbit separation energies $d(Z)$ and $d(N)$ were calculated close to the bottom

of the valley of beta stability for $1 \leqslant Z \leqslant 139$ and $1 \leqslant N \leqslant 239$. These calculations required some further extrapolations of the writer's shell corrections (Cameron 1957*b*).

It is necessary to average the orbit separation energies in the vicinity of the Fermi level. The average must be weighted so that large weight is given to orbits close to the Fermi level and small weight to those far from the Fermi level. The Fermi level is taken to coincide with the highest filled proton and neutron orbits. Following Newton (1956), we choose weights according to the formula:

$$w(E) = \ln(1+\exp -E/t), \tag{14}$$

where E is the energy difference between the orbit in question and the Fermi level. It was found necessary to give equal total weights to the bound and to the unbound orbits. The average spacings are thus given by the expressions:

$$\bar{d}_l(Z) = \sum_{Z_l}^{Z} d(Z_i)\, w_l(Z_i) \Big/ \sum_{Z_l}^{Z} w_l(Z_i), \tag{15}$$

$$\bar{d}_u(Z) = \sum_{Z+1}^{Z_u} d(Z_i)\, w_u(Z_i) \Big/ \sum_{Z+1}^{Z_u} w_u(Z_i), \tag{16}$$

$$\bar{d}_l(N) = \sum_{N_l}^{N} d(N_i)\, w_l(N_i) \Big/ \sum_{N_l}^{N} w_l(N_i), \tag{17}$$

$$\bar{d}_u(N) = \sum_{N+1}^{N_u} d(N_i)\, w_u(N_i) \Big/ \sum_{N+1}^{N_u} w_u(N_i), \tag{18}$$

where

$$w_l(Z_i) = \ln\left[1+\exp -\frac{1}{t}\left\{\sum_{Z_i+1}^{Z} d(Z_j)\right\}\right], \tag{19}$$

$$w_l(Z) = \ln 2 = w_u(Z+1), \tag{20}$$

$$w_u(Z_i) = \ln\left[1+\exp -\frac{1}{t}\left\{\sum_{Z+1}^{Z_i-1} d(Z_j)\right\}\right], \tag{21}$$

and similar expressions for $w_l(N_i)$, $w_l(N)$, $w_u(N_i)$, and $w_u(N+1)$.

The average orbit densities are then

$$\begin{aligned} G_Z &= 2/[\bar{d}_l(Z)+\bar{d}_u(Z)], \\ G_N &= 2/[\bar{d}_l(N)+\bar{d}_u(N)]. \end{aligned} \tag{22}$$

In equations (15) to (18) Z_l, Z_u, N_l, and N_u are limits at which the sums are cut off. In this work it has been customary to cut off the sums for $w < 0.01$.

It may be seen from equation (4) that the nuclear temperature depends upon the total orbit density G, which in turn depends upon the nuclear temperature through the weights w. It is therefore necessary to determine G and t simultaneously by an iterative procedure. One assumes a value of G, calculates t, calculates G, recalculates t, and so on until successive values of t agree sufficiently closely (it has here been required that two successive approximations to t agree to within 1%).

4. THE FIT TO OBSERVED LEVEL SPACINGS

The most accurate experimental information about nuclear level spacings is that derived from low energy neutron interactions with nuclei. The number of partial waves is then very limited (usually only *s*-waves), and the levels which are formed have only two spin states. An attempt was made to fit observed level spacings in 82 nuclei. Most of the observed spacings were taken from a paper on radiation widths by Stolovy and Harvey (1957). The remaining spacings were for nuclei used by Newton (1956) which were not included in the paper by Stolovy and Harvey. The writer has re-estimated the spacings in these latter nuclei through an inspection of BNL-325 (Hughes and Harvey 1955) and its supplement (Hughes and Schwartz 1957). Levels were counted only up to energies at which it appeared likely that nearly all levels had been resolved. In cases where levels above 50 kev were included in the count, corrections were made for *p*-wave interactions (these were important for light nuclei and also near Pb^{208}). These estimates are given in Table II.

TABLE II

SPACINGS OF LEVELS FORMED BY *s*-WAVE NEUTRON INTERACTIONS WITH NUCLEI AS ESTIMATED BY THE WRITER FROM BNL-325

(The Z and A refer to the compound nucleus formed by neutron bombardment)

Z	A	D_{obs}
9	20	110000 ev
11	24	150000
13	28	60000
15	32	50000
17	36	10000
21	46	2000
23	52	2000
25	56	2000
27	60	3000
43	100	14
50	113	150
50	117	150
50	119	300
50	120	150
59	142	110
64	158	2
65	160	2.7
67	166	7.5
72	180	8
81	204	1000
82	207	25000
82	209	400000
83	210	40000
92	235	17
92	237	17
95	242	0.43

When attempts were made to fit equation (7) to these observed level spacings by the procedure which has been outlined, the results were for the most part very encouraging. However, in certain regions the fit was poor. These regions were the transition regions near heavy closed shells in which the addition of a

small number of nucleons is sufficient to cause spherical nuclei to become strongly deformed, or vice versa. In these regions the calculated values of $d(Z)$ and $d(N)$ were negative. It was thus evident that any close correspondence between the second differences of the masses and the spacings of nucleon orbits had been destroyed by collective effects in the transition regions. Accordingly, typical values were assigned to $d(Z)$ and $d(N)$ in the transition regions, usually about two-thirds of the values that $d(Z)$ and $d(N)$ would have if the shell corrections had been zero. When these substitutions had been made, a good fit was also obtained in the transition regions.

It was found also that in certain regions away from shell edges the $d(Z)$ and $d(N)$ fluctuated randomly between moderate and very small values. It was known from the work done in fitting masses (Cameron 1957*b*) that these fluctuations had no physical significance. If the fluctuations were allowed to remain, they would cause large fluctuations in level densities calculated for very low excitation energies. Therefore the $d(Z)$ and $d(N)$ were smoothed locally in such regions. This had very little effect on the fits at the excitation energies corresponding to neutron binding energies. A table of $d(Z)$ and $d(N)$ is given as Appendix I.

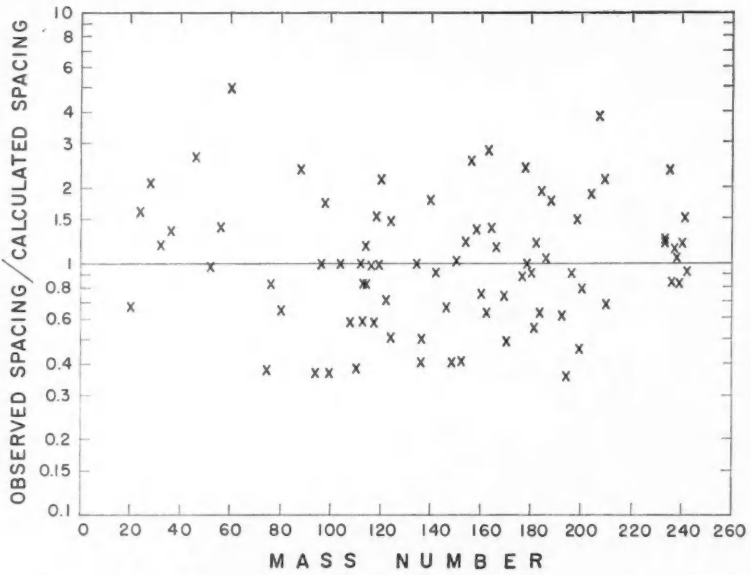

FIG. 1. Ratio of observed to calculated level spacings for 82 nuclei, plotted as a function of mass number.

Figure 1 shows the ratio of the observed to the calculated level spacings as a function of mass number. It may be seen that every region of mass number has been fitted about as well as any other. The normalization to the points in Fig. 1 gives the final level spacing formula:

$$(24) \qquad D(UZNJ) = \frac{3.26\times10^5}{(2J+1)}\left[G_Z G_N G^3 A^2\left(\frac{\pi^2}{3}Gt-\frac{3}{2}\right)t^7\right]^{1/2}\exp-\frac{\pi^2}{3}Gt.$$

Factors of error for the points in Fig. 1 are defined as follows:

$$(25) \qquad \text{Log (error factor)} = \left|\log\frac{D_{\text{obs}}}{D_{\text{calc}}}\right|.$$

The average error factor is 1.53. The root mean square error factor is 1.74. This latter value should be compared with the root mean square error factor of 3 obtained by Newton (1956). It is evident that a further improvement in the fit to level densities has been achieved by the procedure outlined in this paper. A not insignificant part of the error factor of 1.74 may be due to uncertainties in observed level spacings. Many of the values used in the fit are uncertain by at least a factor two.

Figure 2 shows the ratio of the observed to the calculated level spacings plotted against the spin of the target nucleus which is bombarded by neutrons.

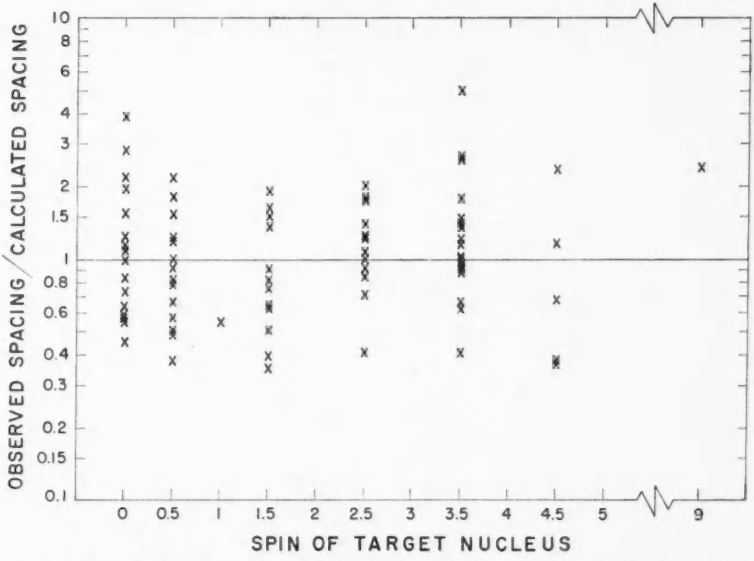

FIG. 2. Ratio of observed to calculated level spacings for 82 nuclei, bombarded by neutrons, plotted as a function of the target spin.

The spins of the compound nuclei will differ from that of the target nucleus by $\pm\frac{1}{2}$. It may be seen that the fit is about equally good for all target spins, thus showing that level spacings vary inversely as $(2J+1)$ to a good approximation.

It should be noted that the level spacing formula has not been tested over a very wide range of excitation energy.

5. APPROXIMATIONS TO THE ORBIT DENSITIES

Although the method outlined in this paper for determining $G_Z(t)$ and $G_N(t)$ has proved quite successful, it is nevertheless a very clumsy and lengthy method. The calculation of one level density takes between 1 and 10 minutes on the Chalk River Datatron, the longer time being characteristic of nuclei near Pb^{208}. Under these circumstances it is not possible to use this procedure as a tool in the solution of other problems which may require the calculation of many level densities. Therefore the regular procedure has been used to calculate $G_Z(t)$ and $G_N(t)$ for a range of values of t (generally corresponding to a range of excitation energy of zero to 100 Mev). These values have then been fitted by the general approximation formula:

$$G_k(t) = \frac{a_0(k)+a_1(k)t+a_2(k)t^2+a_3(k)t^3+a_4(k)t^4}{1+t+t^2+t^3+t^4}, \tag{26}$$

where k stands for Z or N. The five coefficients $a_0(k), \ldots, a_4(k)$ were fitted by a least squares procedure to 15 values of $G_k(t)$. The resulting approximation usually fitted these values to within 1%.

These fits were made for $10 \leqslant Z \leqslant 109$ and $10 \leqslant N \leqslant 189$. The resulting coefficients are given in Tables III and IV. It may be noted that some of the coefficients are negative. However, it has been verified that no set of coefficients gives a negative value of $G_k(t)$ within the useful range of t.

TABLE III

COEFFICIENTS IN THE APPROXIMATION FORMULA (26) FOR $G_Z(t)$.
($G_Z(t)$ is in units of Mev^{-1})

Z	a_0	a_1	a_2	a_3	a_4
10	2.54090	−6.88500	7.06180	−2.66610	0.58669
11	2.05760	−5.25000	5.36770	−1.91450	0.48746
12	1.82440	−3.50200	3.93670	−1.08140	0.49654
13	1.75700	−2.00900	2.97640	−0.49370	0.50516
14	1.23250	−1.19700	2.27190	−0.15630	0.54597
15	1.07400	−1.43700	2.35670	0.11140	0.55716
16	1.07760	−0.66700	1.64230	0.59240	0.56247
17	0.97450	0.22700	1.00450	1.00930	0.57339
18	1.02940	0.77900	0.57730	1.37540	0.59761
19	1.38120	0.12700	0.91440	1.46700	0.64208
20	0.82010	0.53200	0.25000	1.72890	0.68103
21	0.73380	1.12900	−0.35370	1.99080	0.68045
22	1.78550	−0.21700	1.38770	1.61690	0.77693
23	1.30070	1.59400	0.17310	1.96610	0.79870
24	0.94390	2.95310	−1.14950	2.41430	0.78967
25	0.77270	3.52960	−1.62140	2.39850	0.84887
26	−0.04100	6.96580	−5.70350	3.84030	0.71714
27	0.13470	5.62540	−4.67970	3.19150	0.84693
28	−0.01630	4.66900	−4.14950	2.84330	0.93519
29	0.57050	1.29030	−0.13600	1.06950	1.21312
30	0.97740	0.77100	1.03660	0.64720	1.28997
31	1.33880	0.94890	1.38730	0.86970	1.29596
32	1.34420	1.49790	1.43370	1.15010	1.29318
33	1.79310	0.87790	2.57380	0.97090	1.36046
34	2.30220	0.42990	3.05330	1.12470	1.38150
35	2.24120	0.50170	3.28720	1.19380	1.42727
36	1.83260	1.29290	2.40790	1.67410	1.40286
37	1.73610	1.22640	2.55910	1.65670	1.45010

TABLE III (*continued*)

Z	a_0	a_1	a_2	a_3	a_4
38	1.80250	0.98900	2.80540	1.57840	1.50325
39	1.72880	1.66180	1.85380	2.06680	1.46949
40	1.76890	1.64160	1.91960	1.98760	1.51824
41	1.80940	1.66110	2.03090	1.88230	1.57321
42	1.89230	1.34410	2.70580	1.37500	1.70617
43	1.89830	1.51060	2.58460	1.32130	1.75270
44	1.88300	1.77150	2.34820	1.24600	1.80983
45	1.93330	1.83000	2.31840	1.08200	1.88211
46	2.04170	1.64150	2.38290	0.80770	1.97991
47	2.26540	1.03400	2.50520	0.60540	2.05252
48	2.60780	−0.43680	3.28500	0.21940	2.13629
49	2.41160	−1.55210	3.97610	−0.43440	2.29490
50	0.73028	1.61310	−0.79680	1.11850	2.13641
51	0.62134	1.76260	−1.21720	1.77750	1.93396
52	2.20146	−0.70960	2.41220	0.51580	2.15497
53	2.20045	0.97640	1.46610	1.24090	2.08108
54	2.02370	1.96340	1.53190	1.48450	2.08343
55	1.81430	2.68210	1.98800	1.44040	2.13392
56	2.15520	2.44970	2.96980	1.29650	2.18503
57	2.78490	1.95430	3.96360	1.30290	2.21492
58	2.88500	3.45450	2.32200	2.53780	2.05018
59	3.54270	2.91280	2.95300	2.68350	2.05714
60	4.94570	−0.47280	6.80350	1.23850	2.32293
61	5.18540	−1.17040	7.72260	1.00950	2.41191
62	3.87360	2.00980	4.18400	2.62370	2.20457
63	2.84670	3.89310	2.06030	3.55600	2.09311
64	2.65694	3.18680	2.85390	3.09850	2.20282
65	2.66221	2.17600	3.83120	2.57700	2.32124
66	2.48543	2.14120	3.53000	2.72270	2.31589
67	2.31180	2.36530	2.95080	2.98440	2.29285
68	2.37716	2.09170	3.19930	2.77600	2.35510
69	2.60136	1.56730	3.66300	2.48930	2.42417
70	2.49254	1.76560	3.74210	2.26540	2.49443
71	2.35504	2.15640	3.69930	2.04360	2.57392
72	2.37008	2.51860	3.65590	1.81040	2.65373
73	2.52609	3.16450	2.79100	2.20410	2.59819
74	3.02744	3.07870	2.69460	2.17460	2.63103
75	3.40231	3.45160	1.96100	2.41220	2.62283
76	3.61399	4.59460	−0.78900	4.08380	2.29499
77	4.28974	2.91840	0.67410	3.14380	2.48983
78	5.08195	−0.52930	4.57210	0.66070	2.99123
79	5.49290	−4.31320	9.15820	−2.46220	3.63057
80	4.76203	−5.54530	10.60750	−4.23370	4.06301
81	1.56832	2.19680	−0.98880	1.08570	3.15736
82	0.63248	0.91420	−0.02280	1.09140	3.20923
83	0.85952	0.70290	1.71860	−1.25420	3.58958
84	3.88686	−6.40780	12.39100	−6.02830	4.42853
85	5.62571	−7.94070	14.63030	−5.86640	4.36500
86	5.60035	−2.93880	7.46750	−0.53400	3.30689
87	5.37494	1.21960	2.01890	3.42210	2.55312
88	5.15555	3.89580	−0.87940	5.60320	2.17708
89	4.57913	7.29850	−5.00680	8.41830	1.66300
90	4.94414	6.02950	−2.23660	7.06140	1.99504
91	5.84768	1.79290	4.48440	3.45800	2.76167
92	4.96580	3.80280	2.68080	4.35710	2.68089
93	3.99003	5.79620	0.75160	5.43370	2.52601
94	3.52739	5.76460	1.31870	5.09940	2.62699
95	3.36583	5.06740	2.51560	4.48820	2.77705
96	3.46175	4.07180	3.65780	4.03910	2.87281
97	3.45633	3.86930	3.66190	4.05240	2.92873
98	3.50179	3.72480	3.44800	4.25230	2.91469
99	3.55396	3.56250	3.37660	4.31570	2.95171
100	3.62648	3.31610	3.52580	4.19890	3.02965
101	3.72031	2.86080	3.95910	3.84590	3.15330

TABLE III (*concluded*)

Z	a_0	a_1	a_2	a_3	a_4
102	3.76769	2.40420	4.40690	3.50280	3.27771
103	3.67740	1.88570	5.31650	2.84130	3.46659
104	3.27821	2.14940	5.42540	2.51880	3.59350
105	2.85502	2.93760	4.49230	3.06580	3.48965
106	2.89336	2.54480	5.18630	2.70070	3.55147
107	3.15908	2.23410	5.43010	2.73370	3.54030
108	3.31585	2.58470	4.91310	3.18420	3.44506
109	3.35546	3.46910	3.62430	4.20510	3.18402

TABLE IV

COEFFICIENTS IN THE APPROXIMATION FORMULA (26) FOR $G_N(t)$
($G_N(t)$ is in units of Mev^{-1})

N	a_0	a_1	a_2	a_3	a_4
10	−2.01000	6.37300	−3.46800	1.99730	0.37526
11	−2.27300	7.19400	−3.75600	2.11950	0.43772
12	−1.72100	5.93700	−3.11900	1.96670	0.50522
13	0.27400	2.81200	−1.42300	1.55070	0.59158
14	−4.62700	12.49300	−7.28600	2.68610	0.58200
15	−2.24700	7.28500	−4.71400	2.12100	0.66448
16	0.75300	0.89600	−0.20200	0.96220	0.80110
17	−0.01900	3.65100	−1.76400	1.48780	0.80672
18	0.88100	1.63700	−0.16700	1.23570	0.88170
19	1.15900	0.55300	0.90100	1.04210	0.95641
20	0.70400	0.65700	1.04100	1.13680	0.99477
21	0.75900	1.42600	0.76300	1.25750	1.01410
22	1.38900	2.97800	0.11500	1.77780	1.02907
23	2.35200	1.91200	1.19100	1.66390	1.12262
24	2.55600	0.97700	2.20400	1.22460	1.25306
25	1.13800	4.08400	−0.61800	1.92310	1.25547
26	0.65300	4.85000	−1.82800	2.17130	1.29349
27	0.33800	5.13400	−3.16000	2.47540	1.32796
28	−0.52290	5.88800	−4.81400	2.92910	1.33400
29	−0.62330	5.77100	−4.76000	3.07560	1.30398
30	0.85800	3.07600	−1.68500	2.08310	1.44368
31	1.74660	1.68900	0.48200	1.61130	1.55552
32	1.84010	1.65500	1.38800	1.53770	1.62671
33	1.88110	1.68200	1.96400	1.61890	1.66548
34	1.93890	1.74200	2.41200	1.73940	1.70445
35	2.23470	1.42300	3.12600	1.74670	1.75216
36	2.78700	0.31000	4.59800	1.42840	1.85296
37	3.28660	−0.79500	6.15600	1.02330	1.96976
38	3.11860	0.09400	5.49900	1.43550	1.98554
39	2.89480	0.87300	5.15900	1.62700	2.02530
40	2.54000	2.43100	3.73100	2.20970	2.02364
41	2.55200	2.85700	3.37900	2.36250	2.06658
42	2.69850	3.63100	2.42200	2.75370	2.07943
43	3.64080	2.55300	2.99100	2.53680	2.17423
44	4.10290	2.08000	3.13400	2.34950	2.27746
45	3.57860	2.68800	2.55000	2.14260	2.40308
46	2.89790	4.15700	0.39100	2.79400	2.38510
47	2.88360	3.39100	0.49000	2.44650	2.51017
48	2.97650	2.00700	0.69300	2.11510	2.62291
49	2.20430	2.26500	−0.56300	2.25900	2.68696
50	0.36630	4.99800	−4.91500	3.70550	2.57086
51	0.59230	2.56900	−1.84300	2.96190	2.56207
52	1.78910	1.04800	0.45000	1.95430	2.74485
53	1.71180	2.86200	−0.46400	2.46000	2.70429
54	1.65080	4.64700	−1.35500	3.01100	2.64281
55	2.70740	3.86600	−0.13200	3.09680	2.62880

TABLE IV (*continued*)

N	a_0	a_1	a_2	a_3	a_4
56	3.92370	2.35000	2.25100	2.70700	2.72411
57	4.11380	2.75400	2.77700	3.00040	2.74027
58	3.77330	3.94800	2.58000	3.42240	2.74288
59	3.32810	6.17300	0.45000	4.84870	2.57430
60	3.31030	6.45600	0.86400	5.00610	2.59945
61	3.04530	7.99200	−0.52200	6.02320	2.49465
62	3.23470	8.12500	−0.49300	6.35530	2.48990
63	4.50300	5.44300	2.31900	5.51490	2.65379
64	5.43750	4.07200	3.70100	5.34360	2.72528
65	4.62960	7.05800	0.87300	6.69820	2.59748
66	4.10510	8.61300	−0.25100	7.04340	2.63621
67	5.06110	6.23400	2.19100	6.19140	2.80129
68	5.94120	3.96300	4.56000	5.24150	3.01265
69	4.70240	7.40300	0.98400	6.66220	2.87188
70	3.26820	11.79600	−3.81100	8.66880	2.63130
71	3.45980	11.59100	−4.14800	8.84410	2.64101
72	4.82300	7.67400	−0.15700	7.03040	2.96799
73	5.65400	5.97700	0.78300	6.54580	3.08789
74	4.87440	8.97600	−3.34100	8.23430	2.88701
75	4.31010	10.22700	−4.85000	8.43420	2.94242
76	5.55520	6.24490	−1.69400	7.04660	3.17342
77	8.20490	−2.35650	6.45500	3.33950	3.77604
78	9.78170	−8.31620	11.34000	0.92570	4.18195
79	8.89640	−8.09010	9.69600	1.08890	4.22318
80	5.55150	−1.41700	0.63770	4.40940	3.78019
81	1.76200	5.69660	−8.38780	7.98270	3.30502
82	0.79360	2.24950	−3.12110	5.85450	3.67937
83	0.90040	1.91210	−2.22470	4.90410	3.77064
84	2.21280	3.35830	−3.81270	5.35250	3.69503
85	4.48590	1.27410	−0.34820	4.15720	3.89296
86	7.58190	−3.79360	6.37050	1.79000	4.27251
87	10.53330	−8.99900	13.45800	−0.67680	4.68776
88	11.96770	−10.24560	15.88800	−1.13360	4.79335
89	12.31040	−8.40750	14.01100	0.61690	4.49846
90	12.22800	−7.04840	13.50300	1.21760	4.44878
91	11.58070	−5.09040	12.44700	1.89840	4.39150
92	9.86250	−0.43420	7.93500	4.19100	4.05640
93	7.81890	4.43690	3.46800	6.20680	3.78750
94	6.14920	7.43030	1.30400	7.02070	3.71880
95	4.93470	9.37510	−0.23400	7.71410	3.63770
96	4.29580	9.16020	1.07300	6.88460	3.82260
97	4.14940	7.94990	3.20900	5.78790	4.03630
98	4.27180	6.03760	6.30000	4.02360	4.41810
99	4.28080	5.44040	7.13400	3.65850	4.50110
100	4.38820	5.09990	7.36900	3.65780	4.52350
101	4.70600	4.44620	7.80600	3.58260	4.54500
102	5.11340	3.38080	9.29100	2.70850	4.75280
103	5.32590	3.21600	9.23500	2.79070	4.75830
104	5.38920	3.38840	9.20400	2.63050	4.84500
105	5.47650	3.28700	9.55200	2.25120	4.96700
106	5.51350	3.34390	9.76200	1.92910	5.07630
107	5.27980	4.30570	8.80300	2.14540	5.09780
108	5.28230	4.47900	8.82400	1.82290	5.21230
109	5.49430	3.85470	9.93700	0.91550	5.44680
110	5.74000	3.27800	10.68400	0.25920	5.61740
111	5.85290	3.05900	11.13300	−0.43680	5.82450
112	5.75270	3.44930	10.89600	−0.80600	5.99010
113	5.72910	3.71210	10.43500	−0.94970	6.08100
114	5.50360	5.33220	6.89920	1.27590	5.57640
115	5.40300	5.92930	5.61720	1.65350	5.56110
116	5.42110	5.93650	5.03990	1.62540	5.62550
117	5.49550	5.87270	4.07270	1.96120	5.59070
118	5.59090	5.57640	3.27710	2.16750	5.59820
119	5.62980	5.36060	2.01680	2.70800	5.52860

TABLE IV (*continued*)

N	a_0	a_1	a_2	a_3	a_4
120	5.66620	4.73380	1.00260	3.27500	5.44026
121	5.67060	3.50780	0.78880	3.31940	5.45726
122	5.18893	3.31780	−0.98520	4.30800	5.28631
123	4.44115	3.12600	−2.67410	5.34260	5.09107
124	3.94805	0.46200	−0.53990	4.34570	5.27667
125	1.66941	3.65770	−5.70440	7.07060	4.80341
126	0.80912	0.58190	0.84720	4.24580	5.14117
127	1.23839	0.82540	2.48570	−2.45000	6.60541
128	3.23842	−1.91680	8.80140	−4.66090	7.07604
129	7.23749	−13.92430	28.01920	−14.47400	9.02634
130	11.37358	−26.88090	48.45080	−25.29430	11.25946
131	13.62251	−31.13200	55.11310	−27.82330	11.77850
132	14.76010	−30.84020	54.71950	−26.28380	11.48710
133	14.57480	−25.36240	46.77530	−20.65240	10.42810
134	14.15950	−19.75880	38.44600	−14.77130	9.28260
135	13.23160	−13.01450	28.77300	−8.30630	8.03760
136	11.99790	−5.85650	18.35800	−1.44620	6.67990
137	11.18760	−1.62000	12.58600	2.51450	5.91660
138	10.87090	−0.72080	12.16300	3.06420	5.86780
139	10.52770	−0.89560	13.83700	2.18780	6.12870
140	9.41760	1.44650	11.83300	3.35750	5.97910
141	6.33490	12.06220	−2.49200	11.77350	4.36050
142	5.37460	14.86770	−5.20500	13.17730	4.15420
143	6.92580	5.94960	9.31000	4.42380	6.02650
144	6.41020	6.33040	9.87500	3.99240	6.19510
145	4.68490	13.02210	0.54500	9.56500	5.11670
146	5.05440	11.82440	1.90300	9.17060	5.19250
147	7.93780	−0.00180	19.08100	−0.65990	7.21970
148	11.11410	−13.60990	39.45300	−12.59010	9.73350
149	13.45580	−25.31500	57.93300	−23.82260	12.16380
150	11.24360	−19.48420	51.00000	−20.10400	11.53720
151	6.87400	−5.01680	31.93900	−9.37830	9.44750
152	2.51800	9.04440	14.40000	0.05660	7.68050
153	2.85130	7.70580	15.49100	−0.50290	7.74770
154	7.65620	−7.34620	36.24600	−12.40810	10.25200
155	9.76270	−10.98020	39.81700	−13.79610	10.53150
156	9.86980	−6.55190	31.67600	−8.35830	9.41860
157	9.72860	−2.26000	24.28900	−3.50890	8.43560
158	9.32240	2.32390	16.87700	1.15380	7.49220
159	9.17610	4.98160	12.90700	3.47850	7.08120
160	9.08990	6.68370	11.17000	4.09000	7.09430
161	8.76630	9.46520	7.17000	6.28290	6.72320
162	8.63630	11.34140	4.46300	7.66880	6.52450
163	8.63930	12.75230	2.16600	8.90000	6.35900
164	8.63570	14.39110	−0.83600	10.52040	6.08610
165	8.73020	15.52130	−2.68200	11.43760	5.96600
166	9.29130	14.77110	−2.35400	11.12320	6.11070
167	10.30140	12.39950	−0.09200	9.76800	6.44140
168	11.06960	11.16790	0.06400	9.79280	6.46290
169	11.46850	11.61530	−2.64700	11.72790	6.06890
170	12.20170	9.83190	−2.29900	12.08730	5.82800
171	13.02650	7.11960	0.00800	10.72030	6.13250
172	13.27010	6.48600	−1.00100	11.33450	5.99250
173	13.26560	6.07640	−2.18000	12.02210	5.82560
174	13.17270	5.42440	−2.90500	12.28090	5.80400
175	13.21756	3.20470	−1.11600	10.83180	6.12770
176	13.33235	−0.38930	3.26500	7.53960	6.90970
177	13.47239	−5.17700	9.82000	2.59790	8.06580
178	13.61737	−11.34520	19.27830	−4.59480	9.78480
179	13.78681	−19.06110	32.00070	−14.35500	12.14410
180	13.32149	−24.81640	41.72400	−22.31430	14.13590
181	11.47239	−24.29050	40.76040	−23.23280	14.49410
182	6.65768	−8.54540	12.91000	−5.69670	10.56670
183	1.96431	5.31070	−11.70070	9.67710	7.08568

TABLE IV (*concluded*)

N	a_0	a_1	a_2	a_3	a_4
184	0.61563	2.40930	−6.54590	10.29300	6.72776
185	1.01590	0.87910	2.18890	−6.38400	11.07745
186	2.28950	0.29780	5.39480	−6.51590	11.12806
187	3.98508	−2.98150	13.31490	−10.26400	12.07910
188	5.98064	−8.22120	24.19440	−15.98570	13.45220
189	9.85338	−24.06020	53.69850	−35.02590	17.99470

In using these approximations it is still necessary to determine G and t simultaneously by an iterative procedure. It is recommended that an initial value of $G(t)$ be chosen as

$$G(t) \text{ initial} = a_4(Z)+a_4(N). \tag{27}$$

Near closed shells it is often better to choose an initial value about one half of the amount given by equation (27).

The writer is indebted to Dr. T. D. Newton for several stimulating discussions.

REFERENCES

CAMERON, A. G. W. 1957*a*. Chalk River Report CRL-41.
——— 1957*b*. Can. J. Phys. **35**, 1021.
HUGHES, D. J. and HARVEY, J. A. 1955. U.S. Atomic Energy Commission Report BNL-325.
HUGHES, D. J. and SCHWARTZ, R. B. 1957. U.S. Atomic Energy Commission Report, Supp. No. 1, BNL-325.
KLINKENBERG, P. F. A. 1952. Revs. Mod. Phys. **24**, 63.
NEWTON, T. D. 1956. Can. J. Phys. **34**, 804.
STOLOVY, A. and HARVEY, J. A. 1957. Phys. Rev. (in press).

APPENDIX I

A table of the nucleon orbit spacings $d(Z)$ and $d(N)$ calculated from second differences of masses. $[d(Z)]_r$ and $[d(N)]_r$ are reference spacings obtained from the mass formula from which the shell correction terms were omitted in addition to the Coulomb, Coulomb exchange, and pairing energy terms. $[d(Z)]_u$ and $[d(N)]_u$ are the spacings calculated as described in the text, and $[d(Z)]_a$ and $[d(N)]_a$ are the spacings, smoothed and in places adjusted as described in the text, which were used in the final calculations of level spacings. All spacings are in Mev.

Z or N	$[d(Z)]_r$	$[d(Z)]_u$	$[d(Z)]_a$	$[d(N)]_r$	$[d(N)]_u$	$[d(N)]_a$
0			40.000			40.000
1			30.000			30.000
2			20.000	20.251		20.000
3	8.935		8.935	8.961		8.961
4	5.465		5.465	5.713		5.713
5	4.247		4.247	4.035		4.035
6	3.415		3.415	3.247		3.247
7	2.875		2.875	2.742		2.742
8	2.494		2.494	2.390		2.390
9	2.212		2.212	2.126		2.126
10	1.992		1.992	1.920		1.920
11	1.865	10.145	10.145	1.754	0.854	0.854
12	1.715	0.765	0.765	1.554	1.544	1.544
13	1.585	1.555	1.555	1.447	1.407	1.407
14	1.478	0.778	0.778	1.356	0.946	0.946
15	1.411	2.351	2.351	1.275	1.655	1.655

APPENDIX I (*continued*)

Z or N	$[d(Z)]_r$	$[d(Z)]_u$	$[d(Z)]_a$	$[d(N)]_r$	$[d(N)]_u$	$[d(N)]_a$
16	1.327	1.587	1.587	1.205	1.955	1.955
17	1.253	1.433	1.433	1.110	1.150	1.150
18	1.187	1.157	1.157	1.057	1.067	1.067
19	1.146	0.996	0.996	1.010	1.030	1.030
20	1.090	0.610	0.610	0.967	1.037	1.037
21	1.041	2.031	2.031	0.928	1.648	1.648
22	1.010	0.440	0.440	0.869	0.649	0.489
23	0.968	0.728	0.728	0.840	0.010	0.245
24	0.930	0.790	0.790	0.809	0.309	0.310
25	0.904	0.794	0.794	0.782	0.612	0.536
26	0.870	0.800	0.800	0.741	0.651	0.651
27	0.849	0.809	0.809	0.718	0.658	0.658
28	0.821	0.991	0.991	0.698	0.718	0.718
29	0.794	1.564	1.564	0.679	1.749	1.749
30	0.775	1.365	1.365	0.646	1.066	1.066
31	0.750	0.790	0.790	0.630	0.530	0.530
32	0.735	0.765	0.765	0.615	0.575	0.575
33	0.714	0.704	0.704	0.587	0.557	0.557
34	0.698	0.518	0.518	0.573	0.553	0.553
35	0.678	0.448	0.448	0.560	0.510	0.510
36	0.664	0.554	0.554	0.550	0.450	0.450
37	0.648	0.598	0.598	0.526	0.406	0.406
38	0.636	0.606	0.606	0.516	0.356	0.356
39	0.620	0.580	0.580	0.507	0.397	0.397
40	0.607	0.577	0.577	0.487	0.397	0.397
41	0.595	0.565	0.565	0.479	0.389	0.389
42	0.584	0.554	0.554	0.469	0.399	0.399
43	0.571	0.541	0.541	0.455	0.345	0.345
44	0.561	0.541	0.541	0.446	0.166	0.166
45	0.550	0.530	0.530	0.439	0.269	0.269
46	0.539	0.519	0.519	0.425	0.325	0.325
47	0.530	0.500	0.500	0.418	0.358	0.358
48	0.519	0.459	0.459	0.411	0.321	0.321
49	0.513	0.403	0.403	0.400	0.320	0.320
50	0.503	0.233	0.233	0.393	0.323	0.323
51	0.495	2.145	2.145	0.388	1.578	1.578
52	0.488	0.498	0.498	0.376	0.666	0.666
53	0.478	0.488	0.488	0.371	0.501	0.501
54	0.472	0.482	0.482	0.366	0.596	0.576
55	0.465	0.515	0.515	0.356	0.516	0.440
56	0.456	0.536	0.536	0.352	0.132	0.259
57	0.449	0.379	0.379	0.347	0.257	0.226
58	0.444	0.354	0.354	0.339	0.259	0.259
59	0.438	0.338	0.338	0.334	0.274	0.274
60	0.430	0.320	0.252	0.329	0.269	0.269
61	0.426	0.046	0.171	0.323	0.263	0.263
62	0.420	0.270	0.230	0.317	0.287	0.287
63	0.413	0.333	0.317	0.311	0.261	0.261
64	0.409	0.379	0.379	0.308	0.148	0.148
65	0.402	0.362	0.362	0.304	0.154	0.154
66	0.397	0.397	0.397	0.297	0.247	0.247
67	0.393	0.413	0.413	0.293	0.233	0.233
68	0.387	0.447	0.447	0.290	0.140	0.140
69	0.383	0.403	0.403	0.283	0.123	0.123
70	0.378	0.388	0.388	0.282	0.252	0.252
71	0.374	0.434	0.434	0.274	0.264	0.264
72	0.369	0.419	0.419	0.272	0.232	0.217
73	0.366	0.416	0.416	0.271	0.171	0.157
74	0.362	0.362	0.362	0.264	0.054	0.145
75	0.358	0.298	0.298	0.262	0.302	0.226
76	0.353	0.293	0.293	0.256	0.246	0.238
77	0.348	0.258	0.258	0.256	0.156	0.150
78	0.345	0.225	0.225	0.252	0.042	0.082
79	0.343	0.103	0.200	0.246	0.086	0.077

APPENDIX I (*continued*)

Z or N	$[d(Z)]_r$	$[d(Z)]_u$	$[d(Z)]_a$	$[d(N)]_r$	$[d(N)]_u$	$[d(N)]_a$
80	0.338	0.038	0.200	0.244	0.094	0.066
81	0.335	0.075	0.200	0.241	−0.009	0.261
82	0.331	1.051	1.051	0.238	0.968	0.724
83	0.327	1.997	1.997	0.234	1.524	1.524
84	0.324	0.394	0.394	0.231	0.761	0.590
85	0.320	0.120	0.200	0.231	0.261	0.296
86	0.318	−0.042	0.200	0.225	0.185	0.192
87	0.316	0.116	0.200	0.224	0.034	0.090
88	0.313	0.013	0.200	0.221	0.001	0.090
89	0.309	0.059	0.200	0.219	−0.061	0.090
90	0.304	0.234	0.234	0.214	0.024	0.090
91	0.302	0.172	0.172	0.214	0.044	0.090
92	0.300	0.170	0.170	0.212	0.122	0.086
93	0.298	0.238	0.238	0.208	0.148	0.126
94	0.293	0.253	0.253	0.207	0.147	0.147
95	0.292	0.292	0.292	0.203	0.183	0.183
96	0.291	0.281	0.281	0.202	0.202	0.202
97	0.286	0.286	0.286	0.198	0.228	0.228
98	0.285	0.285	0.285	0.197	0.217	0.217
99	0.282	0.282	0.282	0.197	0.227	0.227
100	0.281	0.281	0.281	0.193	0.223	0.223
101	0.276	0.276	0.276	0.192	0.222	0.222
102	0.273	0.273	0.273	0.189	0.199	0.199
103	0.273	0.273	0.273	0.187	0.197	0.197
104	0.270	0.290	0.290	0.186	0.186	0.186
105	0.268	0.338	0.338	0.185	0.195	0.195
106	0.266	0.366	0.366	0.181	0.181	0.181
107	0.263	0.333	0.333	0.179	0.189	0.189
108	0.261	0.311	0.311	0.179	0.199	0.199
109	0.259	0.299	0.299	0.177	0.187	0.187
110	0.256	0.296	0.296	0.177	0.187	0.187
111	0.255	0.265	0.265	0.172	0.172	0.172
112	0.254	0.254	0.254	0.171	0.181	0.181
113	0.252	0.242	0.242	0.170	0.180	0.180
114	0.247	0.227	0.227	0.169	0.179	0.179
115	0.249	0.219	0.219	0.166	0.186	0.186
116	0.244	0.204	0.204	0.164	0.184	0.184
117	0.244	0.194	0.194	0.165	0.185	0.185
118	0.242	0.172	0.172	0.162	0.152	0.180
119	0.241	0.151	0.151	0.160	−0.020	0.180
120	0.239	0.139	0.150	0.158	−0.442	0.180
121	0.238	−0.162	0.150	0.159	−0.331	0.180
122	0.235	−0.065	0.150	0.157	0.147	0.180
123	0.233	0.083	0.150	0.154	0.214	0.214
124	0.232	0.132	0.132	0.155	0.245	0.245
125	0.230	0.180	0.180	0.152	0.252	0.252
126	0.229	1.029	1.029	0.151	0.861	0.861
127	0.226	1.826	1.826	0.149	1.589	1.589
128	0.224	0.164	0.164	0.150	0.060	0.060
129	0.223	0.143	0.143	0.148	0.098	0.098
130	0.221	0.161	0.161	0.147	0.087	0.087
131	0.222	0.112	0.112	0.145	0.025	0.080
132			0.150	0.143	−0.097	0.080
133			0.150	0.143	0.003	0.080
134			0.150	0.140	0.030	0.080
135			0.150	0.139	0.059	0.080
136			0.150	0.140	0.090	0.090
137			0.150	0.139	0.079	0.100
138			0.150	0.136	0.056	0.100
139			0.150	0.137	0.047	0.100
140				0.135	0.025	0.100
141				0.133	0.083	0.100
142				0.132	0.212	0.212
143				0.131	0.141	0.141

APPENDIX I (*continued*)

Z or N	$[d(Z)]_r$	$[d(Z)]_u$	$[d(Z)]_a$	$[d(N)]_r$	$[d(N)]_u$	$[d(N)]_a$
144				0.132	0.132	0.132
145				0.129	0.169	0.169
146				0.130	0.230	0.230
147				0.129	0.149	0.149
148				0.126	0.116	0.116
149				0.127	0.077	0.077
150				0.125	0.035	0.035
151				0.123	0.133	0.133
152				0.123	0.163	0.163
153				0.122	0.492	0.492
154				0.122	0.112	0.112
155				0.120	0.100	0.100
156				0.119	0.109	0.109
157				0.118	0.108	0.108
158				0.119	0.109	0.109
159				0.116	0.116	0.116
160				0.118	0.108	0.108
161				0.114	0.114	0.114
162				0.115	0.115	0.115
163				0.114	0.114	0.114
164				0.112	0.112	0.112
165				0.113	0.113	0.113
166				0.112	0.112	0.112
167				0.111	0.101	0.101
168				0.111	0.091	0.091
169				0.109	0.089	0.089
170				0.110	0.090	0.090
171				0.107	0.077	0.077
172				0.108	0.078	0.078
173				0.107	0.077	0.077
174				0.106	0.066	0.080
175				0.106	0.036	0.080
176				0.104	−0.306	0.080
177				0.105	−0.205	0.080
178				0.103	−0.057	0.080
179				0.101	−0.019	0.080
180				0.103	0.003	0.080
181				0.102	0.032	0.080
182				0.099	0.029	0.080
183				0.101	0.051	0.080
184				0.099	0.859	0.859
185				0.099	1.979	1.979
186				0.097	0.017	0.017
187				0.099	0.019	0.019
188				0.099	0.019	0.019
189				0.095	0.005	0.050
190				0.096	−0.024	0.050
191				0.094	−0.116	0.050
192				0.094	−0.186	0.050
193				0.095	−0.165	0.050
194				0.094	0.014	0.050
195				0.094	0.064	0.064
196				0.091	0.071	0.071
197				0.093	0.103	0.103
198				0.091	0.111	0.111
199				0.093	0.113	0.113
200				0.089	0.109	0.109
201				0.089	0.109	0.109
202				0.090	−0.070	0.090
203				0.088	0.088	0.088
204				0.089	0.089	0.089
205				0.088	0.088	0.088
206				0.086	0.086	0.086
207				0.088	0.088	0.088

APPENDIX I (*concluded*)

Z or N	$[d(Z)]_r$	$[d(Z)]_u$	$[d(Z)]_a$	$[d(N)]_r$	$[d(N)]_u$	$[d(N)]_a$
208				0.086	0.086	0.086
209				0.085	0.085	0.085
210				0.086	0.086	0.086
211				0.085	0.085	0.085
212				0.084	0.084	0.084
213				0.084	0.084	0.084
214				0.084	0.084	0.084
215				0.084	0.084	0.084
216				0.081	0.081	0.081
217				0.082	0.082	0.082
218				0.081	0.081	0.081
219				0.083	0.083	0.083
220				0.082	0.082	0.082
221				0.079	0.079	0.079
222				0.080	0.080	0.080
223				0.081	0.081	0.081
224				0.081	0.081	0.081
225				0.078	0.078	0.078
226				0.078	0.078	0.078
227				0.079	0.079	0.079
228				0.078	0.078	0.078
229				0.079	0.079	0.079
230				0.076	0.076	0.076
231				0.077	0.077	0.077
232						0.075
233						0.075
234						0.075
235						0.075
236						0.075
237						0.075
238						0.075
239						0.075

SCATTERING FROM A SMALL ANISOTROPIC ELLIPSOID[1]

R. A. HURD

ABSTRACT

Scattering of an electromagnetic wave by a small ellipsoid having tensor permeability and dielectric properties is dealt with by expanding the fields as power series in λ^{-1}. Consideration has been given to the first three terms of the expansion.

INTRODUCTION

The problem of solving Maxwell's equations in an anisotropic medium for other than cylindrical coordinate systems is difficult, and to the author's knowledge, has received little attention in the literature. Jones (1945) has considered the case of an anisotropic ellipsoid in a static field, and some work has been done for ferrite-type anisotropy in spheres by Berk and Lengyel (1955), Ament and Passerini (1956), and Artman (1956, 1957).

In this paper we shall study the diffraction of a plane electromagnetic wave by an ellipsoid which has permeability and dielectric properties described by tensors

$$\mu = (\mu_{ij}), \quad \epsilon = (\epsilon_{ij}), \qquad i, j = 1, 2, 3.$$

It is assumed that the dimensions of the ellipsoid are small compared to the wavelength inside the ellipsoid. The solution is obtained by expanding the various field components as power series in λ^{-1} in the manner used by Stevenson (1953 *a*, *b*) for scattering from isotropic ellipsoids.

The first three terms of the series are considered. Explicit determination of the fields is not, however, carried out for the most general permeability and dielectric tensors, since this requires the inversion of matrices of rather large order. When somewhat less general tensors are considered explicit evaluation of the fields becomes feasible.

The case where the tensors have diagonal form is worked out, and in the paper following this, the coefficients are determined for a ferrite in which the steady magnetic field is applied along one of the principal axes of the ellipsoid.

GENERAL

We consider an ellipsoid, having the permeability and dielectric properties described above, with principal semi-axis $\sqrt{a_i}$ $(i = 1, 2, 3)$, and whose equation in rectangular coordinates x_i is*

$$\sum_i x_i^2/a_i = 1. \tag{1}$$

[1]Manuscript received March 3, 1958.
Contribution from the Radio and Electrical Engineering Division, National Research Council, Ottawa, Canada.
Issued as N.R.C. No. 4793.

*Summations and indices range over 1, 2, 3 unless otherwise indicated.

We introduce the elliptical coordinates ξ_i defined by the equations

$$\sum_i x_i^2/(a_i+\xi_j) = 1, \tag{2}$$

where $\xi_1 > -a_3$, $-a_3 > \xi_2 > -a_2$, $-a_2 > \xi_3 > -a_1$, and $a_1 > a_2 > a_3$. Thus the surface of the ellipsoid is described by $\xi_1 = 0$.

On the ellipsoid it is assumed that there is incident a plane electromagnetic wave $\mathscr{E}$, $\mathscr{H}$ whose rectangular components are

$$\mathscr{H}_i = m_i \exp\left(-ik \sum_j n_j x_j + iwt\right), \tag{3}$$

$$\mathscr{E}_i = Z_0 l_i \exp\left(-ik \sum_j n_j x_j + iwt\right), \tag{4}$$

with $Z_0 = \sqrt{\mu_0/\epsilon_0}$ and $k = 2\pi/\lambda$. The time dependence e^{iwt} will henceforth be omitted. Assuming that the magnetic field has unit amplitude, and since the fields $\mathscr{E}$ and $\mathscr{H}$ are orthogonal to each other and to the direction of propagation, it follows that

$$\sum l_i^2 = \sum m_i^2 = \sum n_i^2 = 1, \tag{5}$$

$$\sum l_i m_i = \sum m_i n_i = \sum n_i l_i = 0, \tag{6}$$

plus nine relations of the form

$$l_1 = m_2 n_3 - n_2 m_3. \tag{7}$$

Following Stevenson, the incident field is expanded as a power series in k.

$$\mathscr{H}_i = \sum_{n=0}^{\infty} (ik)^n \mathscr{H}_i^{(n)}. \tag{8}$$

Comparison of equations (3) and (8) yields

$$\mathscr{H}_i^{(n)} = (-1)^n m_i \left(\sum_j n_j x_j\right)^n \Big/ (n!). \tag{9}$$

We denote the external scattered fields by $\mathbf{E}$, $\mathbf{H}$, $\mathbf{D}$, $\mathbf{B}$, the internal fields by $\mathbf{e}$, $\mathbf{h}$, $\mathbf{d}$, $\mathbf{b}$, and expand each as power series in k

$$\mathbf{H} = \sum_{n=0}^{\infty} (ik)^n \mathbf{H}^{(n)}, \text{ etc.} \tag{10}$$

Substitution in Maxwell's equations yields the set of equations

$$\nabla \times \mathbf{H}^{(0)} = \nabla \times \mathbf{E}^{(0)} = \nabla \cdot \mathbf{B}^{(0)} = \nabla \cdot \mathbf{D}^{(0)} = 0, \tag{11}$$

$$\begin{cases} \nabla \times \mathbf{H}^{(n)} = c\mathbf{D}^{(n-1)}, \\ \nabla \times \mathbf{E}^{(n)} = -c\mathbf{B}^{(n-1)}, \\ \nabla \cdot \mathbf{B}^{(n)} = \nabla \cdot \mathbf{D}^{(n)} = 0, \quad \text{for } n > 0, \end{cases} \tag{12}$$

where c is the velocity of light in vacuum. The same set of equations holds for the internal field components. The M.K.S. unit system is employed.

Continuity of field components at $\xi_1 = 0$ leads to

$$(13)\qquad \begin{cases} [\mathbf{H}^{(n)} + \mathscr{H}^{(n)} - \mathbf{h}^{(n)}]_{\tan} = 0, \\ [\mathbf{B}^{(n)} + \mu_0 \mathscr{H}^{(n)} - \mathbf{b}^{(n)}]_{\text{norm}} = 0, \\ [\mathbf{E}^{(n)} + \mathscr{E}^{(n)} - \mathbf{e}^{(n)}]_{\tan} = 0, \\ [\mathbf{D}^{(n)} + \epsilon_0 \mathscr{E}^{(n)} - \mathbf{d}^{(n)}]_{\text{norm}} = 0. \end{cases}$$

We seek step-by-step solutions of equations (11) to (13) as far as $n = 2$ subject to the condition that the scattered fields should vanish at infinity.*

THE STATIC SOLUTION, MAGNETIC FIELD

When $n = 0$, the equations which have to be solved are

$$(14)\qquad \nabla \times \mathbf{H}^{(0)} = 0,$$

$$(15)\qquad \nabla \cdot \mathbf{H}^{(0)} = 0,$$

$$(16)\qquad \nabla \times \mathbf{h}^{(0)} = 0,$$

$$(17)\qquad \nabla \cdot \mathbf{b}^{(0)} = 0,$$

with

$$(18)\qquad b_i^{(0)} = \sum_j \mu_{ij} h_j^{(0)},$$

and $\mathscr{H}_i^{(0)} = m_i$; subject to boundary conditions (13).

From the analogy with the isotropic static case, we assume solutions in the form of gradients of potential functions, thus

$$(19)\qquad \mathbf{h}^{(0)} = \nabla \phi^{(0)},$$

$$(20)\qquad \mathbf{H}^{(0)} = \nabla \Phi^{(0)},$$

with $\phi^{(0)}$ given by

$$(21)\qquad \phi^{(0)} = \sum_i c_i x_i,$$

and

$$(22)\qquad \Phi^{(0)} = \sum_i A_i x_i I_i(\xi_1),\dagger$$

where c_i, A_i are independent of the variables x_i, and

$$(23)\qquad I_i(\xi_1) = \int_{\xi_1}^{\infty} \frac{du}{(a_i+u)R(u)},$$

$$(24)\qquad R(u) = [(a_1+u)(a_2+u)(a_3+u)]^{\frac{1}{2}}.$$

*That the fields vanish at infinity for the first three terms was shown by Stevenson. A similar analysis shows that this is also true for anisotropic scatterers.

†See, for example, Whittaker and Watson, Chap. XXIII.

For continuity of the tangential field components it is sufficient to ensure that the potentials are continuous across $\xi_1 = 0$. This gives

$$\sum_i c_i x_i = \sum_i A_i I_i x_i + \sum_i m_i x_i, \tag{25}$$

where the x_i are evaluated at $\xi_1 = 0$, and $I_i \equiv I_i(0)$. Equation (25) is satisfied independently of ξ_2 and ξ_3 if

$$c_i = A_i I_i + m_i. \tag{26}$$

To evaluate the normal components, we have, for the normal component of any vector $\mathbf{V}$ with rectangular components V_i,

$$V_{\xi 1} = U_1 \sum_i V_i \, \partial x_i / \partial \xi_1 \tag{27}$$

where U_1 is a scale factor whose value is of no consequence. From consideration of equation (2) it follows that

$$\partial x_i / \partial \xi_j = \tfrac{1}{2} x_i / (\xi_j + a_i). \tag{28}$$

Hence, using equations (18), (21), (27), and (28), and putting $\xi_1 = 0$,

$$b_{\xi 1}^{(0)} = \tfrac{1}{2} U_1 \sum_{i,j} x_i \mu_{ij} c_j / a_i, \tag{29}$$

and for the incident field

$$\mathscr{H}_{\xi 1}^{(0)} = \tfrac{1}{2} U_1 \sum_i m_i x_i / a_i. \tag{30}$$

Now taking the ξ_1 gradient of $\Phi^{(0)}$ and putting $\xi_1 = 0$ we obtain

$$H_{\xi 1}^{(0)} = U_1 \sum_i (\tfrac{1}{2} I_i - A) x_i A_i / a_i \tag{31}$$

where $A = (a_1 a_2 a_3)^{-\frac{1}{2}}$.

The continuity of normal components then yields

$$\sum_j \mu_{ij} c_j = \mu_0 (I_i - 2A) A_i + \mu_0 m_i. \tag{32}$$

Eliminating A_i between equations (26) and (32) we find

$$\sum_j [\mu_{ij} - \mu_0 (1 - 2A / I_i) \delta_{ij}] c_j = 2\mu_0 m_i A / I_i, \tag{33}$$

where δ_{ij} is Kronecker's symbol,

$\delta_{ii} = 1$,

$\delta_{ij} = 0$, when $i \neq j$.

Calling the determinant of the system Δ and the minors M_{ij}, the solutions of equation (33) are given by

$$c_j = 2\mu_0 \Delta^{-1} \sum_i m_i M_{ij} / I_i. \tag{34}$$

The A_i are then readily found from equation (26).

The zero order electric fields are written in the form

$$\mathbf{E}^{(0)} = \nabla \bar{\Phi}^{(0)}, \quad \mathbf{e}^{(0)} = \nabla \bar{\phi}^{(0)}$$

with

$$\bar{\Phi}^{(0)} = \sum_i \bar{A}_i x_i I_i(\xi_1), \quad \bar{\phi}^{(0)} = \sum_i \bar{c}_i x_i.$$

The coefficients $\bar{A}_i$, $\bar{c}_i$ are found from the A_i, c_i by making the substitutions $m_i \rightarrow Z_0 l_i$, $\mu_{ij} \rightarrow \epsilon_{ij}$, and $\mu_0 \rightarrow \epsilon_0$ in equations (33) and (26).

In future a bar over a quantity will indicate the corresponding electric component.

THE FIRST ORDER MAGNETIC FIELD

From equation (12) the equations to be solved are

$$\nabla \times \mathbf{H}^{(1)} = c\mathbf{D}^{(0)}, \tag{35}$$

$$\nabla \cdot \mathbf{H}^{(1)} = 0, \tag{36}$$

$$\nabla \times \mathbf{h}^{(1)} = c\mathbf{d}^{(0)}, \tag{37}$$

$$\nabla \cdot \mathbf{b}^{(1)} = 0, \tag{38}$$

with $\mathscr{H}_i^{(1)} = -m_i \sum_j x_j n_j$ and

where the components of $\mathbf{D}^{(0)}$ and $\mathbf{d}^{(0)}$ are given by

$$D_i^{(0)} = \epsilon_0 \left\{ \bar{A}_i I_i(\xi_1) + \sum_j \bar{A}_j x_j \frac{\partial I_j(\xi_1)}{\partial x_i} \right\}, \tag{39}$$

$$d_i^{(0)} = \sum_j \epsilon_{ij} \bar{c}_j. \tag{40}$$

We seek a solution to equations (35) and (36) of the form $\mathbf{H}^{(1)} = \mathbf{G}^{(1)} + \mathbf{F}^{(1)}$ where $\mathbf{G}^{(1)}$ is a particular solution of $\nabla \times \mathbf{G}^{(1)} = c\mathbf{D}^{(0)}$, $\nabla \cdot \mathbf{G}^{(1)} = 0$, and $\mathbf{F}^{(1)}$ is the gradient of a harmonic function. The particular function $\mathbf{G}^{(1)}$ can be taken from Stevenson's paper. Thus

$$G_i^{(1)} = \sum_j G_{ij} x_j I_j(\xi_1), \tag{41}$$

where $G_{ii} = 0$, $G_{ij} = -G_{ji}$,

and

$$G_{12} = \epsilon_0 c \bar{A}_3, \qquad (P)^*. \tag{42}$$

To find the complementary function we put $\mathbf{F}^{(1)} = \nabla \Phi^{(1)}$, where $\Phi^{(1)}$ is a potential function of degree 2. The most general exterior harmonic function of this degree is

$$\Phi^{(1)} = BX_r T_r(\xi_1) + B'X_r' T_r'(\xi_1) + x_1 x_2 x_3 \sum_i B_i J_i(\xi_1)/x_i \tag{43}$$

*The symbol (P) following an equation will henceforth be used to indicate that the cyclic permutations of the equation hold.

where B, B', and B_i are coefficients to be determined, and

$$X_\nu = R^2(\nu)\Theta(\nu),$$

$$\Theta(\nu) = \sum_i x_i^2/(a_i+\nu) - 1,$$

$$T_\nu(\xi_1) = \int_{\xi_1}^{\infty} \frac{du}{(u-\nu)^2 R(u)},$$

$$J_i(\xi_1) = \int_{\xi_1}^{\infty} \frac{(a_i+u)du}{R^3(u)},$$

and ν, ν' are roots of the quadratic equation

$$\beta(\nu) \equiv \sum_i (a_i+\nu)^{-1} = 0. \tag{44}$$

To satisfy equations (37) and (38), the interior fields are taken to be of the form

$$h_i^{(1)} = \sum_j g_{ij}x_j; \tag{45}$$

and therefore

$$b_i^{(1)} = \sum_{j,k} \mu_{ij}g_{jk}x_k. \tag{46}$$

Using equations (37) and (45) we obtain

$$g_{21} - g_{12} = cd_3^{(0)}, \qquad (P). \tag{47}$$

Substitution of equation (46) into equation (38) gives

$$\sum_{i,j} \mu_{ij}g_{ji} = 0. \tag{48}$$

Matching of the normal fields at $\xi_1 = 0$ leads to

$$\begin{aligned} &-\sum_{i,j} n_i m_j x_i x_j/a_j + \sum_{i,j} G_{ij}I_j x_i x_j/a_i \\ &+2BR^2(\nu)(T_\nu + A/\nu)\sum_i x_i^2 a_i^{-1}(a_i+\nu)^{-1} + 2B'R^2(\nu')(T_\nu' + A/\nu') \\ &\qquad \times \sum_i x_i^2 a_i^{-1}(a_i+\nu')^{-1} \\ &+x_1x_2x_3 \sum_i B_i x_i^{-1}[J_i(\beta(0) - a_i^{-1}) - 2Aa_i] = \mu_0^{-1} \sum_{i,j,k} x_i x_k \mu_{ij} g_{jk}/a_i. \end{aligned} \tag{49}$$

Continuity of the tangential components yields

$$\begin{aligned} &-\sum_{i,j} n_i m_j x_i x_j/(a_j+\xi) + \sum_{i,j} G_{ij}I_j x_i x_j/(a_i+\xi) \\ &+2BT_\nu R^2(\nu) \sum_i x_i^2 (a_i+\nu)^{-1}(a_i+\xi)^{-1} + 2B'T_\nu' R^2(\nu') \\ &\qquad \times \sum_i x_i^2 (a_i+\nu)^{-1}(a_i+\xi)^{-1} \\ &+x_1x_2x_3 \sum_i B_i J_i[\beta(\xi) - (a_i+\xi)^{-1}] = \sum_{i,j} g_{ij}x_i x_j/(a_i+\xi), \end{aligned} \tag{50}$$

where ξ stands for either of tangential variables ξ_2 or ξ_3. Equating coefficients of $x_i x_j$ in equation (49) gives

$$(51)\quad -n_i m_i + 2BR^2(\nu)(T_\nu + A/\nu)/(a_i+\nu) + 2B'R^2(\nu')(T_\nu + A/\nu')/(a_i+\nu') = \mu_0^{-1} \sum_j \mu_{ij} g_{ji},$$

and

$$(52)\quad -n_i m_j/a_j - n_j m_i/a_i + G_{ij} I_j/a_i + G_{ji} I_i/a_j + B_l[J_l(1/a_i + 1/a_j) - 2a_l A^3] = \mu_0^{-1}\left(\sum_k \mu_{ik} g_{kj}/a_i + \sum_k \mu_{jk} g_{ki}/a_j\right).$$

In equation (52) the indices i, j, l are unequal. The tangential equations (50) yield

$$(53)\quad -n_i m_i + 2BT_\nu R^2(\nu)/(a_i+\nu) + 2B'T_\nu' R^2(\nu')/(a_i+\nu') - g_{ii} = 2\lambda/a_i,$$

$$(54)\quad -n_i m_j + G_{ji} I_i + B_k J_k = g_{ji} \qquad (i, j, k \text{ unequal}).$$

In equation (53) a new unknown λ is introduced because the variables $x_i^2/(a_i+\xi)$ are not all independent, being connected by

$$(55)\quad \sum_i x_i^2 a_i^{-1}(a_i+\xi)^{-1} = 0.$$

Relation (55) is established by differentiating the equation of the ellipsoid (1) with respect to either of the tangential variables ξ and using equation (28).

It is apparent that equation (54) and the electric version of equation (32) imply equation (47). Also, by summing equation (51) with respect to i, using equation (44) and the orthogonal property of the m_i and n_i, we find $\sum_{i,j} \mu_{ij} g_{ji} = 0$ and hence equation (48) is satisfied. We are thus reduced to 15 equations in the 15 unknowns B_i, B, B', λ, and g_{ij}. The g_{ij} can be eliminated from equations (51) to (54) leaving a set of six equations. The 6×6 matrix of the set has all but three of its positions non-zero, so inversion of it will be, in general, a tiresome task.

Before proceeding to the third term, we need expressions for the second term electric field. These are obtained by writing $-A_i$, $-c_i$ for $\bar{A}_i$ and $\bar{c}_i$; and making the substitutions $\mu_{ij} \leftrightarrow \epsilon_{ij}$, $\mu_0 \leftrightarrow \epsilon_0$ and $m_i \rightarrow Z_0 l_i$ elsewhere.

THE SECOND ORDER MAGNETIC FIELD

The fields of order k^2 satisfy the equations

$$(56)\quad \nabla \times \mathbf{H}^{(2)} = c\mathbf{D}^{(1)},$$

$$(57)\quad \nabla \cdot \mathbf{H}^{(2)} = 0,$$

$$(58)\quad \nabla \times \mathbf{h}^{(2)} = c\mathbf{d}^{(1)},$$

$$(59)\quad \nabla \cdot \mathbf{b}^{(2)} = 0,$$

with an incident field component given by

$$(60)\quad \mathscr{H}_i^{(2)} = \tfrac{1}{2} m_i \left(\sum_j n_j x_j\right)^2.$$

As before, solutions in the form of $\mathbf{H}^{(2)} = \mathbf{F}^{(2)}+\mathbf{G}^{(2)}$ are sought. The particular function $\mathbf{G}^{(2)}$ may be taken from Stevenson's paper:

$$(61)\quad \mathbf{G}_1^{(2)} = -\tfrac{1}{2}A_1[\sum_i x_i^2 I_i(\xi_1)-I(\xi_1)]-\tfrac{1}{2}\epsilon_0 c\bar{B}_1[x_1^2 J_2(\xi_1)+x_2^2 J_1(\xi_1)$$
$$+3x_3^2 I_{33}(\xi_1)-I_3(\xi_1)]+\epsilon_0 c\bar{B}_2 x_1 x_2 J_3(\xi_1)+\epsilon_0 c\bar{C}_1 x_2 x_3 J_1(\xi_1)+\partial\psi/\partial x_1, \quad (P),$$

where

$$\psi = \sum_i A_i\psi_i,$$

$$\psi_i = (1/10)x_i I_i(\xi_1)\sum_j x_j^2-(1/5)x_i I(\xi_1),$$

and

$$I(\xi_1) = \int_{\xi_1}^{\infty}\frac{du}{R(u)},$$

$$I_{11}(\xi_1) = \int_{\xi_1}^{\infty}\frac{du}{(a_i+u)^2 R(u)}, \quad (P),$$

$$\bar{C}_1 = (a_2-a_3)[(a_1+\nu)\bar{B}+(a_1+\nu')\bar{B}'], \quad (P).$$

In equation (61) the quantities $\bar{B}_i$, $\bar{B}$ are the coefficients of the first order electric field.

The complementary function takes the form $\mathbf{F}^{(2)} = \nabla\Phi^{(2)}$ where $\Phi^{(2)}$ is the third degree exterior harmonic function.

$$(62)\quad \Phi^{(2)} = \sum_i x_i[\Theta_i K_i(\xi_1)E_i+\Theta_i' K_i'(\xi_1)E_i']+Ex_1x_2x_3K(\xi_1)+\sum_i D_i x_i I_i(\xi_1),$$

with

$$\Theta_i = \sum_j x_j^2/(a_j+\nu_i)-1,$$

$$K_i(\xi_1) = \int_{\xi_1}^{\infty}\frac{du}{(a_i+u)(u-\nu_i)^2 R(u)},$$

$$K(\xi_1) = \int_{\xi_1}^{\infty}\frac{du}{R^3(u)},$$

and the ν_i, ν_i' are defined as the two roots of the equation

$$(63)\qquad \sum_j (1+2\delta_{ij})/(a_j+\nu_i) = 0.$$

E_i, E_i', E, and D_i are 10 coefficients which have to be determined.

For the internal field we assume an expansion of the form

$$(64)\qquad h_i^{(2)} = \tfrac{1}{2}\sum_{j,k} d_{ijk}x_j x_k+e_i$$

with $d_{ijk} = d_{ikj}$.

Substitution in the curl equation (58) yields

$$(65)\qquad \sum_{j,k}\epsilon_{ijk}d_{kje} = c\sum_j \epsilon_{ij}\bar{g}_{je},$$

where ϵ_{ijk} is the permutation symbol; $\epsilon_{ijk} = 0$ if any of i, j, k are equal; $\epsilon_{ijk} = 1$ if i, j, k are an even permutation of 1, 2, 3, and otherwise $\epsilon_{ijk} = -1$.

Since d_{ijk} is symmetric in j, k and ϵ_{ijk} is skew in these indices, it follows that

$$\sum_{i,j,k} \epsilon_{ijk} d_{kji} = 0.$$

Hence

$$\sum_{i,j} \epsilon_{ij} \bar{g}_{ji} = 0, \tag{66}$$

which is satisfied in virtue of the electric analogue of equation (48).

Taking the divergence of $\mathbf{b}^{(2)}$ and equating coefficients of x_k to zero gives

$$\sum_{i,j} \mu_{ij} d_{jik} = 0. \tag{67}$$

The normal field components are now calculated. When the coefficients of x_1^3, $x_1x_2^2$, $x_1x_3^2$, x_1 etc. are successively equated to zero, we obtain

$$\mu_0[g_iE_i/(a_j+\nu_i)+g_i'E_i'/(a_j+\nu_i')+X_{ij}]-(1/4a_i)\sum_k \mu_{ik}d_{kjj} - (1/2a_j)(1-\delta_{ij})\sum_k \mu_{jk}d_{kij} = \lambda_i/a_j, \tag{68}$$

$$\mu_0[g_iE_i+g_i'E_i'-(\tfrac{1}{2}I_i-A)D_i/a_i-U_i]+(1/2a_i)\sum_k \mu_{ik}e_k = \lambda_i, \tag{69}$$

where

$$\left.\begin{aligned}
X_{11} &= a_1^{-1}[\tfrac{1}{4}m_1n_1^2-\tfrac{1}{4}(A_1I_1+\epsilon_0c\bar{B}_1J_2)+(1/10)A_1(\tfrac{1}{2}I_1-A)],\\
X_{12} &= a_1^{-1}[\tfrac{1}{4}m_1n_2^2-\tfrac{1}{4}(A_1I_2+\epsilon_0c\bar{B}_1J_1)+(1/10)A_1(\tfrac{1}{2}I_1-A)]\\
&\qquad +(1/2a_2)m_2n_1n_2,\\
X_{13} &= a_1^{-1}[\tfrac{1}{4}m_1n_3^2-\tfrac{1}{4}(A_1I_3+3\epsilon_0c\bar{B}_1I_{33})+\tfrac{1}{2}\epsilon_0c\bar{B}_1J_2+(1/10)A_1(\tfrac{1}{2}I_1-A)]\\
&\qquad +(1/2a_3)m_3n_1n_3,\\
U_1 &= (1/4a_1)(A_1I+\epsilon_0c\bar{B}_1I_3)+(1/10)A_1(I_1+2A-I/a_1),\\
g_i &= (1/2a_i-1/\nu_i)K_i-A/a_i\nu_i^2,
\end{aligned}\right\} \quad (P)$$

with $K_i \equiv K_i(0)$, and where λ_i is introduced because the variables x_i are constrained by equation (1).

The E_i, E_i' are eliminated from equations (58) by multiplying by $1+2\delta_{ij}$, summing on j, and using equation (63). This gives λ_i in terms of the coefficients d_{ijk}, thus

$$(\gamma_i+1)\lambda_i = a_i\mu_0\left(2X_{ii}+\sum_j X_{ij}\right)-\tfrac{1}{4}\sum_{k,j}\mu_{ik}d_{kjj}-\tfrac{1}{2}\sum_k \mu_{ik}d_{kii} - \tfrac{1}{2}a_i\sum_{j,k}(1-\delta_{ij})\mu_{jk}d_{kij}/a_j, \tag{70}$$

where $\gamma_1 = 2+a_1/a_2+a_1/a_3$, (P).

An additional relation is obtained by setting the coefficient of $x_1x_2x_3$ equal to zero:

$$(71)\quad E(K\beta(0)-A^3)+m_1n_2n_3/a_1+m_2n_3n_1/a_2+m_3n_1n_2/a_3 +\epsilon_0 c\sum_i \bar{C}_i J_i/a_i = \mu_0^{-1}\sum_i (\mu_{1i}d_{i23}+\mu_{2i}d_{i31}+\mu_{3i}d_{i12}).$$

Matching the tangential fields leads to a more complicated set of equations. From the terms in $x_1^3/(a_1+\xi)$, $x_1x_2^2/(a_2+\xi)$, $x_1x_3^2/(a_3+\xi)$ we have

$$(72)\quad (3/2)[E_1K_1/(a_1+\nu_1)+E_1'K_1'/(a_1+\nu_1')]+Y_{11}-\tfrac{1}{4}d_{111}+N_1 = 2M_1/a_1,$$

$$(73)\quad E_1K_1/(a_2+\nu_1)+E_1'K_1'/(a_2+\nu_1')+Y_{12}-\tfrac{1}{2}d_{212} = M_1/a_2,$$

$$(74)\quad E_1K_1/(a_3+\nu_1)+E_1'K_1'/(a_3+\nu_1')+Y_{13}-\tfrac{1}{2}d_{313} = M_1/a_3.$$

From the terms involving $x_1^3/(a_1+\xi)$, $x_1x_2^2/(a_1+\xi)$, $x_1x_3^2/(a_1+\xi)$, and $x_1/(a_1+\xi)$ we find

$$(75)\quad (3/2)[E_1K_1/(a_1+\nu_1)+E_1'K_1'/(a_1+\nu_1')]+Y_{11}-\tfrac{1}{4}d_{111}-N_1 = 2\Lambda_1/a_1,$$

$$(76)\quad \tfrac{1}{2}[E_1K_1/(a_2+\nu_1)+E_1'K_1'/(a_2+\nu_1')]+Z_{12}-\tfrac{1}{4}d_{122} = \Lambda_1/a_2,$$

$$(77)\quad \tfrac{1}{2}[E_1K_1/(a_3+\nu_1)+E_1'K_1'/(a_3+\nu_1')]+Z_{13}-\tfrac{1}{4}d_{133} = \Lambda_1/a_3,$$

$$(78)\quad -\tfrac{1}{2}(E_1K_1+E_1'K_1')+V_1+\tfrac{1}{2}D_1I_1-\tfrac{1}{2}e_1 = -\Lambda_1,$$

where

$$\left.\begin{aligned} Y_{11} &= \tfrac{1}{4}m_1n_1^2-\tfrac{1}{4}(A_1I_1+\epsilon_0c\bar{B}_1J_2)+(3/20)A_1I_1,\\ Y_{12} &= \tfrac{1}{2}m_2n_1n_2+(1/10)A_1I_1,\\ Y_{13} &= \tfrac{1}{2}m_3n_1n_3+\tfrac{1}{2}\epsilon_0c\bar{B}_1J_2+(1/10)A_1I_1,\\ Z_{12} &= \tfrac{1}{4}m_1n_2^2-\tfrac{1}{4}(A_1I_2+\epsilon_0c\bar{B}_1J_1)+(1/20)A_1I_1,\\ Z_{13} &= \tfrac{1}{4}m_1n_3^2-\tfrac{1}{4}(A_1I_3+3\epsilon_0c\bar{B}_1I_{33})+(1/20)A_1I_1,\\ V_1 &= \tfrac{1}{4}(A_1I+\epsilon_0c\bar{B}_1I_3)-(1/10)A_1I. \end{aligned}\right\}\quad (P).$$

There are two more sets of cyclic permutations of equations (72) to (78). The coefficients Λ_1 and M_1 have been introduced because of the restraints contained in equations (1) and (55) respectively. N_1 is needed to ensure that the two sets of tangential equations are consistent.

An additional relation is obtained from the terms involving $x_1x_2x_3/(a_1+\xi)$:

$$(79)\quad EK+m_1n_2n_3+\epsilon_0c\bar{C}_1J_1-d_{123} = 0, \qquad (P).$$

By using equation (51) (electric) and equation (65) it may be shown that the cyclic variations of equation (79) are redundant.

To determine Λ_1, M_1, N_1 we proceed as follows: equation (72) is multiplied by 2 and added to equations (73) and (74). Equation (63) is used, thus eliminating E_1 and E_1' and yielding

$$(80)\quad -\tfrac{1}{2}\sum_j d_{j1j}+2N_1 = (\gamma_1+2)M_1/a_1.$$

Similarly from equations (75) to (77)

$$(81)\qquad \tfrac{1}{4}m_1-\tfrac{1}{2}AA_1+\tfrac{1}{4}A_1I-\tfrac{1}{2}\epsilon_0c\bar{B}_1A/a_3-\tfrac{1}{4}\sum_j d_{1jj}-N_1=\gamma_1\Lambda_1/a_1.$$

Furthermore, from equations (72) and (75)

$$(82)\qquad \Lambda_1 = M_1-a_1N_1.$$

Equations (80) to (82) may now be solved for Λ_1, M_1, N_1. It turns out that only Λ_1 is required for subsequent use, since equations (73) and (74) can be shown to be implied by equations (76) and (77). It is found that

$$(83)\qquad 4(\gamma_1+1)\Lambda_1 = -a_1\sum_j d_{1jj}+4(\gamma_1+1)\Lambda_1',$$

where

$$(84)\quad 4(\gamma_1+1)\Lambda_1' = a_1(\gamma_1-2)^{-1}\Big\{2c\Big[\sum_j \epsilon_{3j}\bar{g}_{j2}-\sum_j \epsilon_{2j}\bar{g}_{j3}\Big] +\gamma_1[m_1-A_1(I_2+I_3)-2\epsilon_0c\bar{B}_1A/a_3]\Big\}.$$

If we now eliminate E_1, E_1' from equations (68), (76), and (77) we get

$$\begin{aligned}(85)\qquad &(2\mu_0g_1/K_1)\{[(\Lambda_1/a_2)-Z_{12}+\tfrac{1}{4}d_{122}](a_2+\nu_1')-[(\Lambda_1/a_3)-Z_{13}+\tfrac{1}{4}d_{133}](a_3+\nu_1')\}\\ &=\Big[\lambda_1-a_2X_{12}-\tfrac{1}{2}\sum_i \mu_{2i}d_{i12}-\tfrac{1}{4}(a_2/a_1)\sum_i \mu_{1i}d_{i22}\Big](1+\nu_1'/a_2)\\ &\quad-\Big[\lambda_1-a_3X_{13}-\tfrac{1}{2}\sum_i \mu_{3i}d_{i13}-\tfrac{1}{4}(a_3/a_1)\sum_i \mu_{1i}d_{i33}\Big](1+\nu_1'/a_3).\end{aligned}$$

A similar equation also holds except that ν_1 and ν_1' are interchanged throughout. Two more equations of cyclic form are obtained when the other E_i, E_i' are eliminated.

If E is eliminated between equations (71) and (79) we have

$$\begin{aligned}(86)\quad &\mu_0^{-1}\sum_i (\mu_{1i}d_{i23}+\mu_{2i}d_{i31}+\mu_{3i}d_{i12})-m_1n_2n_3/a_1-m_2n_3n_1/a_2-m_3n_1n_2/a_3\\ &-\epsilon_0c\sum_i \bar{C}_iJ_i/a_i = \Big(\sum_i a_i^{-1}-A^3/K\Big)(d_{123}-m_1n_2n_3-\epsilon_0c\bar{C}_1J_1).\end{aligned}$$

The above seven equations involve only the unknowns d_{ijk}. Together with the eight equations (65), and the three equations (67), we have a set of 18 equations in the 18 d_{ijk}. However, equations (65) and (67) are simple in form and may be used to eliminate 11 of the d_{ijk}, and we are left with a 7×7 set of equations in which all the matrix positions are non-zero.

Once the d_{ijk} have been determined the external coefficients E_i, E_i', E follow readily from the tangential equations (76), (77), and (79). Knowing the E's, the D_i, e_i may now be calculated from equations (69) and (78). If the e_i's are eliminated, the matrix which must be inverted is of order 3×3.

To find the electrical components of order 2, we make the substitutions $A_i\rightarrow\bar{A}_i$, $\bar{B}_i\rightarrow-B_i$, $\bar{B}\rightarrow-B$ wherever they occur explicitly, and make the substitutions $\mu_{ij}\leftrightarrow\epsilon_{ij}$, $\mu_0\leftrightarrow\epsilon_0$, $m_i\rightarrow Z_0l_i$, $Z_0l_i\rightarrow-m_i$ elsewhere.

THE FAR FIELD

Since the exterior fields for an anisotropic scatterer have the same form as in the isotropic case, the expression derived by Stevenson for the far field may be applied here, provided that the exterior coefficients are modified as above.

If R, θ, ϕ are the polar coordinates of the field point in the wave zone, then Stevenson shows that

$$(87)\qquad \begin{cases} E_\theta = Z_0 H_\phi = \left(\dfrac{\partial \bar{P}}{\partial \theta} + \dfrac{Z_0}{\sin\theta}\dfrac{\partial P}{\partial \phi}\right)\dfrac{e^{-ikR}}{R}, \\ E_\phi = -Z_0 H_\theta = \left(\dfrac{1}{\sin\theta}\dfrac{\partial \bar{P}}{\partial \phi} - Z_0\dfrac{\partial P}{\partial \theta}\right)\dfrac{e^{-ikR}}{R}, \end{cases}$$

where

$$(88)\qquad P = \tfrac{1}{2}k^2 S_1^{(0,3)} + k^4\left[-\tfrac{1}{2}S_1^{(2,3)} - (1/18)S_2^{(1,4)} + (1/18)S_3^{(2,3)}\right]$$

and

$$(89)\qquad \begin{aligned} S_1^{(0,3)} &= -(4/3)\sum_i \alpha_i A_i, \\ S_2^{(1,4)} &= \sum_i p_i \alpha_i^2 + \alpha_1\alpha_2\alpha_3 \sum_i q_i/\alpha_i, \\ S_1^{(2,3)} &= \sum_i r_i \alpha_i, \\ S_3^{(2,3)} &= (2/5)\sum_i A_i \alpha_i\left[\sum_j a_j \alpha_j^2 - (1/5)\sum_j a_j(1+2\delta_{ij})\right], \end{aligned}$$

where

$$\alpha_i = x_i/R,$$

and

$$(P)\qquad \left.\begin{aligned} p_1 &= -(6/5)[(a_2+\nu)(a_3+\nu)B + (a_2+\nu')(a_3+\nu')B'], \\ q_1 &= (2/5)[\epsilon_0 c(a_2-a_3)\bar{A}_1 - 3B_1], \\ r_1 &= (2/75)[3(2a_1-a_2-a_3)A_1 - 5\epsilon_0 c\bar{B}_1 - 50D_1]. \text{*} \end{aligned}\right\}$$

The expression for $\bar{P}$ is obtained from equation (89) by substituting electric for magnetic coefficients.

DIAGONAL DIELECTRIC AND PERMEABILITY TENSORS

When the dielectric and permeability tensors have the form

$$\epsilon = \begin{pmatrix} \epsilon_1 & 0 & \\ 0 & \epsilon_2 & \\ & & \epsilon_3 \end{pmatrix}, \qquad \mu = \begin{pmatrix} \mu_1 & 0 & \\ 0 & \mu_2 & \\ & & \mu_3 \end{pmatrix},$$

*The formulae differ from Stevenson's because we use a slightly different definition for the coefficients and a different time dependence.

explicit determination of the fields becomes quite easy. It is found that the coefficients for the first term are

$$c_i = \frac{2\mu_0 m_i A}{(\mu_i-\mu_0)I_i+2\mu_0 A}, \tag{90}$$

$$A_i = \frac{(\mu_0-\mu_i)m_i}{(\mu_i-\mu_0)I_i+2\mu_0 A}. \tag{91}$$

For the second term we find

$$B_1 = \frac{a_3(1-\mu_2/\mu_0)(n_3m_2-\epsilon_0 c\bar{A}_1 I_3)+a_2(1-\mu_3/\mu_0)(n_2m_3+\epsilon_0 c\bar{A}_1 I_2)}{J_1[a_3(1-\mu_2/\mu_0)+a_2(1-\mu_3/\mu_0)]-2a_1A} \quad (P), \tag{92}$$

$$2BR^2(\nu) = \frac{S_1T_2'-S_2T_1'}{T_1T_2'-T_2T_1'}, \tag{93}$$

where

$$T_i = \frac{T_\nu(1-\mu_i/\mu_0)+A/\nu}{a_i+\nu}+\frac{\mu_i}{\mu_0}\frac{T_\nu}{a_i}\frac{\sum_j \mu_j(a_j+\nu)^{-1}}{\sum_j \mu_j/a_j} \qquad i=1,2,$$

$$S_i = (1-\mu_i/\mu_0)n_im_i+\frac{\mu_i}{a_i\mu_0}\frac{\sum_j \mu_j n_j m_j}{\sum_j \mu_j/a_j} \qquad i=1,2,$$

the primed quantities being obtained by replacing ν by ν' everywhere.

The internal coefficients g_{ij} may be readily obtained from equations (53) and (54), using equation (93) and the value of λ obtained from

$$\frac{2\lambda}{\mu_0}\sum_j \frac{\mu_j}{a_j} = -\frac{1}{\mu_0}\sum_j \mu_j n_j m_j+\frac{2BR^2(\nu)T_\nu}{\mu_0}\sum_j \frac{\mu_j}{a_j+\nu} + \frac{2B'R^2(\nu')T_\nu'}{\mu_0}\sum_j \frac{\mu_j}{a_j+\nu'}. \tag{94}$$

We shall not write down the complete set of coefficients for the third term since only the coefficients D_i are required to find the far field. The D_i are given by

$$10[(\mu_1-\mu_0)I_1+2\mu_0A]D_1 = m_1(\mu_0-\mu_1)\sum_i a_i n_i^2-\frac{2m_1\mu_1a_1}{\gamma_1-2} + \frac{2\mu_i c a_1(\epsilon_2\bar{g}_{23}-\epsilon_3\bar{g}_{32})}{\gamma_1-2}+A_1\Big\{2(\mu_0-\mu_1)I+\frac{1}{5}(3a_1+a_2+a_3)[(\mu_0-\mu_1)I_1-2\mu_0A] + 4\mu_0a_1A-\frac{2\mu_1a_1(I_1-2A)}{\gamma_1-2}\Big\}+2\epsilon_0c\bar{B}_1\Big\{(\mu_0-\mu_1)I_3+\frac{2\mu_1a_1A}{a_3(\gamma_1-2)}\Big\}, \quad (P). \tag{95}$$

The electric coefficients may be obtained from the magnetic terms by carrying out the substitutions referred to above; the far field may then be evaluated by using equations (87) to (89). The resulting expressions are rather lengthy, so will not be written down here.

REFERENCES

AMENT, W. S. and PASSERINI, H. J. 1956. Naval Research Laboratory Report 4747.
ARTMAN, J. O. 1956. Lincoln Laboratory Group Report M35-54.
——— 1957. J. Appl. Phys. **28**, 92.
BERK, A. D. and LENGYEL, B. A. 1955. Proc. Inst. Radio Engrs. **43**, 1587.
JONES, R. C. 1945. Phys. Rev. **68**, 93.
STEVENSON, A. F. 1953*a*. J. Appl. Phys. **24**, 1134.
——— 1953*b*. J. Appl. Phys. **24**, 1143.
WHITTAKER, E. T. and WATSON, G. N. 1946. A course of modern analysis (Cambridge University Press, London).

THE MAGNETIC FIELDS OF A FERRITE ELLIPSOID[1]

R. A. HURD

ABSTRACT

Approximate expressions are found for the internal and the adjacent external magnetic fields of a small ferrite ellipsoid under plane wave excitation. Consideration is given to the variation of apparent susceptibility with the size of the ferrite.

INTRODUCTION

In the preceding paper a power series solution in $1/\lambda$ (λ = wavelength) for the scattering of a plane wave from a small anisotropic ellipsoid was outlined. In the present paper these results are used to compute the magnetic field in and near a ferrite ellipsoid.

A plane wave is assumed to be incident on a ferrite particle whose permeability has the form

$$\mu = \begin{pmatrix} \mu & -i\kappa & 0 \\ i\kappa & \mu & 0 \\ 0 & 0 & \mu_3 \end{pmatrix}, \tag{1}$$

with a scalar dielectric constant. Terms as far as λ^{-1} are found for a general ellipsoid; the term in λ^{-2} is computed for a spheroid whose axis of symmetry is in the x_3 direction, i.e., the direction of the static magnetic field applied to the ferrite.

THE FORM OF THE FIELDS

A small ferrite ellipsoid with permeability properties described by equation (1) is located at the origin of the rectangular coordinate system x_i ($i=1, 2, 3$). The equation of the ellipsoid is

$$\sum_{i=1}^{3} x_i^2/a_i = 1.$$

Upon the ellipsoid there is incident a plane electromagnetic wave $\mathscr{E}$, $\mathscr{H}$ whose rectangular components are

$$\mathscr{H}_i = m_i \exp\left(-ik \sum_j n_j x_j + iwt\right),$$

$$\mathscr{E}_i = Z_0 l_i \exp\left(-ik \sum_j n_j x_j + iwt\right),$$

where $k = 2\pi/\lambda$ and $Z_0 = (\mu_0/\epsilon_0)^{\frac{1}{2}}$.

[1]Manuscript received March 3, 1958.
Contribution from the Radio and Electrical Engineering Division, National Research Council, Ottawa, Canada.
Issued as N.R.C. No. 4831.

The internal fields of the body are denoted by **e**, **h**; and the external scattered fields near the ellipsoid by **E**, **H**.

According to the previous paper the rectangular components of these fields are given by

$$h_i = c_i + ik\sum_j g_{ij}x_j - k^2\left[\tfrac{1}{2}\sum_{j,k} d_{ijk}x_jx_k + e_i\right] + O(k^3), \tag{2}$$

$$H_i = \partial\Phi^{(0)}/\partial x_i + ik[\partial\Phi^{(1)}/\partial x_i + G_i^{(1)}] - k^2[\partial\Phi^{(2)}/\partial x_i + G_i^{(2)}] + O(k^3), \tag{3}$$

with $d_{ijk}=d_{ikj}$, and where

$$\begin{aligned}
\Phi^{(0)} &= \sum_i A_i x_i I_i(\xi_1),\\
\Phi^{(1)} &= BX_\nu T_\nu(\xi_1) + B'X_\nu' T_\nu'(\xi_1) + x_1x_2x_3\sum_i B_i x_i^{-1} I_i(\xi_1),\\
\Phi^{(2)} &= \sum_i x_i\Theta_i E_i K_i(\xi_1) + \sum_i x_i\Theta_i' E_i' K_i'(\xi_1) + Ex_1x_2x_3K(\xi_1)\\
&\qquad + \sum_i D_i x_i I_i(\xi_1),\\
G_1^{(1)} &= \epsilon_0 c[\bar{A}_3 x_2 I_2(\xi_1) - \bar{A}_2 x_3 I_3(\xi_1)],\\
G_1^{(2)} &= -\tfrac{1}{2}A_1\left[\sum_i x_i^2 I_i(\xi_1) - I(\xi_1)\right] - \tfrac{1}{2}\epsilon_0 c\bar{B}_1[x_1^2 J_2(\xi_1) + x_2^2 J_1(\xi_1)\\
&\qquad + 3x_3^2 I_{33}(\xi_1) - I_3(\xi_1)] + \epsilon_0 c\bar{B}_2 x_1x_2 J_3(\xi_1) + \epsilon_0 c x_2x_3(a_2-a_3)\\
&\qquad \times[(a_1+\nu)\bar{B} + (a_1+\nu')\bar{B}']J_1(\xi_1) + \partial/\partial x_1\sum_i A_i\psi_i,
\end{aligned} \tag{4}$$

and in which

$$\psi_i = (1/10)x_iI_i(\xi_1)\sum_j x_j^2 - (1/5)x_iI(\xi_1).$$

In the above expressions, c is the velocity of light in vacuum, ξ_1 is the radial-type ellipsoidal coordinate ($\xi_1=0$ is the surface of the ferrite), and the coefficients c_i, g_{ij}, d_{ijk}, e_i, A_i, B, B', B_i, E_i, E_i', D_i, $\bar{A}_i$, $\bar{B}_i$, $\bar{B}$, $\bar{B}'$ are independent of the variables x_i, ξ_1. In equation (4) the x_1 components of the vectors $\mathbf{G}^{(1)}$ and $\mathbf{G}^{(2)}$ are given; the other components are obtained by cyclic permutation of all subscripts excepting of course the subscripts on ϵ_0, μ_0, and ξ_1. The remaining functions are given by

$$I(\xi_1) = \int\frac{du}{R(u)}, \qquad I_i(\xi_1) = \int\frac{du}{(a_i+u)R(u)},$$

$$I_{ii}(\xi_1) = \int\frac{du}{(a_i+u)^2R(u)}, \qquad J_i(\xi_1) = \int\frac{(a_i+u)du}{R^3(u)},$$

$$T_\nu(\xi_1) = \int\frac{du}{(u-\nu)^2R(u)}, \qquad K(\xi_1) = \int\frac{du}{R^3(u)},$$

$$K_i(\xi_1) = \int\frac{du}{(a_i+u)(u-\nu_i)^2R(u)},$$

$$X_\nu = R^2(\nu)\left[\sum_i x_i^2/(a_i+\nu)-1\right],$$

$$\Theta_i = \sum_j x_j^2/(a_j+\nu_i)-1,$$

where $R(u) = [(a_1+u)(a_2+u)(a_3+u)]^{\frac{1}{2}}$. The range of the integrations is from ξ_1 to ∞. The primed functions T_ν', K_i', etc. are obtained by substituting ν' and ν_i' for ν and ν_i respectively. The quantities ν, ν' are the two roots of the quadratic equation

$$\sum_i (a_i+\nu)^{-1} = 0$$

and ν_i, ν_i' are the roots of

$$\sum_j (1+2\delta_{ij})(a_j+\nu_i)^{-1} = 0.$$

The electric field components for the first two terms (which are needed to compute the higher order magnetic fields) are given by expressions identical in form with equations (2), (3), and (4) except that the coefficients c_i, g_{ij} . . . are replaced by $\bar{c}_i$, $\bar{g}_{ij}$ . . . etc.; and the vector $\mathbf{G}^{(1)}$ is replaced by $\bar{\mathbf{G}}^{(1)}$, $\bar{\mathbf{G}}^{(1)}$ being obtained from $\mathbf{G}^{(1)}$ by making the substitutions $\bar{A}_i \rightarrow -A_i$ and $\epsilon_0 \rightarrow \mu_0$.

THE ZERO ORDER TERM

The coefficients c_i, A_i are found to be

$$(5)\qquad \begin{cases} c_1 = \dfrac{2\mu_0 A}{\Delta_0}\left(\dfrac{m_1 f_2}{I_1}+\dfrac{i\kappa m_2}{I_2}\right), \\ c_2 = \dfrac{2\mu_0 A}{\Delta_0}\left(-\dfrac{i\kappa m_1}{I_1}+\dfrac{m_2 f_1}{I_2}\right), \\ c_3 = \dfrac{2\mu_0 m_3}{2\mu_0+(\mu_3-\mu_0)I_3/A}, \end{cases}$$

$$(6)\qquad A_i = (c_i-m_i)/I_i,$$

where

$$f_i = \mu-\mu_0(1-2A/I_i),$$
$$\Delta_0 = f_1 f_2-\kappa^2,$$
$$A = (a_1a_2a_3)^{-\frac{1}{2}}.$$

The electrical coefficients $\bar{c}_i$, $\bar{A}_i$ are

$$\bar{c}_i = \frac{2l_i A}{cI_i\bar{f}_i},$$

$$\bar{A}_i = \frac{l_i(1-\epsilon/\epsilon_0)}{cI_i\bar{f}_i},$$

where

$$\bar{f}_i = \epsilon-\epsilon_0(1-2A/I_i),$$

and

$$I_i \equiv I_i(0).$$

(This notation will be adopted for the other elliptic functions defined above.)

THE FIRST ORDER TERM

It is found that

$$B_1J_1 = (S_1R_2+i\kappa a_3S_2)(a_3^2\kappa^2-R_1R_2)^{-1},$$

$$B_2J_2 = (S_2R_1-i\kappa a_3S_1)(a_3^2\kappa^2-R_1R_2)^{-1},$$

$$B_3J_3\Delta_1 = O_3(W_1W_2'-W_2W_1')-i\kappa T_\nu Y(O_2W_1'-O_1W_2')-i\kappa T_\nu' Y'(O_1W_2-O_2W_1),$$

$$2BR^2(\nu)\Delta_1 = R_3(O_2W_1'-O_1W_2')-i(\kappa/\mu)O_3(a_1W_2'+a_2W_1')+(\kappa^2/\mu)T_\nu' Y'(a_1O_2+a_2O_1),$$

$$2B'R^2(\nu')\Delta_1 = R_3(O_1W_2-O_2W_1)+i(\kappa/\mu)O_3(a_1W_2+a_2W_1)-(\kappa^2/\mu)T_\nu Y(a_1O_2+a_2O_1),$$

where

$$S_1 = a_2(\mu_3-\mu_0)(n_2m_3+\epsilon_0c\bar{A}_1I_2)+a_3(\mu-\mu_0)(n_3m_2-\epsilon_0c\bar{A}_1I_3)+i\kappa a_3(n_3m_1+\epsilon_0c\bar{A}_2I_3),$$

$$S_2 = a_1(\mu_3-\mu_0)(n_1m_3-\epsilon_0c\bar{A}_2I_1)+a_3(\mu-\mu_0)(n_3m_1+\epsilon_0c\bar{A}_2I_3)-i\kappa a_3(n_3m_2-\epsilon_0c\bar{A}_1I_3),$$

$$R_1 = a_2(\mu_0-\mu_3)+a_3(\mu_0-\mu)-2\mu_0A/J_1,$$

$$R_2 = a_3(\mu_0-\mu)+a_1(\mu_0-\mu_3)-2\mu_0A/J_2,$$

$$R_3 = (\mu_0-\mu)(a_1+a_2)-2\mu_0A/J_3,$$

$$O_1 = (1-\mu_0/\mu_3)a_3n_3m_3-a_1[(1-\mu_0/\mu)n_1m_1-i(\kappa/\mu)(n_1m_2+\epsilon_0c\bar{A}_3I_1)],$$

$$O_2 = (1-\mu_0/\mu_3)a_3n_3m_3-a_2[(1-\mu_0/\mu)n_2m_2+i(\kappa/\mu)(n_2m_1-\epsilon_0c\bar{A}_3I_2)],$$

$$O_3 = (\mu-\mu_0)[a_2n_2m_1+a_1n_1m_2+\epsilon_0c\bar{A}_3(a_1I_1-a_2I_2)]-i\kappa(a_2n_2m_2-a_1n_1m_1),$$

$$W_i = \frac{a_i[(\mu_0-\mu)T_\nu+\mu_0A/\nu]}{\mu(a_i+\nu)}-\frac{a_3[(\mu_0-\mu_3)T_\nu+\mu_0A/\nu]}{\mu_3(a_3+\nu)}, \qquad i=1,2;$$

$$Y = \frac{a_2}{a_2+\nu}-\frac{a_1}{a_1+\nu},$$

$$\Delta_1 = -R_3(W_1W_2'-W_2W_1')+(\kappa^2/\mu)[T_\nu Y'(a_1W_2+a_2W_1)-T_\nu Y(a_1W_2'+a_2W_1')].$$

The internal coefficients g_{ij} are calculated from

$$g_{12} = -n_2m_1+\epsilon_0c\bar{A}_3I_2+B_3J_3,$$

$$g_{21} = g_{12}+\epsilon c\bar{c}_3,$$

and cyclic permutations thereof. The coefficients g_{ii} are given by

$$g_{ii} = -n_i m_i + (a_3/a_i)(1-\mu_0/\mu_3)n_3 m_3 + g(\nu) + g(\nu'),$$

where

$$g(\nu) = \frac{2BR^2(\nu)}{a_i(a_3+\nu)}\left[\frac{a_i-a_3}{a_i+\nu}\nu T_\nu + \frac{a_3\mu_0}{\mu_3}(T_\nu + A/\nu)\right].$$

The electric terms are

$$\bar{B}_1 J_1 = \frac{(\epsilon-\epsilon_0)[Z_0(a_2 n_2 l_3 + a_3 n_3 l_2) + \mu_0 c A_1(a_3 I_3 - a_2 I_2)]}{(\epsilon-\epsilon_0)(a_2+a_3)+2\epsilon_0 A/J_1},$$

with $\bar{B}_2$, $\bar{B}_3$ cyclic permutations of $\bar{B}_1$.

$$\bar{B} = Z_0(\epsilon_0-\epsilon)\sum_i n_i l_i (a_i+\nu)^{-1} \Big/ 6(\nu-\nu')[(\epsilon-\epsilon_0)T_\nu - \epsilon_0 A/\nu],$$

$\bar{B}'$ = same as $\bar{B}$ with ν and ν' interchanged.

$$\bar{g}_{12} = -Z_0 n_2 l_1 - \mu_0 c A_3 I_2 + \bar{B}_3 J_3$$

and cyclic permutations thereof. The remaining $\bar{g}_{ij}$ may be obtained from:

$$\bar{g}_{12} - \bar{g}_{21} = \mu_3 c c_3,$$

$$\bar{g}_{23} - \bar{g}_{32} = c(\mu c_1 - i\kappa c_2),$$

$$\bar{g}_{31} - \bar{g}_{13} = c(i\kappa c_1 + \mu c_2),$$

$$\bar{g}_{ii} = -Z_0 n_i l_i + \frac{2\bar{B}R^2(\nu)T_\nu}{a_i+\nu} + \frac{2\bar{B}'R^2(\nu')T_\nu'}{a_i+\nu'}.$$

THE SECOND ORDER TERM

Computation of the second order term for a general ellipsoid would involve considerable work; however, a reasonable simplification occurs if the calculation is done for a spheroid with $a_1=a_2$. In this case the quantities ν_i, ν_i' defined above become

$$\nu_1 = \nu_2 = \nu_3 = -a_1,$$
$$\nu_1' = \nu_2' = -(1/5)(a_1+4a_3),$$
$$\nu_3' = -(1/5)(3a_1+2a_3).$$

Furthermore it may be assumed without loss of generality that the direction of incidence lies in the x_1-x_3 plane, and thus $n_2=0$.

The following abbreviations are introduced:

$$\beta_i = \mu_0[a_i^{-1} - 2\nu_i^{-1} - 2A(a_i\nu_i^2 K_i)^{-1}],$$

β_i' = same as β_i with ν_i', K_i' replacing ν_i, K_i,

$$N_1 = \epsilon c[\mu_3\bar{g}_{23} - \mu\bar{g}_{32} + i\kappa\bar{g}_{31}],$$

$$N_2 = \epsilon c[\mu\bar{g}_{31} - \mu_3\bar{g}_{13} + i\kappa\bar{g}_{32}],$$

$$N_3 = \epsilon c[\mu(\bar{g}_{12} - \bar{g}_{21}) + i\kappa\bar{g}_{33}],$$

$$\Delta_2 = (\beta_1-3\mu/a_1)^2-(3\kappa/a_1)^2,$$

$$\Delta_3 = \tfrac{1}{4}a_1^{-1}\{3\mu_3[4+(a_1/a_3)(\mu_3/\mu)]-\beta_3'[2a_3+3a_1\mu_3/\mu]\},$$

$$\Delta_4 = [\beta_3-(2\mu/a_1)-\mu_3/a_3]^2-(2\kappa/\mu)^2,$$

$$\Delta_5 = \tfrac{1}{2}\mu_3 I_3+\mu_0 I_1,$$

$$\begin{aligned} Q_1 = {} & -\tfrac{1}{4}N_1+\tfrac{1}{4}i(\kappa/\mu)N_2-\tfrac{1}{2}\epsilon\mu_3 c(1-a_1/a_3)\bar{g}_{23} \\ & +\tfrac{1}{4}\mu_0[m_1-2n_1m_3n_3(1-a_1/a_3)] \\ & -\mu_0\{AA_1+\tfrac{1}{4}A_1I_1+\tfrac{1}{2}\epsilon_0 c\bar{B}_1[J_1(1-a_1/a_3)+A/a_3]\}, \end{aligned}$$

$$\begin{aligned} Q_2 = {} & -\tfrac{1}{4}N_2-\tfrac{1}{4}i(\kappa/\mu)N_1+\tfrac{1}{2}\epsilon\mu_3 c(1-a_1/a_3)\bar{g}_{13}+\tfrac{1}{4}\mu_0 m_2 \\ & -\mu_0[AA_2+\tfrac{1}{4}A_2I_1+\tfrac{1}{2}\epsilon_0 c\bar{B}_2A/a_1], \end{aligned}$$

$$\begin{aligned} X_1 = {} & \tfrac{1}{2}\epsilon\mu_3 c\bar{g}_{23}/a_3+\tfrac{1}{4}\mu_0(m_1n_3^2/a_1+2m_3n_1n_3/a_3)+\mu_0\{-\tfrac{1}{4}a_1^{-1}(A_1I_3 \\ & +3\epsilon_0 c\bar{B}_1I_{33})+\tfrac{1}{2}\epsilon_0 c\bar{B}_1J_1/a_3-(1/20)(I_1+I_3)A_1/a_1\}, \end{aligned}$$

$$\begin{aligned} X_2 = {} & -\tfrac{1}{2}\epsilon\mu_3 c\bar{g}_{13}/a_3+\tfrac{1}{4}\mu_0 m_2n_3^2/a_1-\mu_0\{\tfrac{1}{4}a_1^{-1}(A_2I_3+\epsilon_0 c\bar{B}_2J_1) \\ & +(1/20)(I_1+I_3)A_2/a_1\}, \end{aligned}$$

$$Z_1 = \tfrac{1}{4}m_1n_3^2-\tfrac{1}{4}(A_1I_3+3\epsilon_0 c\bar{B}_1I_{33})+(1/20)A_1I_1,$$

$$Z_2 = \tfrac{1}{4}m_2n_3^2-\tfrac{1}{4}(A_2I_3+\epsilon_0 c\bar{B}_2J_1)+(1/20)A_2I_1,$$

$$P_1 = \tfrac{1}{4}ca_1\{(\epsilon-\epsilon_0)(3+a_1/a_3)\bar{g}_{32}+\epsilon(1-\mu_3/\mu)\bar{g}_{23}-i\epsilon(\kappa/\mu)\bar{g}_{31}\},$$

$$P_2 = \tfrac{1}{4}c\{(\epsilon-\epsilon_0)(3a_3+a_1)\bar{g}_{31}-\epsilon a_1(1-\mu_3/\mu)\bar{g}_{13}-i\epsilon a_1(\kappa/\mu)\bar{g}_{32}\},$$

$$\begin{aligned} P_3 = {} & \tfrac{1}{4}c[4(1+a_3/a_1)(\epsilon-\epsilon_0)\bar{g}_{21}+2\epsilon(a_3/a_1)(\bar{g}_{12}-\bar{g}_{21})+3N_3/\mu] \\ & +(3+2a_3/a_1)[-\tfrac{1}{4}m_3n_1^2+\tfrac{1}{2}(I_1A_3+2\epsilon_0 c\bar{B}_3J_3)-(1/10)I_3A_3], \end{aligned}$$

$$L_1 = (a_2-a_3)[(a_1+\nu)\bar{B}+(a_1+\nu')\bar{B}'],$$

$$s_i = (4+a_3/a_1)(\beta_1'Z_i-X_i)+a_3^{-1}(Q_i-\beta_1'P_i), \quad i=1,2;$$

$$r_1 = -\tfrac{1}{4}i\kappa[4a_1^{-1}+\mu_3(a_3\mu)^{-1}],$$

$$r_2 = -\mu a_1^{-1}-(11/4)\mu_3a_3^{-1}+\tfrac{1}{4}\beta_1'[4+a_1\mu_3(a_3\mu)^{-1}],$$

$$\begin{aligned} T_1 = {} & i\kappa\epsilon ca_1^{-1}(\bar{g}_{12}+\bar{g}_{21})+\mu\epsilon ca_1^{-1}\bar{g}_{33}-\mu_3\epsilon ca_3^{-1}\bar{g}_{22}-\epsilon_0\mu_0 c\sum_j L_jJ_j/a_j \\ & -\mu_0m_2n_3n_1/a_1+\beta_3\epsilon_0 cL_1J_1, \end{aligned}$$

$$\begin{aligned} T_2 = {} & 2\epsilon ca_1^{-1}[\mu(\bar{g}_{12}+\bar{g}_{21})-i\kappa\bar{g}_{33}]+2\epsilon_0\mu_0 c\bar{B}_3(J_1a_1^{-1}-J_3a_3^{-1}) \\ & -\beta_3\epsilon_0 cL_1J_1-\mu_0(m_3n_1^2a_3^{-1}+2m_1n_3n_1a_1^{-1}), \end{aligned}$$

$$T = \Delta_4^{-1}[(\beta_3-2\mu a_1^{-1}-\mu_3a_3^{-1})T_2-4i\kappa T_1/a_1],$$

$$M_1 = -(1/5)[P_1+(a_3-a_1)Z_1]-\tfrac{1}{4}(A_1I+\epsilon_0 c\bar{B}_1I_3)+(1/10)A_1I,$$

$$M_2 = -(1/5)[P_2+(a_3-a_1)Z_2]-\tfrac{1}{4}(A_2I+\epsilon_0 c\bar{B}_2I_1)+(1/10)A_2I,$$

$$\begin{aligned} M_3 = {} & -(1/5)[Q_1+(a_3-a_1)X_1]-(1/20)\mu_0A_1(12I_1+5I_3) \\ & -\tfrac{1}{4}\mu_0\epsilon_0 ca_1^{-1}\bar{B}_1I_3, \end{aligned}$$

$$M_4 = -(1/5)[Q_2+(a_3-a_1)X_2]-(1/20)\mu_0 A_2(12I_1+5a_3I_3/a_1) -\tfrac{1}{4}\mu_0\epsilon_0 c a_1^{-1}\bar{B}_2 I_1,$$

$$M_5 = -(1/20)c[2(a_1+a_3)(\epsilon-\epsilon_0)\bar{g}_{21}+\epsilon(a_3-a_1)(\bar{g}_{12}-\bar{g}_{21})-i(\kappa/\mu)\epsilon a_1\bar{g}_{33}] +(1/5)(a_3-a_1)[\tfrac{1}{4}m_3n_1^2-\tfrac{1}{2}A_3I_1-\epsilon_0 c\bar{B}_3J_3+(1/10)A_3I_3] -(3/20)A_3I-\tfrac{1}{4}\epsilon_0 c\bar{B}_3I_1,$$

$$M_6 = -(1/20)\mu_0 m_3[n_3^2+(a_1/a_3)(1-n_3^2)]+(1/20)(a_1/a_3)(\mu_3/\mu)N_3 -(1/30)\epsilon_0\mu_0 c\bar{B}_3(J_1+4a_1J_3/a_3)+(1/50)\mu_0 A_3[7(I_1-a_1I_3/a_3)-3I_3 -22a_1I_1/a_3].$$

The coefficients then are

$$d_{133} = (r_1s_2+r_2s_1)(r_1^2+r_2^2)^{-1},$$

$$d_{122} = -\tfrac{1}{4}(\mu_3/\mu)d_{133}+\tfrac{1}{4}N_1/\mu-\tfrac{1}{2}\epsilon c\bar{g}_{32}-\tfrac{1}{4}\Delta_2^{-1}(\beta_1-3\mu_0/a_1)[(\beta_1-3\mu/a_1) \times m_1n_1^2-3i\kappa m_2n_1^2/a_1],$$

$$d_{111} = -d_{122}-(\mu_3/\mu)d_{133}+N_1/\mu,$$

$$d_{233} = (r_2s_2-r_1s_1)(r_1^2+r_2^2)^{-1},$$

$$d_{211} = -\tfrac{1}{4}(\mu_3/\mu)d_{233}+\tfrac{1}{4}N_2/\mu+\tfrac{1}{2}\epsilon c\bar{g}_{31}+\tfrac{1}{4}\Delta_2^{-1}(\beta_1-3\mu_0/a_1) \times[(\beta_1-3\mu/a_1)m_2n_1^2+3i\kappa m_1n_1^2/a_1],$$

$$d_{222} = -d_{211}-(\mu_3/\mu)d_{233}+N_2/\mu,$$

$$\Delta_3 d_{333} = 3a_3^{-1}\{\tfrac{1}{4}\mu_3N_3/\mu+\tfrac{1}{4}\mu_0m_3(4n_3^2a_3/a_1-n_1^2)+\mu_0A_3[(1/10)I_1(7-2a_3/a_1) -\tfrac{1}{2}I_3a_3/a_1]+\mu_0\epsilon_0 c\bar{B}_3(J_3-J_1a_3/a_1)\}-\beta_3'P_3,$$

$$\Delta_4 d_{123} = (\beta_3-2\mu a_1^{-1}-\mu_3a_3^{-1})T_1+i\kappa T_2/a_1,$$

$$d_{311} = \tfrac{1}{2}[T-(\mu_3/\mu)d_{333}+N_3/\mu],$$

$$d_{322} = \tfrac{1}{2}[-T-(\mu_3/\mu)d_{333}+N_3/\mu],$$

$$e_1 = -(1/10)(a_3-a_1\mu_3/\mu)d_{133}+2\Delta_0^{-1}\{f_1[\mu_0M_1(1-2A/I_1)-a_1M_3] +i\kappa[\mu_0M_2(1-2A/I_1)-a_1M_4]\},$$

$$e_2 = -(1/10)(a_3-a_1\mu_3/\mu)d_{233}+2\Delta_0^{-1}\{f_1[\mu_0M_2(1-2A/I_1)-a_1M_4] -i\kappa[\mu_0M_1(1-2A/I_1)-a_1M_3]\},$$

$$e_3 = -(1/10)(a_3-a_1\mu_3/\mu)d_{333}-\Delta_5^{-1}(2\mu_0I_1M_5+a_3I_3M_6),$$

$$\tfrac{1}{2}I_1D_1 = M_1+\tfrac{1}{2}e_1+(1/20)(a_3-a_1\mu_3/\mu)d_{133},$$

$$\tfrac{1}{2}I_2D_2 = M_2+\tfrac{1}{2}e_2+(1/20)(a_3-a_1\mu_3/\mu)d_{233},$$

$$D_3 = \Delta_5^{-1}(\mu_3M_5-a_3M_6),$$

$$\tfrac{1}{2}K_1'E_1' = (1/5)(a_3-a_1)(4+a_1/a_3)^{-1}\{[1+\tfrac{1}{4}a_1\mu_3(a_3\mu)^{-1}]d_{133}+a_3^{-1}P_1 -(4+a_1/a_3)Z_1\},$$

$$\tfrac{1}{2}K_2'E_2' = (1/5)(a_3-a_1)(4+a_1/a_3)^{-1}\{[1+\tfrac{1}{4}a_1\mu_3(a_3\mu)^{-1}]d_{233}+a_3^{-1}P_2 -(4+a_1/a_3)Z_2\},$$

$$\tfrac{1}{2}K_3'E_3' = (1/5)(a_3-a_1)(3+2a_3/a_1)^{-1}\{[\tfrac{1}{2}(a_3/a_1)+\tfrac{3}{4}\mu_3/\mu]d_{333}+P_3\},$$

$$E_1 = E_2 = E_3 = 0,$$

$$EK = d_{123}-\epsilon_0 cL_1J_1.$$

The electric components may be obtained from the above by making the substitutions given in the previous paper. The detailed results will not, however, be given here.

APPARENT SUSCEPTIBILITY AS A FUNCTION OF PARTICLE SIZE

Of current interest is the apparent susceptibility tensor which is defined as the ratio of the internal magnetization to the applied magnetic field. Thus, denoting the apparent susceptibility components by $\tilde{\mu}-\mu_0$ and $\tilde{\kappa}$, one has

$$b_1-\mu_0 h_1 = (\tilde{\mu}-\mu_0)m_1 - i\tilde{\kappa}m_2,$$

$$b_2-\mu_0 h_2 = i\tilde{\kappa}m_1 + (\tilde{\mu}-\mu_0)m_2,$$

where b_i is the internal magnetic induction. Using the static approximations for b_i and h_i it is found that

$$\tilde{\mu}-\mu_0 = \frac{2\mu_0 A}{I_1\Delta_0}[(\mu-\mu_0)f_1-\kappa^2],$$

$$\tilde{\kappa} = \frac{2\mu_0\kappa A}{I_1\Delta_0}[f_1+\mu_0-\mu]. \tag{7}$$

These relations are true when $a_1=a_2$; if $a_1 \neq a_2$ it is found that the apparent susceptibility no longer has the antisymmetric form of the ordinary susceptibility matrix.

From equation (7) it follows that, for a spheroid,

$$\tilde{\mu}\pm\tilde{\kappa}-\mu_0 = \frac{2\mu_0 A}{I_1}\cdot\frac{\mu\pm\kappa-\mu_0}{f_1\pm\kappa}. \tag{8}$$

This reduces to the values given by Spencer, Ault, and LeCraw (1956) in the particular cases of sphere, cylinder, and disk.

To find how the apparent susceptibility behaves as a function of particle size, higher order approximations to the interior fields are necessary. It is clear, however, that since the higher order magnetic components are functions of position within the ferrite, some other approach than the one above must be used. Two methods of handling this problem have been devised. Artman (1956, 1957) defines the apparent permeability in terms of the exterior fields, using the dipole moment of the particle as the fundamental quantity. The other approach, used by Tompkins and Spencer (1957), makes use of the cavity perturbation formula to define the apparent permeability. In this paper both methods are employed.

Consider two incident waves, ${}_1\mathscr{H}$ and ${}_2\mathscr{H}$, proceeding in the $+x_3$ direction, whose only non-vanishing field components are described by

$${}_1\mathscr{H}: \quad m_1 = 1,\ l_2 = 1$$

$${}_2\mathscr{H}: \quad m_2 = i,\ l_1 = -i.$$

Under this form of excitation one finds that, from equation (6),

$$A_1 I_1 = -(\mu+\kappa-\mu_0)(f_1+\kappa)^{-1},$$

and thus, writing $\psi_0 \equiv \tilde{\mu}+\tilde{\kappa}-\mu_0$, and using equation (8), it follows that

$$\psi_0 = -2\mu_0 A A_1.$$

Taking the third term of the series into account, the apparent susceptibility at finite size ψ may be defined by

$$\psi = -2\mu_0 A (A_1 - k^2 D_1), \tag{9}$$

so that for a spheroid, using the value of D_1, it is found that

$$\begin{aligned}\psi = \psi_0 &+ (1/5)\mu_0 k^2 (1+a_1/a_3)^{-1}\{(\psi_0/\mu_0)^2[\tfrac{1}{4}a_1(\epsilon/\epsilon_0)A^{-2}(I_1+I_3)^2 \\ &+ (\epsilon-\epsilon_0)(a_3 I_3 - a_1 I_1)^2 (2a_3 J_1 A \bar{R}_1)^{-1} + \tfrac{1}{4}A^{-1}(6a_1 I_1(1+a_1/a_3) \\ &+ 2a_3 I_3 - a_1 I_1^2/A)] + (\psi_0/\mu_0)[(\epsilon/\epsilon_0)a_1(I_1+I_3)/A - (\epsilon-\epsilon_0)(a_3 I_3 - a_1 I_1) \\ &\times (1-a_1/a_3)(\bar{R}_1 J_1)^{-1} - \tfrac{1}{2}(6a_1 - 2a_1 I_1/A + (4/5)a_3 + (6/5)a_1^2/a_3)] \\ &+ a_1(\epsilon-\epsilon_0)[\epsilon_0^{-1} + 2A(\bar{R}_1 J_1)^{-1}]\},\end{aligned} \tag{10}$$

where

$$\bar{R}_1 = (\epsilon-\epsilon_0)(a_1+a_3)J_1 + 2\epsilon_0 A.$$

For a cylinder of radius a, length c, $a \ll c$ formula (10) becomes

$$\begin{aligned}\psi = \psi_0[1-(2/25)k^2c^2] &+ (1/20)\mu_0 k^2 a^2[(1+\epsilon/\epsilon_0)(2+\psi_0/\mu_0)^2 \\ &+ (8/5)(\psi_0/\mu_0) - 8\epsilon(\epsilon+\epsilon_0)^{-1}(2+3\psi_0/\mu_0)] + O(k^2a^3/c).\end{aligned} \tag{11}$$

For the disk of radius a, thickness c, $a \gg c$ we obtain

$$\begin{aligned}\psi = \psi_0[1-(3/25)k^2a^2] &+ (1/20)\pi\mu_0 k^2 ac[3(\psi_0/\mu_0)^2 + (1-\epsilon_0/\epsilon)(\psi_0/\mu_0)] \\ &+ O(k^2c^2).\end{aligned} \tag{12}$$

The case of greatest current interest is that of the sphere, for which we find

$$\begin{aligned}\psi = \psi_0 &+ \mu_0 k^2 a^2[(1/90)(5+\epsilon/\epsilon_0)(3+2\psi_0/\mu_0)^2 - \psi_0/\mu_0 - 3/5 \\ &- \tfrac{1}{2}(\epsilon-\epsilon_0)(2\epsilon+3\epsilon_0)^{-1}],\end{aligned} \tag{13}$$

a being the radius of the sphere.

If the static magnetic field at which ψ_0 is resonant is denoted by H_0 and the resonant field of ψ by H; then from equation (13) it is found that

$$H \simeq H_0 + 4\pi M(5+\epsilon/\epsilon_0)(2/45)k^2a^2, \tag{14}$$

where $4\pi M$ is the magnetization. Formula (14) is derived under the assumptions that the imaginary part of ψ_0 is much larger than its real part near resonance, and that the resonance shift $H-H_0$ is much less than half the line width.

The method of Tompkins and Spencer makes use of the cavity perturbation formula

$$E\frac{\delta f}{f} = (\mu+\kappa-\mu_0)\int_v \mathbf{h} \cdot \mathscr{H}^* d\tau \tag{15}$$

where f is the frequency, E is a constant, and $\mathscr{H}$, $\mathbf{h}$ are the circularly polarized incident and internal magnetic fields. The integration is taken over the volume of the ferrite. Equation (15) holds when the sample is placed at a zero of electric field. For a sphere of radius a, it is found that

$$(16) \qquad E\frac{\delta f}{f} = \frac{8\pi a^3}{3}(\mu+\kappa-\mu_0)\left\{c_1-k^2\left[e_1+\frac{a^2}{10}(d_{111}+d_{122}+d_{133}+c_1)\right]\right\}.$$

As $a \to 0$, one has,

$$\psi_0 = \frac{3E}{8\pi a^3}\frac{\delta f}{f}.$$

Defining the apparent susceptibility at radius a by

$$(17) \qquad \psi = \frac{3E}{8\pi a^3}\frac{\delta f}{f}$$

and substituting for the coefficients in equation (16), one obtains

$$(18) \qquad \psi = \psi_0+k^2a^2\psi_0[(1/45)(5+\epsilon/\epsilon_0)(3+2\psi_0/\mu_0)-3/5].$$

This formula, though different in form from equation (13), leads to approximately the same resonance shift formula as equation (14).

DISCUSSION OF RESULTS

It is of some interest to compare our results on the susceptibility size effect with those of other investigators. Artman (1956, 1957),* using an approximation to the actual ferrite matrix, obtains a formula which in our notation is

$$(19) \qquad \psi = \psi_0+(1/90)(\epsilon/\epsilon_0)\mu_0k^2a^2(3+2\psi_0/\mu_0)^2+O(k^4),$$

from which he derives the resonance shift formula

$$(20) \qquad H \simeq H_0+4\pi M(\epsilon/\epsilon_0)(2/45)k^2a^2.$$

Thus our formula (14) predicts a resonance shift greater than Artman's by $(5\epsilon_0+\epsilon)/\epsilon$, which for most ferrites is $\simeq 1.4$.

Artman has also proposed the empirical formula

$$(21) \qquad H \simeq H_0+4\pi M(\epsilon/\epsilon_0)(4/45)k^2a^2,$$

which fits well with the available experimental data. It will be seen that our result, while not in agreement with experiment, is somewhat better than Artman's theoretical formula.

Ament and Passerini (1956) have also used the exterior fields to compute the size effect. They find a resonance shift formula with a coefficient 9/8 that of equation (21). However, it would appear that their result applies to *intrinsic* rather than apparent susceptibility. Indeed, when their analysis is applied to the apparent susceptibility, a resonance shift with a coefficient

*There are some errors in equations (23) and (24) of Artman's 1957 paper. The mistakes do not appear, however, in the 1956 paper.

$(\epsilon_0+\epsilon)/\epsilon$ that of equation (20) is predicted. This point seems to have been overlooked by Artman in quoting the Ament–Passerini results.

The formula derived by Tompkins and Spencer (1957) has leading terms which are

$$\psi = \psi_0+(1/45)k^2a^2(\epsilon/\epsilon_0)\psi_0(3+2\psi_0/\mu_0). \tag{22}$$

This should be compared with equation (18). From equation (22) can be derived a resonance shift formula which is almost identical with equation (20).

In conclusion, it is expected that equations (13) and (18), being based on a solution rigorous to $O(k^2)$ for plane wave excitation, will be more accurate than the other formulas quoted above; and this is to some extent borne out by the better agreement of the resonance shift formula (14) with the experimental result of Artman (equation (21)). As far as choosing between the two approaches to the problem, as represented by equations (13) and (18), it would seem that the cavity perturbation formulation adheres more closely to the way in which the "actual" apparent susceptibility is measured, although there is little difference in the predicted resonance shifts to $O(k^2)$.

APPENDIX

Values of the Elliptic Integrals

When $a_1=a_2$, the various elliptic integrals reduce to elementary functions. Thus if $a_3 > a_1$

$$I = (a_3-a_1)^{-\frac{1}{2}} \log \frac{a_3^{\frac{1}{2}}+(a_3-a_1)^{\frac{1}{2}}}{a_3^{\frac{1}{2}}-(a_3-a_1)^{\frac{1}{2}}}.$$

When $a_3 < a_1$

$$I = 2(a_1-a_3)^{-\frac{1}{2}}\cos^{-1}(a_3/a_1)^{\frac{1}{2}}.$$

The remaining functions are then found from the relations

$$\sum_i I_i = 2A,$$

$$\sum_i a_i I_i = I,$$

$$J_1 = (I_2-I_3)(a_3-a_2)^{-1}, \text{ etc.},$$

$$3I_{11}+J_2+J_3 = 2A/a_1, \text{ etc.},$$

$$T_\nu = \tfrac{1}{2}\sum_i I_i(a_i+\nu)^{-1}-A/\nu,$$

$$K_1 = \tfrac{1}{2}\left(\frac{3I_{11}}{a_1+\nu_1}+\frac{J_3}{a_2+\nu_1}+\frac{J_2}{a_3+\nu_1}\right)-A(\nu_1 a_1)^{-1}, \text{ etc.},$$

$$K = (J_2-J_3)(a_3-a_2)^{-1}.$$

For a sphere of radius a

$$I = 2/a, \quad I_i = (2/3)a^{-3},$$

$$J_i = I_{ii} = T_\nu = T_\nu' = (2/5)a^{-5},$$

$$K = K_i = (2/7)a^{-7}.$$

REFERENCES

AMENT, W. S. and PASSERINI, H. J. 1956. Naval Research Laboratory Report 4747.
ARTMAN, J. O. 1956. Lincoln Laboratory Group Report M35-54.
——— 1957. J. Appl. Phys. **28**, 92.
SPENCER, E. G., AULT, L. A., and LECRAW, R. C. 1956. Proc. Inst. Radio Engrs. **44**, 1311.
TOMPKINS, J. E. and SPENCER, E. G. 1957. J. Appl. Phys. **28**, 969.

EXPERIMENTAL EVIDENCE FOR AXIAL VECTOR INTERACTION IN THE DISINTEGRATION OF Pr^{144} [1]

R. L. Graham, J. S. Geiger, and T. A. Eastwood

ABSTRACT

A detailed study of the disintegration scheme of Pr^{144} has been carried out using lens spectrometers, scintillation spectrometers, and fast coincidence techniques The 2293 kev β-component (1.3%) studied in coincidence with γ 691 has a predominantly first forbidden unique shape and the β–γ directional correlation is strongly anisotropic. The results indicate a probable spin-sequence $0-(\beta)2+(\gamma)0+$, but the accuracy is not sufficient to exclude completely a $1-$ assignment for the Pr^{144} ground state. The β 803 component (1.0%) observed in coincidence with γ 2181 has an allowed shape and the β–γ directional correlation is isotropic. The shape of the total β-spectrum was studied in a double lens spectrometer having good anti-scattering properties using sources of Ce^{144} oxide sublimed onto 200 $\mu g/cm^2$ Al leaf. Subtraction of a unique (B_{ij}) shape 2293 kev 1.3% component and an allowed shape 803 kev 1.0% component yields the ground state β-spectrum. Analyses were made using the electronic functions of Zerianova which assume uniform charge distribution with $\rho = 1.2\ A^{1/3}\ 10^{-13}$ cm as well as the point charge functions of Rose with $\rho = 1.41\ A^{1/3}\ 10^{-13}$ cm. The observed spectrum shape can be explained on $0-$ to $0+$ selection rules only by the axial vector interaction. Limits on the permissible tensor or pseudoscalar admixtures with the axial vector are discussed. No acceptable fit is possible with tensor, pseudoscalar, or any TP admixture (interfering or not) using Rose and Osborn's pseudoscalar formalism.

I. INTRODUCTION

Since the non-conservation of parity in β-decay was demonstrated, by Wu *et al.* (1957), the nature of the β-interaction has been the subject of renewed speculation. The He^6 recoil experiment by Rustad and Ruby (1955) resulted in the general acceptance of the tensor interaction as the principal contributor to GT decay. The more recent recoil experiment on A^{35}, when considered in conjunction with the recoil experiments on Ne^{19} (Herrmannsfeldt *et al.* 1957) and the neutron (Robson 1955 and 1958), and the measurement of the β-asymmetry in aligned neutron decay (Burgy *et al.* 1958), require for their explanation a dominance of the axial vector interaction in GT decay. Re-examination of the He^6 measurements (Rustad 1958) revealed several previously unsuspected sources of large systematic error which render the interpretation of this experiment ambiguous. The measurements of the Pr^{144} ground state spectrum presented in this paper provide additional evidence in favor of a dominating axial vector contribution in GT decay.

The study of β-spectrum shapes does not, in general, provide conclusive evidence about the nature of the β-interactions. However, for $0-$ to $0+$ β-spectra the interactions which can contribute, T, A, and P, give markedly different spectrum shapes. A single nuclear matrix element is responsible for the possible pure tensor or pure pseudoscalar contribution to this type of transition and unique spectral shapes are predicted for these cases.

[1]Manuscript received May 8, 1958.
Contribution from Physics and Chemistry Divisions, Atomic Energy of Canada Limited, Chalk River, Ontario.
Issued as A.E.C.L. No. 644.

Pr^{144} (17 minutes) appears to be the most convenient nucleus for an extensive study of a 0− to 0+ β-spectrum shape. Its decay scheme is shown in Fig. 1. Pr^{144} has a long-lived (285-day), low energy (0.3 Mev) precursor Ce^{144}. The ground state β-transition, 0− to 0+, is energetic (2.98 Mev) requiring a minimum of corrections for counter sensitivity and source thickness. The lower energy components of the total β-spectrum are weak and can be corrected for with adequate precision for shape analysis.

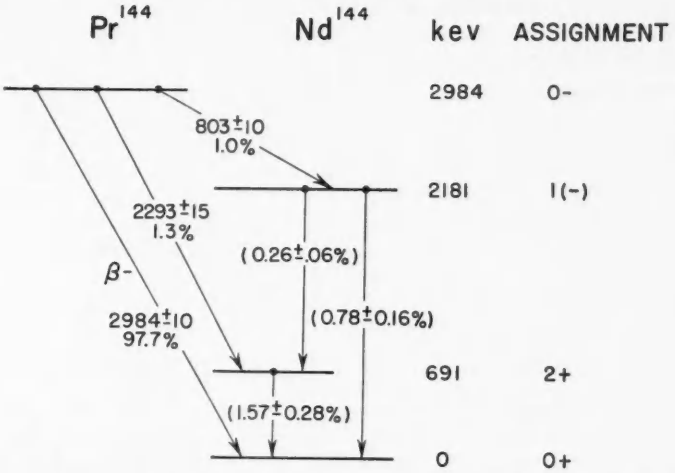

FIG. 1. Disintegration scheme for Pr^{144} showing radiation intensities derived in this work.

Experimental evidence for a 0− assignment for Pr^{144} has been based on studies of the 2293 kev β-component taken in coincidence with γ 691. Ketelle and Brosi (see Laubitz 1956) and Laubitz (1956) both find agreement with a first forbidden unique shape. The 691 kev level in Nd^{144} has been assumed to be 2+, as for almost all first excited states of even–even nuclei (Scharff-Goldhaber 1953). The γ 1490–γ 691 angular correlation studies of Alburger and Kraushaar (1952) and Steffen (1954) are consistent with a 1—2—0 spin-sequence, but provide no unambiguous information (see Section II). Brazos and Roberts (cf. Steffen 1954) find evidence from polarization-correlation studies for a parity change in this sequence which leads to the 1− assignment of Fig. 1.

Various values of the β branching ratios for the 803, 2293, and 2984 kev components have been deduced experimentally. The γ-ray intensity measurements by Emmerich, Auth, and Kurbatov (1954) give 1.9%, 0.8%, and 97.4% respectively and those of Kreger and Cook (1954) give 1.26%, 1.44%, and 97.3%. Estimates made from Kurie plot analysis (cf. Porter and Cook 1952; Alburger and Kraushaar 1952) can have only qualitative significance since the shape of the dominating ground state β-component is in question.

Magnetic analyses of the Pr^{144} β-spectrum have been made by four sets of experimenters. Porter and Cook (1952) and Emmerich, Auth, and Kurbatov

(1954) found their results consistent with a 96% ground state spectrum having an allowed shape. Alburger and Kraushaar (1952) and Laubitz (1956), however, found more low energy electrons, i.e., their Kurie plots were concave upward. Alburger and Kraushaar interpreted their spectrum in terms of an allowed shape 90% ground state component as well as two lower energy components each with ~5% intensity. Laubitz, on the other hand, concluded that the ground state spectrum had a non-allowed shape.

The spectral shape predicted for a 0− to 0+ transition assuming pure tensor (T) interaction disagrees with all of the observed shapes. Laubitz introduced an interfering pseudoscalar (P) contribution with a very strong coupling constant, $C_P/C_T = 107$, in order to obtain theoretical agreement with his data. Zerianova (1956) found that a similar PT admixture was necessary to fit the essentially allowed shape data of Emmerich, Auth, and Kurbatov (1954). More recently Alaga *et al.* (1957*a*) have extended the pseudoscalar theory of Rose and Osborn to include nuclear force effects. They also found that a large pseudoscalar contribution was necessary in order to fit qualitatively the experimental data of Laubitz with a tensor pseudoscalar admixture.

The experimental work described below was undertaken since the spectrum shapes derived from the various earlier experiments are not in agreement. The directional correlation experiments were carried out in an attempt to establish, in a less ambiguous manner, the assignment of 0− for the ground state of Pr^{144}. The evidence described below strongly supports this assignment but the possibility of a 1− assignment cannot be completely excluded. It is possible, therefore, that the conclusions from the spectrum shape analysis may be invalid since it is quite easy (cf. Laubitz 1956) to account for the ground state spectrum shape on the basis of a $1 \rightarrow 0$, yes, type transition.

II. DIRECTIONAL CORRELATION MEASUREMENTS

(*a*) *Experimental Apparatus and Procedure*

The directional correlation measurements were carried out using the experimental arrangements shown schematically in the insets of Figs. 2 and 3*b*. γ-Rays were recorded in 2 in.×2 in. NaI(Tl) crystals and the β-rays in a 3 cm diam.×1 cm thick *trans*-stilbene crystal covered by 2 layers of 2 mg/cm^2 Al foil. These scintillators were mounted on RCA-type 6342 photomultipliers. The photomultipliers were operated at high voltages (> 2000 v) and were connected to a fast–slow coincidence circuit ($2\tau_0 \sim 3\times10^{-8}$ second) similar to that described by Bell, Graham, and Petch (1952).

Gain stabilization was used on the counters in order to minimize systematic errors. The stabilization method used for the 691 kev γ-counter was the following. A collimated beam of γ-rays from a Hg^{203} source near the γ 691 counter produced a strong photopeak at 280 kev which was monitored continuously by a dual differential pulse height analyzer connected to two counting-rate meters. The two pulse height windows were set one on each half of the intense 280 kev photopeak. The two ratemeter outputs, connected in opposition, provided a difference signal which when applied to a variable

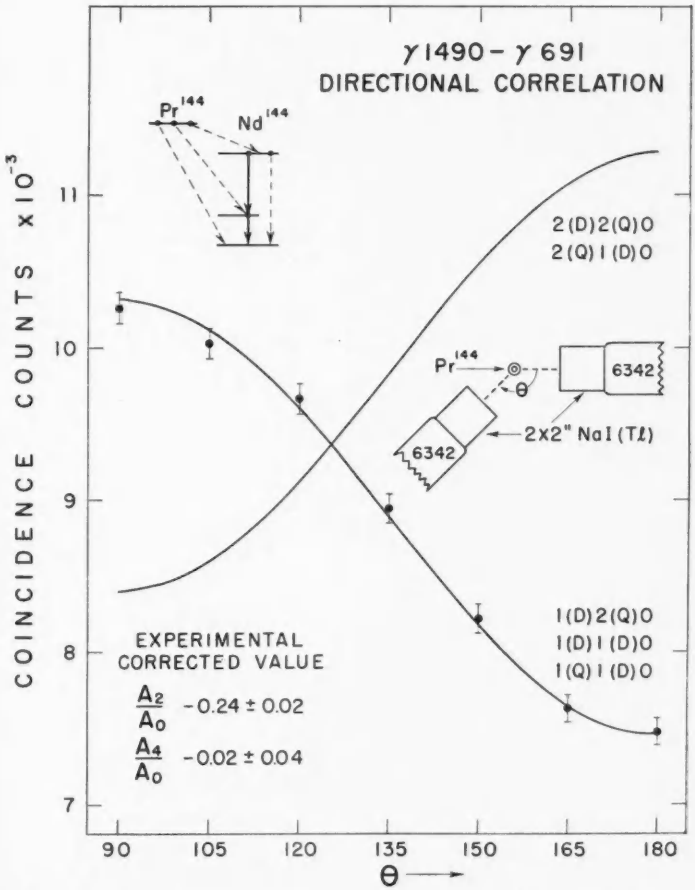

FIG. 2. The directional correlation between γ 691 and γ 1490 taken with the experimental arrangement shown in the inset. The data taken in the 180° to 270° sector were averaged with those taken in the 180° to 90° sector. The combined data have been corrected for random coincidences and for the small variations in the individual counting rates with angular setting ($< 1\%$). Standard deviations are shown by the error bars. The theoretical curves allow for the experimentally measured counter solid angles. The coefficients listed are the least squares fits to the experimental data after correction for counter solid angles.

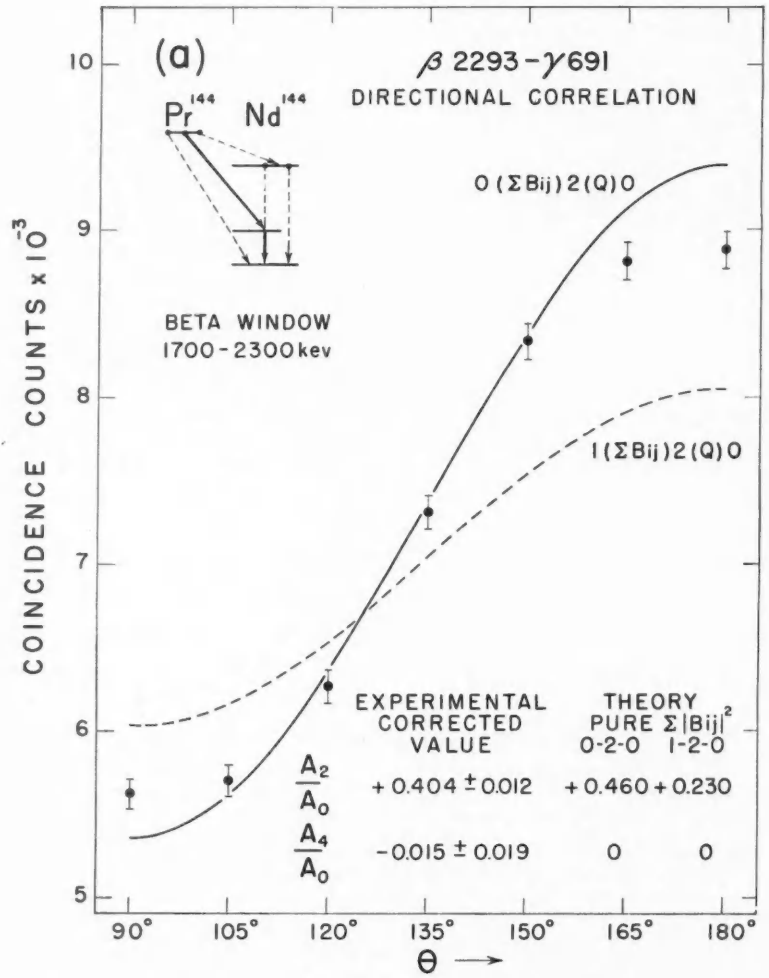

FIG. 3. Beta–gamma directional correlation results taken with the experimental arrangement shown in the inset in (*b*). The data taken in the 180° to 270° sector were averaged with those taken in the 180° to 90° sector. The combined data have been corrected for random coincidences and for the small variations in the individual counting rates with angular setting

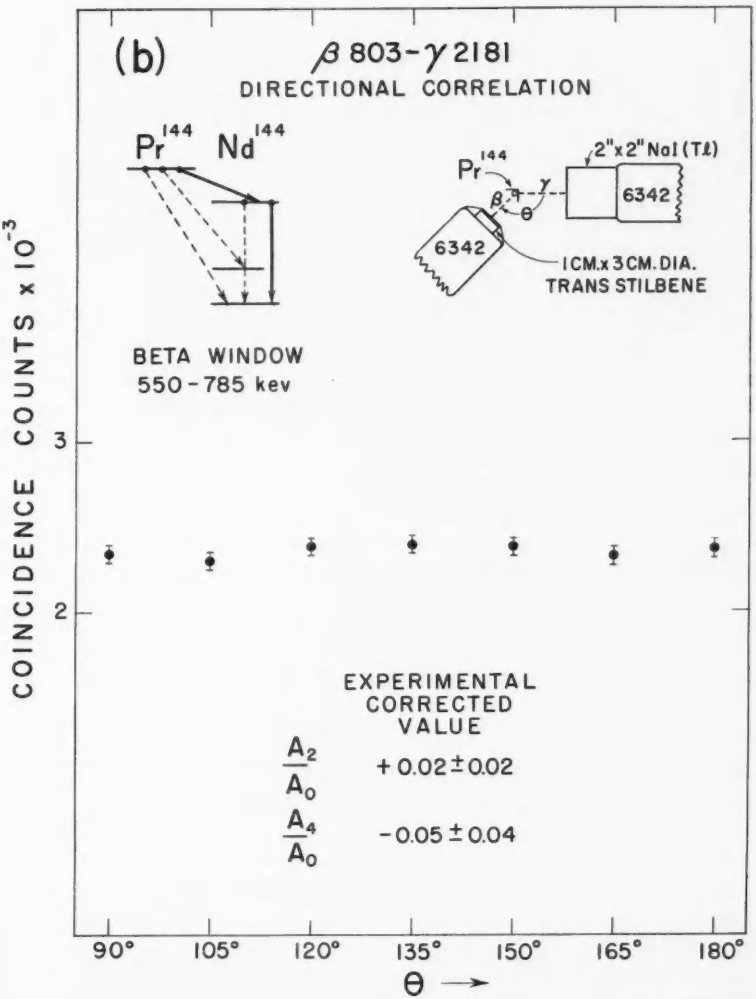

(< 2%). The standard deviations are shown by the error bars. The theoretical curves in 3(*a*) (at left) allow for the measured counter solid angles and for the β energy window shown assuming pure $\sum|B_{ij}|^2_{(L=2)}$ β-radiation. The coefficients listed are the least squares fits corrected for counter solid angles. The theoretical values shown are for the β energy window used in this experiment assuming pure $\sum|B_{ij}|^2_{(L=2)}$ radiation.

gain first amplifier stage kept the over-all gain of the system constant. In this way the over-all gain was kept constant to $\sim 1\%$ over long periods of time. This system can accommodate photomultiplier gain drifts of as much as 50%. A similar arrangement using the 661 kev γ-ray from a Cs^{137} source was used to stabilize the γ 1490 counter.

A different type of gain stabilizer was used with the β-counter. Instead of the differential method used for the γ-counters a simpler integral method was employed. Here a single counting-rate meter is fed from a discriminator set high on the β pulse height spectrum. The counting-rate meter output voltage is compared with a preset voltage and the difference is applied as above to a variable gain amplifier stage to maintain a constant counting rate. This method is applicable only to long-lived sources where decay corrections are unimportant and when background fluctuations can be ignored.

The directional correlation apparatus was run continuously in a 17-step automatic program. At the end of each 10-minute counting interval the angular setting was advanced through a 15° increment. The angular range was from 90° to 270° and provision was included for measuring random coincidence rates at the 105°, 180°, and 255° settings. The coincidence data were printed, along with a code indicating the angular and coincidence delay settings, by a solenoid-operated electric typewriter. The counter channel rates were monitored separately with counting-rate meters and pen-recorders.

The sources were in each case carefully aligned and the net coincidence rates were corrected for positioning errors by normalizing to constant counting rates in both counters for each angular position. The corrected true coincidence counting rates for pairs of angles symmetric about 180° were averaged.

The averaged data were analyzed by the least squares method to obtain the coefficients A_0, A_2, and A_4 of the Legendre polynomials appearing in the assumed expression for the correlation,

$$N(\theta) = A_0 + A_2 P_2(\cos\theta) + A_4 P_4(\cos\theta).$$

The resulting coefficients were then corrected for the finite solid angle subtended by the two counters in the manner suggested by Lawson and Frauenfelder (1953).

(*b*) *Preparation of the Source Material*

Cerium 144 and praseodymium 144 in radioactive equilibrium were used for all the experiments. A "cerium concentrate" extracted from fission products several years old was supplied by the Commercial Products Division of Atomic Energy of Canada Limited. The concentrate also contained some La, Pb, Zn, and other elements so that further purification was necessary. The trivalent cations were separated from the other elements by fluoride and hydroxide precipitations. They were then separated from each other by cation exchange using ammonium α-hydroxy isobutyric acid solution (Choppin and Silva 1956). Those fractions of the eluate which contained Ce^{144} were adjusted to pH 1.0 by the addition of conc. HCl and were passed through another cation exchange column. The absorbed cerium was eluted with 7 *N* HCl (Diamond *et al.* 1954).

The eluate was evaporated to dryness and the cerium chloride was redissolved in 0.1 *N* HCl. Sources were prepared from this solution.

(c) γ 1490–γ 691: Results and Discussion

The experimental arrangement used to measure the γ 1490–γ 691 cascade correlation is indicated in the inset of Fig. 2. Both of the 2 in.×2 in. NaI(Tl) counters subtended a solid angle of about 1.5% of 4π at the source. The 50 μc Ce^{144}–Pr^{144} source used was prepared by evaporating Ce^{144} chloride to dryness in a 1 mm I.D. glass container. The counter outputs were fed through pulse height selectors adjusted to record the respective photopeaks.

The experimental data yield the counter-corrected coefficient ratios $A_2/A_0 = -0.24\pm0.02$ and $A_4/A_0 = -0.02\pm0.04$. The more probable spin-sequences which, with suitable multipolarities for the γ-rays, give theoretical correlation coefficients agreeing with those observed are listed in Table I. Steffen (1954) has measured this directional correlation and has obtained the values $A_2/A_0 = -0.210\pm0.015$ and $A_4/A_0 < 0.01$. He interprets his results in

TABLE I

γ 1490–γ 691 DIRECTIONAL CORRELATION

Spin-sequence			γ 1490 multipolarity*	γ 691 multipolarity	A_2/A_0	A_4/A_0
1	1	0	D	D	−0.25	0
			Q	D	−0.25	0
1	2	0	D	Q	−0.25	0
2	2	0	$D+(\pm\delta)^2Q$	Q		No fit
3	2	0	$D+(-0.22)^2Q$	Q	−0.24	+0.02
2	3	0	$D+(+0.037)^2Q$	Q	−0.24	0.00
Experimental results (this work)					-0.24 ± 0.02	-0.02 ± 0.04

*Amplitude and phase according to Biedenharn and Rose, 1953, Revs. Modern Phys. **25**, 729.

terms of a $1-(\gamma\ 1490)2+(\gamma\ 691)0+$ transition sequence in which γ 1490 is *E*1 radiation with a 0.1% admixture of *M*2 radiation. His results are consistent with our present measurements and the $1- \rightarrow 2+ \rightarrow 0+$ spin-sequence is incorporated in the decay scheme of Fig. 1.

(d) β 2293–γ 691: Results and Discussion

The β–γ directional correlations were measured with the counter arrangement shown in Fig. 3(*b*). The 2 in.×2 in. NaI(Tl) γ-crystal and the 3 cm diam.×1 cm thick *trans*-stilbene β-crystal subtended solid angles at the source of about 1.5% of 4π. A 10 μc open source of Ce^{144}–Pr^{144}, prepared by evaporating a solution of Ce^{144} chloride on 20 mg/cm² Al foil, was used. The source was mounted on the axis of rotation of the moving β-counter and rotated with it.

The observed β 2293–γ 691 correlation is shown in Fig. 3(*a*). The net coincidence count plotted for each angular setting is the sum of the counts for that position and for its equivalent position in the 180°–270° quadrant, e.g., 120° and 240°. The coefficients for this correlation, obtained by the least

squares method and corrected for finite counter solid angles, are $A_2/A_0 = +0.404\pm0.012$ and $A_4/A_0 = -0.015\pm0.019$. These values were obtained with a β-energy window of 1700 to 2300 kev. As a check on the experimental procedure separate analyses have been made of the data obtained in the two quadrants. The counter-corrected results are, for 90°–180°: $A_2/A_0 = +0.408 \pm0.018$, $A_4/A_0 = -0.019\pm0.029$; and for 180°–270°: $A_2/A_0 = +0.393 \pm0.018$, $A_4/A_0 = -0.030\pm0.029$. In these calculations no allowance has been made for the effect of back-scattering in the source material and backing or for air scattering of the β-rays between the source and the counter. The angular response of the β-counter, measured with a narrowly collimated ($< 2°$) beam of β-rays from the Ce^{144}–Pr^{144} source and with identical bias settings, showed no evidence of air scattering.

The coefficients, A_2/A_0, one would expect under our experimental conditions have been evaluated for the $0-(\beta)\ 2+(\gamma)\ 0+$ and $1-(\beta)\ 2+(\gamma)\ 0+$ sequences for all first forbidden matrix element combinations listed by Biedenharn and Rose (1953). Allowance was made in each probable case for the β-energy window used in the experiment (1700–2300 kev).

For the $0-(\beta)\ 2+(\gamma)\ 0+$ case, first forbidden selection rules permit only tensor interaction with pure $\sum_{ij}|B^{\beta}_{ij}|^2$, or axial vector interaction with pure $\sum_{ij}|B_{ij}|^2$. The theoretical results for both of these are $A_2/A_0 = +0.460$. The theoretical coefficient A_4/A_0 is zero for all first forbidden β-ray correlations. The discrepancy between the observed value of A_2/A_0 (0.404 ± 0.012) and the value predicted for the $0-(\beta)2+(\gamma)0+$ sequence may result from an attenuation of the directional correlation as observed experimentally due to (*a*) back-scattering from the relatively thick source mounting, (*b*) undetected large angle air scattering of the β particles, (*c*) nuclear precession in the 691 kev state (which is dependent on the solid state conditions of the source). Furthermore, the theoretical coefficients listed by Biedenharn and Rose (1953) are strictly valid only for low Z. It has been pointed out by Alaga *et al.* (1957*b*) that relativistic nuclear corrections to the theory may be several per cent. It should also be noted that the present theory takes no account of the finite distribution of nuclear charge.

For the spin-sequence $1-(\beta)2+(\gamma)0+$, the coefficients A_2/A_0 which agree with experiment are realized for transitions involving mixed β-matrix elements. For tensor interaction these are $\sum B^{\beta}_{ij}$ with $\int\beta\boldsymbol{\alpha}$ and also $\sum B^{\beta}_{ij}$ with $\int\beta\boldsymbol{\sigma}\times\mathbf{r}$ and for axial vector $\sum B_{ij}$ with $\int\boldsymbol{\sigma}\times\mathbf{r}$. Two of the cases are illustrated in Fig. 4. In all cases it is possible to get agreement with the observed experimental correlation anisotropy, if the B_{ij} contribution to the decay intensity is ~92% or ~40% and the interfering contribution is ~8% or ~60%.

The 40% B_{ij} possibility is excluded by the shape factor analysis discussed in Section III. The effect of attenuation is to reduce the B_{ij} contribution for the other possibility below 92%. Our shape factor results do not exclude such an admixture. There are, however, no known cases where the B_{ij} ($L = 2$) contributions compete favorably with $L = 1$ first forbidden contributions. Our reasons for choosing $0-$ as the correct assignment for the ground state of Pr^{144} are discussed in detail in Section VI.

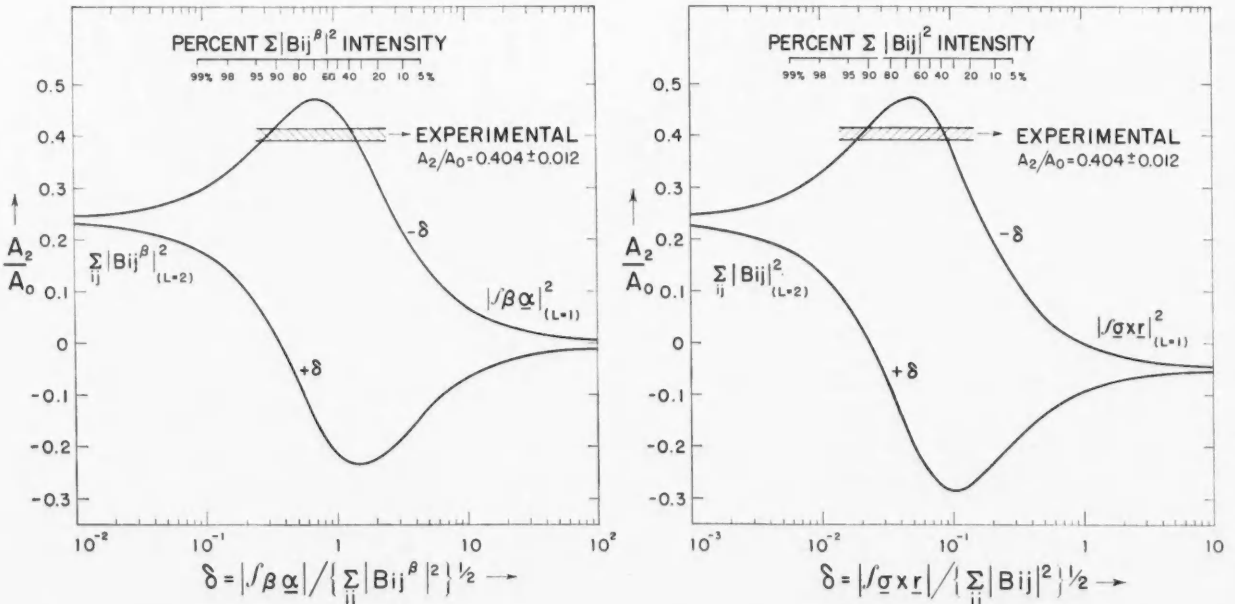

FIG. 4. Theoretical curves of A_2/A_0 as a function of $L = 1$ and $L = 2$ β-radiation admixtures for an assumed $1-(\beta\,2293)2+(\gamma\,691)0+$ directional correlation with a β energy window of 1700 to 2300 kev. For both $\int\beta\alpha$ (tensor) and $\int\boldsymbol{\sigma}\cdot\mathbf{r}$ (axial vector) admixtures the experimental value agrees with $\sim 40\%$ and $\sim 92\%\sum|B_{ij}|^2$ contribution. The β 2293 spectrum shape excludes the 40% possibility but is not accurately enough known to rule out the 92% possibility.

(e) β 803–γ 2181: Results and Discussion

The β 803–γ 2181 directional correlation was measured in the same manner as that for β 2293–γ 691. The energy calibration of the β-counter was determined with the 625 kev K conversion peak from an open Cs^{137} source. For this correlation a β-energy window of 550–785 kev was used. The counter angular response for this energy window was measured using a strong Cs^{137} source and the same collimator as used for the β 2293 tests. The response curve was broader than that for the β 2293 energy window, and revealed some large angle scattering.

The results for this β 803–γ 2181 directional correlation are displayed in Fig. 3 (*b*). The coefficients deduced from these results, $A_2/A_0 = +0.02\pm0.02$ and $A_4/A_0 = -0.05\pm0.04$, are corrected for counter solid angles but not for the effects of large angle scattering. If this β-transition is first forbidden, small but significant anisotropies are expected for several of the possibilities. For a spin-sequence $0-(\beta)1+(\gamma)0+$ the experimental results exclude pure scalar interaction, and pure vector unless the nuclear matrix element $|\int \mathbf{a}|^2$ dominates. Both tensor and axial vector predictions are consistent with the experiment. For the spin-sequence $1-(\beta)1+(\gamma)0+$ the anisotropies predicted for all interactions are small and lie within the experimental limits. No anisotropy is expected for allowed β-spectra, e.g. for $0-(\beta)1-(\gamma)0+$ or for $1-(\beta)1-(\gamma)0+$.

This experiment provides no conclusive evidence for spin and parity assignments but is consistent with the decay scheme proposed in Fig. 1.

III. COINCIDENCE BETA SPECTRA

These experiments were carried out using the double lens, point focus spectrometer shown in the inset of Fig. 5. It was adjusted to a resolution of 2.7% as shown by the width of the K 133 conversion line shown in Fig. 5 (inset). The source was prepared by subliming, in vacuum, Ce^{144} oxide from a tungsten filament at $\sim$2000° C onto an aluminum foil backing of $\sim$800 $\mu g/cm^2$. The quality of the source is evident from the profile of the K 134 conversion line which has an energy of $\sim$90 kev. It does not have the low energy tail which is characteristic of a thick source. The β scintillation counter and the 2 in.$\times$2 in. NaI (Tl) γ scintillation counter were connected to a fast–slow ($2\tau_0 \simeq 2\times10^{-8}$ second) coincidence circuit (Bell, Graham, and Petch 1952). The β-counter sensitivity was deduced from integral pulse height bias curves taken at several spectrometer current settings. At the bias setting used the variation of sensitivity was small ($< 3\%$) over the energy range under study. The γ-counter was pulled back about 1 in. from the source and was covered with 3/16 in. Pb and 1/16 in. Al in order to shield it from β-rays and to attenuate the intense low energy γ-rays from the Ce^{144} decay.

The coincidence data were automatically recorded using a solenoid-operated electric typewriter. A 10-step repeating cycle changed the current setting of the spectrometer in equal increments at 10-minute intervals. The random coincidence rates for these experiments were negligible and were occasionally checked manually. The γ-counter circuit was gain stabilized using an Hg^{203}

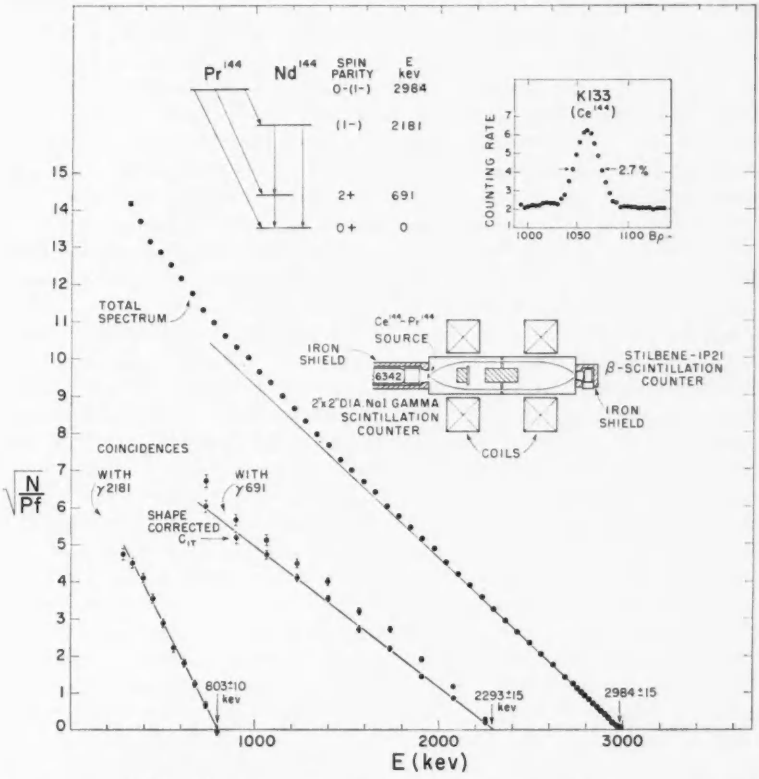

FIG. 5. Analysis of the β-ray spectrum of Pr^{144} obtained by coincidence methods using the double lens spectrometer shown in the inset. The Fermi plot of the component in coincidence with γ 691 has a first forbidden unique shape while that in coincidence with γ 2181 is allowed. The error bars indicate the standard deviations of the counts. The subcomponents are plotted to arbitrary scales. The coincidence data are plotted without applying the directional correlation corrections discussed in the text.

γ-source, in the manner discussed in Section II, in order to avoid errors due to drift and the imperfectly shielded spectrometer magnetic field.

The β-spectrometer was calibrated with a $\sim$200 μc source of thorium active deposit using the F, I, L, M, and X lines whose energies are accurately known (Siegbahn and Gerholm 1955).

Fig. 5 shows allowed Kurie plots of the total spectrum and the two subcomponents. The β 2293 kev spectrum component was observed in coincidence with the γ 691 photopeak and the β 803 kev spectrum component with a γ pulse height window including both the γ 2181 and the γ 1490 photopeaks. Corrections have been made for source decay, background, and the variation of the β-counter sensitivity with energy. No allowance has been made for backscattering.

The allowed Kurie plot of the β 2293 component (uncorrected set of points in Fig. 5) shows the "α" shape characteristic of a first forbidden "unique" spectrum. The matrix element $\sum_{ij}|B_{ij}|^2$ ($L = 2$) therefore makes the dominant contribution to this transition. The β 2293–γ 691 directional correlation result of Section II suggests that there is an $\sim$8 or 60% $L = 1$ β-contribution to this transition. In order to determine the $L = 1$ β-contribution permitted by the experimental spectrum shape, a detailed analysis of these data was performed after they had been corrected for back-scattering. This correction was based on the discrepancy between the ground state spectrum shape obtained with this spectrometer and that found using the double lens, ring focus spectrometer described in Section V. The ratio between these ground state spectrum shapes, scaled in energy by the end-point energy ratio (2293 to 2984) was applied to the β 2293 coincidence data as the back-scattering correction. The maximum correction here is $< 6\%$.

The corrected coincidence β-spectrum data do not represent the true shape of this component because the anisotropy of the β–γ directional correlation varies with β-energy; the exact manner depends on the matrix element admixture assumed. Spectrum shape factors (see Section V) were deduced from the data for two assumptions, (*a*) pure $\sum|B_{ij}|^2$ contribution, and (*b*) 86% $\sum|B_{ij}|^2$ ($L = 2$) with 14% ($L = 1$) allowed shape contribution. The angular correlation effects were removed from the data using the correlation coefficients measured in Section II, the angular apertures appropriate to the coincidence arrangement, and the theoretical energy dependence of the correlation coefficients for the admixture assumed. The resulting data were then treated with the appropriate theoretical shape factor correction and plotted versus energy. The shape factor for the correct admixture will be a horizontal straight line. The least squares fitted slopes to our data on the two assumptions are: for (*a*) $-(3.4\pm4.6)\%$ per Mev, and for (*b*) $+(3.7\pm4.6)\%$ per Mev. Since zero slope corresponds to an exact fit we can only conclude that the β 2293 component contains more than $\sim$75% $\sum B_{ij}$.

The Kurie plot of the β 803 coincidence data is consistent with an allowed spectrum shape. No corrections have been applied to the data shown in Fig. 5. The slight drop in counter efficiency at low energies and the rise at low energies due to back-scattering, in any case, tend to cancel each other. An allowed shape for this spectrum is consistent with the correlation result of Section II.

IV. BRANCHING RATIOS

In order to arrive at an accurate experimental result for the shape of the main ground state β-spectrum from Pr^{144} it is necessary to know the intensities of the two β-subcomponents as well as their shapes. As pointed out in Section I, earlier experimenters do not agree on these intensities and it seemed worth while to make a new determination. The method of measurement used, that most readily carried out with the apparatus at hand, was to determine the relative intensities of the 134 (Ce^{144} decay), 691, 1490, and 2293 kev γ-rays with a calibrated scintillation counter and to obtain the intensity of the K 134 conversion electron line relative to the Pr^{144} total β-spectrum intensity using

a magnetic lens spectrometer. These results, together with the conversion coefficient for γ 134, determine the absolute intensities of the γ-rays occurring in the Pr^{144} decay and hence the β branching ratios.

The experimental values for the γ 134 K conversion coefficient, α_K, are of low accuracy. These measurements, however, together with those of the K/L ratios indicate an $M1$ multipolarity for this γ-ray. Pullman and Axel (1956) find $\alpha_K = 0.71 \pm 0.25$ and $K/L = 7.1 \pm 0.5$. Emmerich *et al.* (1954) find $K/L = 8$, Porter and Cook (1952) find $K/L = \sim 8.8$, and our experimental value is $K/L+M = 7.2 \pm 1.0$. These results are consistent with pure $M1$ but do not exclude $E2$ admixture up to $\sim 15\%$. The limits of error are also too large to rule out completely an admixture of $\sim 90\%$ $E1$ with $\sim 10\%$ $M2$. Cork *et al.* (1954) find $K:L1:L2:L3: = 53:10:0: \sim 1$. The interpretation of this result is not clear, but theoretically one expects $L2:L3 > 1$ for all $M1$ radiation. Sliv's M_1 conversion coefficient $\alpha_K = 0.49$ (Sliv and Band 1956) was chosen in preference to that of Rose since Sliv's values are in better agreement with experiment (cf. Ewan *et al.* 1957). While their results suggest that Sliv's values of $M1$ conversion coefficients are some 10% high, such a discrepancy has no serious effect on the interpretation of our spectral shape results.

The relative γ-ray intensities were obtained using a packaged 4 in. $\times$ 4 in. diam. NaI(Tl) scintillation counter mounted on a 5 in. Dumont phototube. The scintillation spectra obtained with the ~ 50 μc source of Ce^{144}–Pr^{144} are shown in Fig. 6 (*a*) and (*b*). The variation with energy of the total absorption peak efficiency was determined using sources of Na^{22}, Na^{24}, Zn^{65}, and Cs^{137} under the same conditions. After allowing for absorption in the glass source container and NaI(Tl) crystal container and applying escape peak corrections (cf. Bell 1955) we obtain the relative quantum intensities listed in Table II. The absolute intensities listed in Table II are obtained according to

TABLE II

QUANTUM INTENSITIES

	Relative intensities			Quantum intensity per Pr^{144} β-disintegration in %			
Photon energy	This work[a]	Alburger and Krauschaar[b]	Kreger and Cook[a]	This work[f]	Emmerich *et al.*	Kreger and Cook[d]	Pullman and Axel[e]
134	6.75±1.0		8.6	10.6 ±1.1		15.4	8.3
691	1.0	1.0	1.0	1.57±0.28	1.25±0.2	1.79	
1490	0.17±0.02	0.4	0.20	0.26±0.06	0.50 (*c*)	0.35	
2181	0.50±0.05	1.1	0.51	0.78±0.16	1.37 (*c*)	0.91	

[a] By scintillation spectrometer method.
[b] By external conversion method.
[c] Values deduced using Alburger and Krauschaar's relative intensities.
[d] Assuming the 134 kev level is fed in 22% of the disintegrations; cf. Emmerich *et al.* (1954).
[e] From disintegration scheme considerations.
[f] Assuming γ 134 $\alpha_K = 0.49$.

the relation: $I_\gamma/I_\beta = (I_\gamma/I_{\gamma 134})(1/\alpha_{K134})(K134/I_\beta)$. The value of $K134/I_\beta(Pr^{144}) = 0.052$, which we use here, was obtained using the lens spectrometer

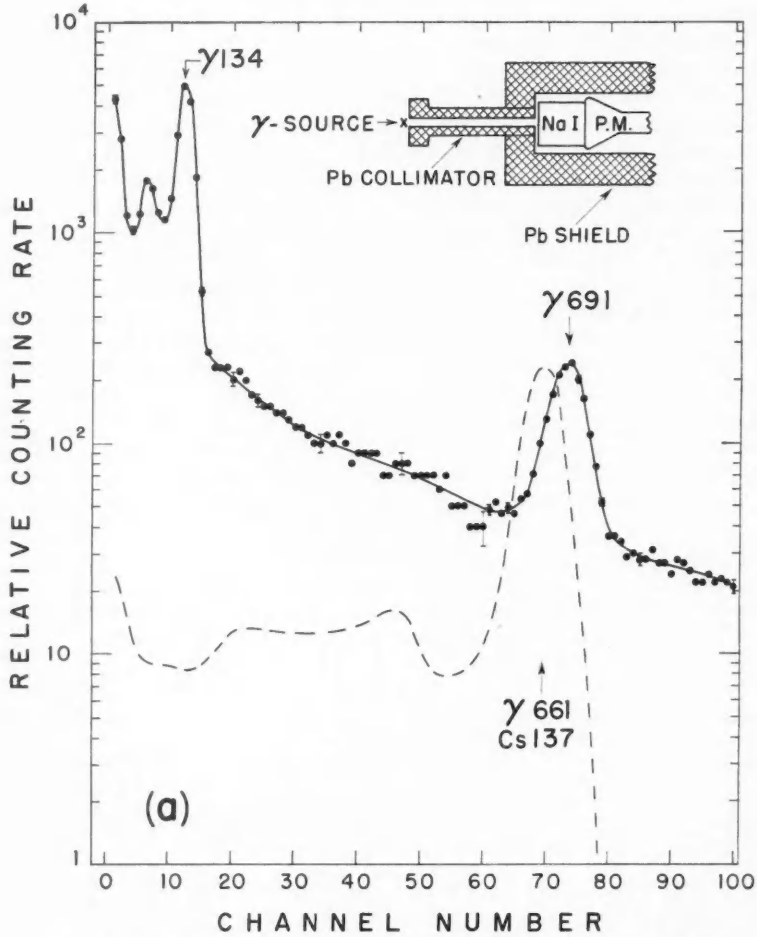

FIG. 6. Scintillation spectra of the γ-radiations from Ce^{144} and Pr^{144} in equilibrium taken with a 4 in. × 4 in. diam. NaI(Tl) packaged crystal mounted on a Dumont-type 6364 photomultiplier. The data were recorded with an Atomic Instruments 20-channel pulse height

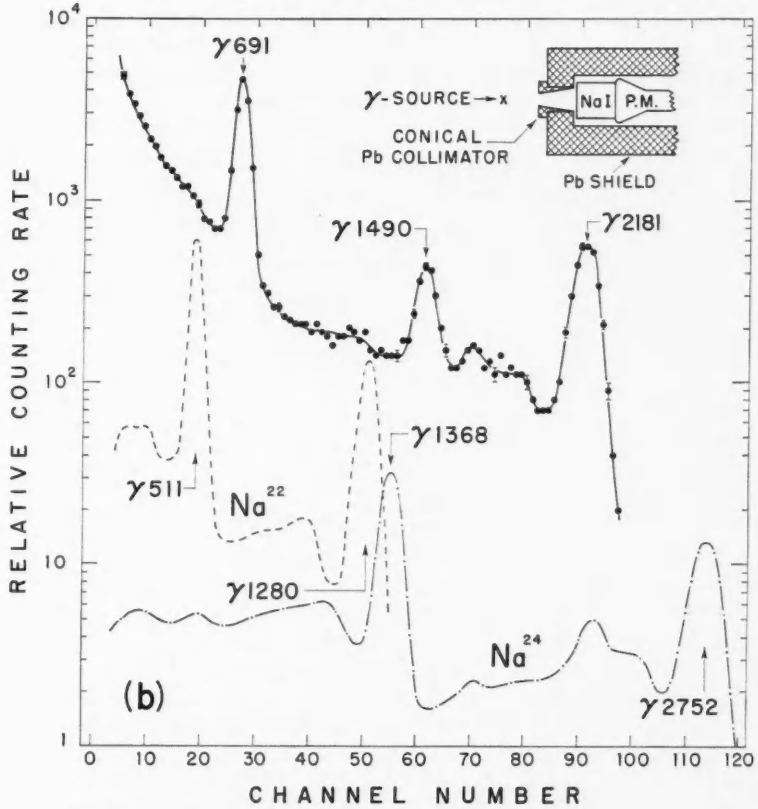

analyzer. The background has been subtracted. Typical standard deviations are indicated by the error bars. Calibration curves are shown for comparison in broken lines. Plot *a* shows the low energy region using the geometry shown in the inset. Plot *b* shows the high energy region.

shown in Fig. 5. Porter and Cook's (1952) value is 0.058. For comparison some relative and absolute intensities of other workers are listed as well.

The β branching ratios deduced from these absolute γ intensity measurements for the Pr^{144} decay scheme as shown in Fig. 1 are β 803 $(1.04\pm0.22)\%$ and β 2293 $(1.31\pm0.34)\%$, implying a $(97.65\pm0.44)\%$ intensity for the β 2984 ground state transition.

V. GROUND STATE β-SPECTRUM SHAPE

In order to study the total β-spectrum with as much freedom from scattering as possible, the double lens spectrometer shown in Fig. 7 was used. It was adjusted for a transmission of 0.3% and a resolution of 0.5%. The vacuum chamber and spiral and ring-focus baffle assembly have been carefully designed

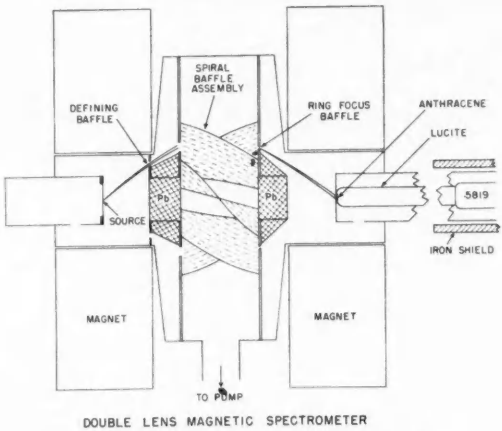

FIG. 7. Cross-sectional diagram of the double lens spectrometer used for the detailed examination of the Pr^{144} β-spectrum shape. Modifications for these experiments which differ from the diagram are the use of (1) a smaller source mount ring and (2) a larger light pipe.

to prevent the detection of scattered electrons. A detailed study carried out by Elliott *et al.* (1954) with a strong P^{32} source has shown that at a setting of 5 line widths beyond the spectrum end-point the scattered rate is $\ll 10^{-5}$ of the peak rate on the spectrum and at higher momentum settings could not be detected.

The source used for this study was made by subliming Ce^{144} oxide from a tungsten ribbon filament at $\sim$2000° C onto 200 $\mu g/cm^2$ aluminum backing. The resulting deposit of 2 μc was just visible and had an estimated surface density of $\lesssim 100\ \mu g/cm^2$. The foil was supported on a 7/8 in. I.D., 0.060 in. thick brass ring which is smaller than the one illustrated in Fig. 7. As shown, the region behind the source is free of scattering materials but it is possible that some of the β-rays scattered from the inside edges of the brass support ring could reach the counter.

The detector is a 16 mm diam. by 2 mm thick disk of anthracene set in the

end of a 2-ft long lucite pipe which leads to a Dumont 6292 photomultiplier. The anthracene crystal is covered with a 200 $\mu g/cm^2$ aluminum foil light reflector. The photomultiplier was carefully selected for efficiency and low noise and was operated at room temperature. The discriminator bias was set above the noise and after pulse region and bias curves were run at many spectrometer current settings. The detector efficiency at the bias setting chosen for this spectrum study was deduced from these bias curves in a manner similar to that described by Porter *et al.* (1956).

In order to obtain the shape of the ground state spectrum the contributions due to the 803 kev and 2293 kev β-components must be subtracted from the total spectrum. The intensities of the components used in this subtraction were those deduced from the γ-studies in Section IV. It was assumed that the 803 kev component had a theoretically allowed shape and that the 2293 kev component had a pure first forbidden unique $\sum|B_{ij}|^2$ shape as suggested by the coincidence spectrum studies described in Section III. The spectrum shape was analyzed using F values obtained from the compilation of Dzelepov and Zerianova (1956). These F values incorporate the factor L_0, which is usually evaluated separately, and allow for uniform nuclear charge distribution and for screening by the orbital electrons. The F values used in this analysis were those appropriate to a nuclear radius $\rho = 1.2\times10^{-13}\ A^{1/3}$ cm and were obtained from Dzelepov and Zerianova's tabulated values, $\rho = 1.5\times10^{-13}\ A^{1/3}$ cm, by scaling in the prescribed manner (for this case F corresponds to F_0L_0 where F_0 and L_0 have the definitions given by Rose *et al.* (1953)). The ratio of $F(\rho_0 = 1.2)$ to $F_0L_0(\rho_0 = 1.41)$ varies less than 0.5% over the energy range of interest, i.e., 300 to 3000 kev.

To compare experiment with theory we divide the observed momentum distribution (N = counting rate/$B\rho$) by the theoretically allowed distribution Fp^2q^2. This ratio is plotted as a function of β kinetic energy in Fig. 8 and is hereinafter referred to as a shape factor. The shape near the high energy end-point is very sensitive to the end-point assumed because of the q^2 factor. We have chosen the end-point value (2984 kev) to minimize the fluctuation above 2500 kev. The effect of different end-point assumptions is illustrated in Fig. 8 by broken lines.

As a check on possible systematic errors in the procedures used for the Pr^{144} work the P^{32} $1+ \rightarrow 0+$, β-ray spectrum was examined in the same apparatus and was analyzed using the same procedure. Two sources were used: one was made by evaporating $P^{32}Cl$ solution on 800 $\mu g/cm^2$ Al backing and the second was prepared by subliming $P^{32}Cl$ from a tungsten filament onto $\sim$200$\mu g/cm^2$ foil. The brass support rings were identical with that of the Pr^{144} source. Consistent shape factor plots were obtained with these two sources. That for the sublimed source is shown in Fig. 9 together with the data of Porter *et al.* (1956). Our results indicate slightly more low energy electrons than found by Porter *et al.* The reason for the discrepancy is not fully understood at present. Even if the discrepancy is entirely due to systematic errors in our experiment the interpretation of the ground state spectrum (see next section) in terms of axial vector interaction is not affected.

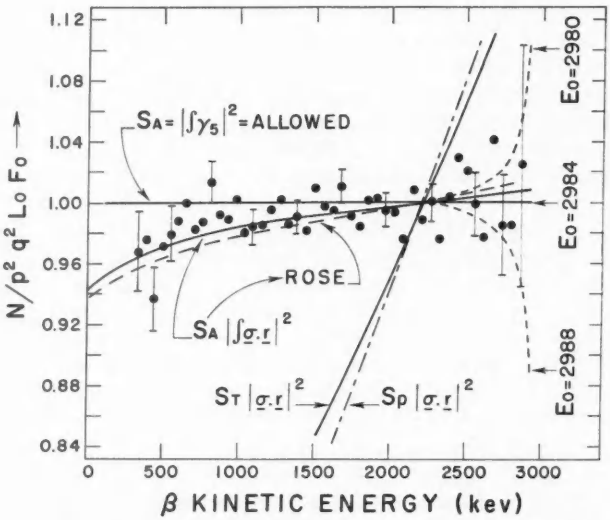

FIG. 8. Experimental shape factor for the ground state β-spectrum of Pr^{144} after subtracting the 1.3% β 2293 and the 1.0% β 803 components from the total spectrum. An allowed shape is a horizontal straight line. Errors which can arise from the wrong end-point assumption are illustrated by the broken lines at the right. Theoretical shape factors shown are for pure tensor, pure pseudoscalar, and two possibilities for pure axial vector interaction assuming a 0− to 0+ spin-sequence. Typical standard deviations are shown by the error bars.

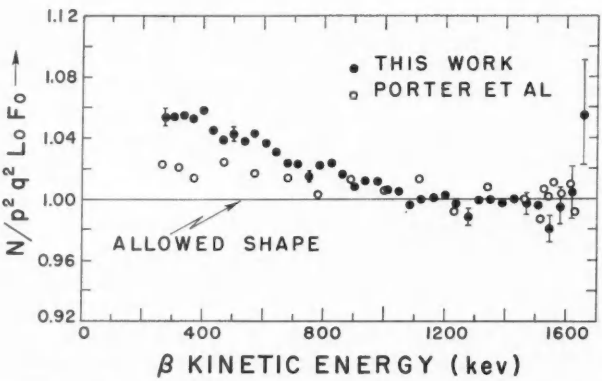

FIG. 9. Experimental shape factor for P^{32} obtained in the spectrometer shown in Fig. 7 using the same procedure as for Pr^{144}. The results of Porter *et al.* (1957), divided by L_0, are plotted as open circles for comparison.

VI. DISCUSSION

The spin assignment of Pr^{144} has not been established with complete certainty. While the assignment 0− has been favored by most authors to date, it

is clear from the coincidence studies above that a $1-$ assignment should also be considered. As has been discussed in Section III this assignment would require that the β 2293 component have $> 75\%\ \sum|B_{kj}|^2$ ($L = 2$). This transition has a $\log f_0 t = 7.9$ and $\log f_1 t = 8.0$ which is typical of a first forbidden, pure $L = 2$ transition where $|J_1 - J_2| = 2$ (cf. Wu 1955). No cases of $L = 2$ transitions have been identified so far where the spin difference involved is only 1, i.e., $|J_1| - |J_2| = \pm 1$, although such contributions are always possible except, of course, where one of the spins is zero. A pertinent example is the 884 kev β-component ($1-$ to $2+$) which occurs in the decay of Tm^{170} (Graham *et al.* 1952). This component has an unusually large ft value of 9.3 yet it has an allowed shape and is not consistent with any significant $L = 2$ contribution. This agrees with the theoretical expectation that the $L = 2$ contributions are inhibited by a factor of $(\alpha Z/2\rho)^2 \simeq 10^2$ relative to competing $L = 1$ contributions. For these reasons it is difficult to accept a $1-$ assignment for the ground state of Pr^{144}; in the discussion that follows we assume that the correct one is $0-$.

Only three interactions, tensor (T), axial vector (A), and pseudoscalar (P), may contribute to a first forbidden $0-$ to $0+$ β-transition. The shape factor formulae for the pure interaction S_{1T}, S_{1A}, S_{1P} and two of the interference terms are taken from Rose and Osborn (1954). Lee-Whiting (1957) has deduced the interference formula S_{1TA} for us. These formulae are:

$$(1)\quad S_{1T} = (|C_T|^2+|C_T'|^2)\left|\int \boldsymbol{\sigma}\cdot\mathbf{r}\right|^2\left[M_0+\frac{2}{3}qN_0+\frac{1}{9}q^2L_0\right],$$

$$(2)\quad S_{1A} = (|C_A|^2+|C_A'|^2)\left\{\left|\int \boldsymbol{\sigma}\cdot\mathbf{r}\right|^2\left[M_0-\frac{2}{3}qN_0+\frac{1}{9}q^2L_0\right]+\left|\int\gamma_5\right|^2 L_0+2i\left(\int\gamma_5\right)\left(\int\boldsymbol{\sigma}\cdot\mathbf{r}\right)^*\left[\frac{1}{3}qL_0-N_0\right]\right\},$$

$$(3)\quad S_{1P} = (|C_P|^2+|C_P'|^2)\left|\int \boldsymbol{\sigma}\cdot\mathbf{r}\right|^2\frac{1}{4M^2}\left\{(U^2+1)M_0-2UQ_0+\frac{2}{3}q[(U^2-1)N_0+4(UM_0-Q_0)]+\frac{q^2}{9}[(U^2+1)L_0-2UP_0+16M_0+8(UN_0-R_0)]\right\},$$

$$(4)\quad S_{1TP} = -\mathrm{Re}(C_TC_P^*+C_T'C_P'^*)\left|\int \boldsymbol{\sigma}\cdot\mathbf{r}\right|^2\frac{1}{M}\left\{UM_0-Q_0+\frac{2}{3}q[2M_0+UN_0]+\frac{q^2}{9}[UL_0-P_0+4N_0]\right\},$$

$$(5)\quad S_{1TA} = 2\mathrm{Re}(C_AC_T^*+C_A'C_T'^*)\left\{\left(\int\boldsymbol{\sigma}\cdot\mathbf{r}\right)\left(\int\boldsymbol{\sigma}\cdot\mathbf{r}\right)^*\left[Q_0+\frac{1}{9}q^2P_0\right]+i\left(\int\gamma_5\right)\left(\int\boldsymbol{\sigma}\cdot\mathbf{r}\right)^*\left[R_0+\frac{1}{3}qP_0\right]\right\},$$

$$(6)\quad S_{1AP} = \mathrm{Re}(C_A C_P^* + C_A' C_P'^*)\left\{\left|\int \boldsymbol{\sigma}\cdot\mathbf{r}\right|^2 \frac{1}{M}\left[-UQ_0 + M_0 - \frac{2}{3}q(2Q_0+N_0) + \frac{q^2}{9}(L_0 - UP_0 - 4R_0)\right] - i\left(\int \gamma_5\right)\left(\int \boldsymbol{\sigma}\cdot\mathbf{r}\right)^* \frac{\sqrt{3}}{M}\left[UR_0 + N_0 + \frac{1}{3}q\left(UP_0 - L_0 + 4R_0 - \rho^2(UQ_0 - M_0)\right) - \frac{1}{9}q^2\rho^2(4Q_0 - UR_0 + N_0)\right]\right\},$$

where q = neutrino momentum, M = nucleon mass in units of the electron rest mass $\simeq 1836$. The potential $U = W - V_c - q$ where V_c = the potential of the field in which the β-particle moves (units of m_0c^2). We take $V_c = Ze/\rho$ where ρ = nuclear radius (units of $\hbar/m_0c = 3.84\times10^{-11}$ cm). We assume, with Rose and Osborn (1954), that $\int\beta\boldsymbol{\sigma}.\mathbf{r}$ which is the correct nuclear matrix element for tensor interaction $\simeq \int\boldsymbol{\sigma}.\mathbf{r}$.*

If two interactions contribute to the transition the shape factor S for the spectrum is obtained by adding the pertinent formulae, e.g., for a TP mixture $S = S_{1T} + S_{1TP} + S_{1P}$. The primed coupling constants denote the non-parity conserving contributions. The functions L_0, M_0, N_0, etc. have been defined by Greuling (1942).

In our analyses the theoretical shape factors appropriate to the first forbidden $0- \rightarrow 0+$ axial vector and tensor interactions, i.e., S_{1T}, S_{1A}, and S_{1TA}, were evaluated using the accurate values of M_0, N_0, P_0, Q_0, and R_0 calculated by Zerianova (1956) for a $Z = 60$ nucleus of radius $\rho = 1.2\times10^{-13}\,A^{1/3}$ cm. These include allowance for a uniform nuclear charge distribution. Her evaluation of these functions assumes that the "allowed" factor L_0 is incorporated into the Fermi function F and L_0 is therefore replaced by unity in evaluating the shape factor formulae. In addition the shape factors S_{1T}, S_{1A}, S_{1P}, S_{1TP}, and S_{1AP} have been evaluated using values of L_0, M_0, N_0, P_0, Q_0, and R_0 from Rose's tabulation where $\rho = 1.41\ A^{1/3}\ 10^{-13}$ cm. These shape factor values must be divided by L_0 since this factor is already taken account of in F. Except for the regions of destructive interference, which are discussed below, the differences in the normalized shape factors computed from these two sets of functions is typically $< 1\%$.

The experimental points are in reasonable agreement with the allowed theoretical shape factor which appears as a horizontal line in Fig. 8. The theoretical shape factor for a $0-$ to $0+$ spectrum assuming pure tensor interaction has a strong positive slope, and is in obvious disagreement with the experimental results as evident in Fig. 8. The pure pseudoscalar shape factor has a similar slope and can also be rejected.

Only a qualitative fit to the data can be obtained with a tensor–pseudoscalar combination using Rose's and Osborn's (1954) theory. This occurs when destructive interference is approached which requires a large pseudoscalar coupling constant, i.e., $|C_P|/|C_T| \sim 10^2$. To illustrate this we show theoretical

Note added in proof:

Dr. M. E. Rose has recently advised us that the factor $\sqrt{3}$ which appears in the final term of equation (6) resulted from an arithmetic error and should be unity. This change will alter slightly the pseudoscalar limits given in Table III for $\lambda = 14$ and $\lambda = 200$, yes cases.

shape factors for TP admixtures in Fig. 10 for several ratios of C_P/C_T. All have been arbitrarily normalized to unity at 2100 kev. Our evaluation assumes time reversal invariance (C's all real) and also

$$C_P'/C_P = +C_T'/C_T,$$

i.e., the interference term present, as expected on the two-component neutrino theory. In evaluating V_c, ρ was taken equal to the same nuclear radius

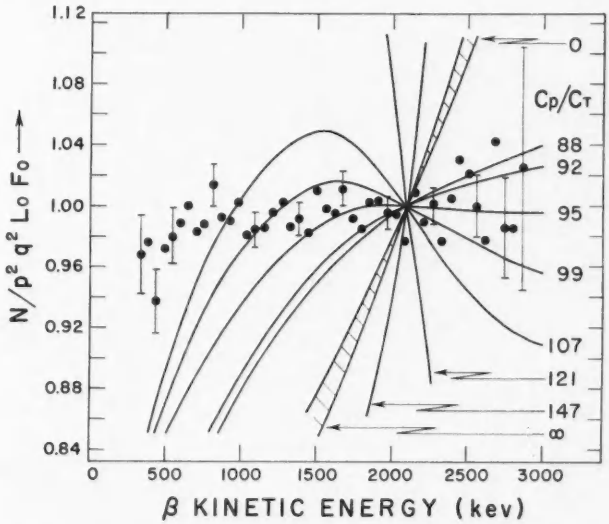

FIG. 10. Attempts to fit the Pr^{144} 0− to 0+ β-spectrum shape factor with pseudoscalar tensor admixtures near the region of destructive interference. The formulation of Rose and Osborn (1954) was used and the tables of Rose *et al.* (1953) were used taking $\rho = 1.41\ A^{1/3}$ 10^{-13} cm. The theoretical shape factors are all arbitrarily normalized to unity at 2100 kev.

assumed in the Rose *et al.* (1953) tabulation, i.e., $\rho = \frac{1}{2}\alpha\ A^{1/3} = 1.41\ A^{1/3}$ 10^{-13} cm. The theoretical factors were divided by L_0 to conform to the treatment used in Fig. 8 so that again an allowed shape is a horizontal straight line. It is apparent that no quantitative fit can be achieved. Since destructive interference is required, $\sim$98%, one cannot calculate these factors from Rose's 4-figure tables to an accuracy of better than $\sim$2%.

Two nuclear matrix elements are present in the theoretical shape factor for pure axial vector interaction. The shape factor for $|\int \boldsymbol{\sigma}.\mathbf{r}|^2$ and for $|\int \gamma_5|^2$ alone are both shown in Fig. 8 evaluated using Zerianova's functions (1956). The shape of the interference term is midway between these two. The results seem to favor $|\int \boldsymbol{\sigma}.\mathbf{r}|^2$ but with the present accuracy either matrix element could be dominant. Admixtures are also acceptable both without interference and with interference provided that it is constructive, i.e., $\lambda = i(\int \gamma_5)/(\int \boldsymbol{\sigma}.\mathbf{r}) > 0$. Pearson (1958) has shown that λ is positive if one assumes a j–j

coupling single particle model with harmonic oscillator potentials of approximately the same strength for parent and daughter states. Destructive interference in the range $\lambda = -3$ to -40 gives rise to shape factor slopes which are inconsistent with the experimental results as shown in Fig. 11.

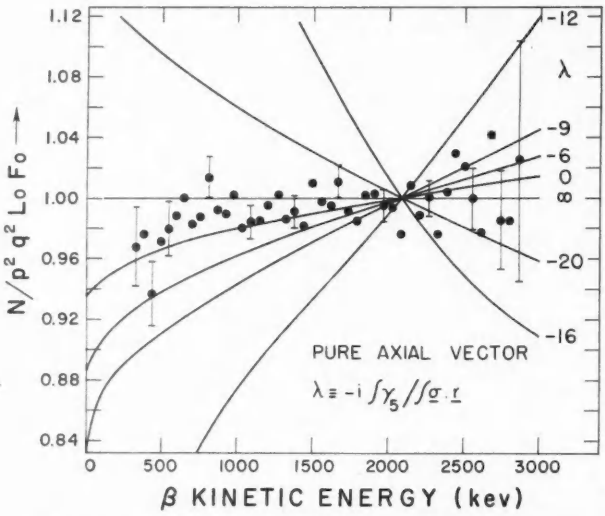

FIG. 11. Attempts to fit the Pr^{144} $0-$ to $0+$ β-spectrum shape factor with pure axial vector for negative values of $\lambda = i\{\int\gamma_5\}/\{\int\boldsymbol{\sigma}.\mathbf{r}\}$, i.e., destructive interference. The shapes for positive values of λ lie in the narrow region between $\lambda = 0$ and $\lambda = \infty$ and are consistent with the experimental results.

In Section V we noted that the shape factor for P^{32} obtained in our equipment differed slightly from that of Porter *et al.* (1957). If we assume that the discrepancy is entirely due to a systematic error in our experiment it does not alter the conclusion regarding axial vector interaction except perhaps to favor dominance of the $|\int\boldsymbol{\sigma}.\mathbf{r}|^2$ contribution.

It should be pointed out that agreement with axial vector interaction is not sensitive to nuclear radius or finite distribution of nuclear charge. To illustrate this point we have also evaluated the theoretical shape factor appropriate to the conditions assumed in Fig. 8 using the Rose *et al.* functions (1953). This is shown in Fig. 8 by the broken line $S_{1A}|\int\boldsymbol{\sigma}.\mathbf{r}|^2$ (Rose). As is evident, the experimental results are again consistent with this factor.

It is of interest to see what admixture of tensor or pseudoscalar interaction with axial vector interaction is permitted by the experimental results. The slope of the axial vector shape factor varies violently in the region of destructive interference of $i\int\gamma_5$ with $\int\boldsymbol{\sigma}.\mathbf{r}$ and it is difficult to make generalizations for this region. There are TA or PA admixtures which are consistent with the experimental data for certain ranges of the ratio $\lambda = i\int\gamma_5/\int\boldsymbol{\sigma}.\mathbf{r}$. The admixture required will be a sensitive function of λ. The situation for con-

structive interference between $i\int\gamma_5$ and $\int\boldsymbol{\sigma}.\mathbf{r}$ is much clearer. Since the experimental data are consistent with any such axial vector shape factor one can then explore the amount of admixture of tensor or pseudoscalar interaction which is still consistent with experiment. We have carried out computations for a variety of values of λ and summarize our conclusions in Table III which lists the approximate limits of TA and PA admixtures for three values of λ.

TABLE III

LIMITS ON T–A and P–A ADMIXTURES FOR THE 0− TO 0+ Pr^{144} GROUND STATE SPECTRUM[a]

Axial vector		Interference term[a]	Tensor		Pseudoscalar	
$\lambda = \{i\int\gamma_5/\int\boldsymbol{\sigma}.\mathbf{r}\}$[b]	$\int\gamma_5$ contribution[c]		C_T/C_A	S_{1T}/S_{1A}[d]	C_P/C_A	S_{1P}/S_{1A}[d]
0	0	Yes	<0.1	<.007	<15	<.009
		No	<0.3	<.06	<50	<.10
14	50%	Yes	<0.2	<.007	<37	<.014
		No	<0.8	<.11	<120	<.14
200	99.5%	Yes	<2	<.012	<180	<.005
		No	<7	<.15	<1000	<.20

[a]Experimental data analyzed with the formalism and the functions of Rose *et al.* (1954) using $\rho = 1.41\ A^{1/3}\ 10^{-13}$ cm. Invariance under time reversal is assumed.

[b]We here consider constructive interference only for reasons discussed in text.

[c]$\{|\int\gamma_5|^2 L_0\}/\{|\int\gamma_5|^2 L_0 + |\int\boldsymbol{\sigma}.\mathbf{r}|^2 (M_0 - \frac{2}{3}q\ N_0 + \frac{1}{9}q^2 L_0)\}$ at $E_\beta \sim 1100$ kev.

[d]Numerical contributions evaluated at $E_\beta \sim 1100$ kev using equations 1, 2, and 3.

[e]S_{1AT} for tensor and S_{1AP} for pseudoscalar admixtures.

The limits were arrived at graphically. A typical example is shown in Fig. 12 for the case $\lambda = 0$. It is clear from the table that no substantial contribution from either tensor or pseudoscalar interaction is permissible with axial vector with any positive value of λ.

Laubitz (1956) obtained an experimental shape factor which differs appreciably from that shown in Fig. 8. In contrast to our experimental shape factor his drops $\sim$20% in the energy region 800 to 2800 kev. The drop above 2200 kev would appear to have two causes. Laubitz did not apply a correction for the 6% resolution of his instrument which is important for his last three points. This may have influenced him in choosing too high an end-point energy value which in turn influences the values of neutrino momentum used in his analysis. If one makes the appropriate resolution correction and assumes an end-point energy $\sim$20 kev lower the pronounced droop at the high energy end is largely eliminated. The rise at low energy may have been caused by back-scattering from the rear of the source mount. This is suggested by the ground state spectrum derived from our 3% lens spectrometer results shown in Fig. 5. This gives an experimental shape factor almost identical with that of Laubitz' below 2000 kev. For these reasons we feel that his analysis of his experimental data does not provide good evidence for a strong pseudoscalar contribution in this 0− to 0+ spectrum.

Zerianova (1956) has evaluated more precise TP shape factors in the region of destructive interference for Pr^{144} in attempting to fit the experimental results of Emmerich, Auth, and Kurbatov (1954). She has computed the pertinent electronic wave functions to 6-figure accuracy taking into

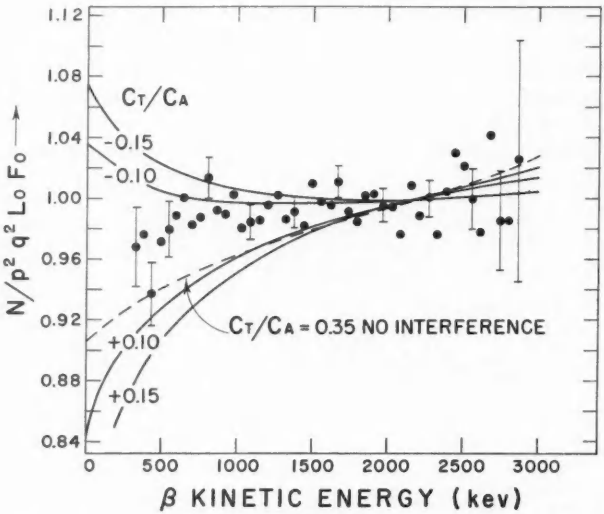

FIG. 12. Attempts to fit the Pr^{144} 0− to 0+ β-spectrum shape factor with axial vector, $\lambda = 0$, and a small admixture of tensor interaction, both with the interference terms,

$$C_T'/C_A' = +C_T/C_A,$$

and without the interference terms,

$$C_T'/C_A' = -C_T/C_A.$$

The theoretical curves were calculated using Zerianova's (1956) functions with $\rho = 1.2\ A^{1/3}\ 10^{-13}$ cm. The shape factors are arbitrarily normalized at 2200 kev.

account screening and uniform distribution of nuclear charge, assuming a nuclear radius value $\rho = 1.2\ A^{1/3}\ 10^{-13}$ cm. Her conclusion is similar, i.e. one cannot obtain quantitative agreement with an experimental shape factor that is essentially allowed using the pseudoscalar formulae of Rose and Osborn (1954).

The value of log $ft = 6.5$ for the Pr^{144} ground state transition is typical of those of other first forbidden transitions. In that region of PT destructive interference which qualitatively fits the experimental data, e.g., for $C_P/C_T = 107$ (see Fig. 10), the presence of pseudoscalar interaction reduces the total decay probability to ~3% of that expected for the pure tensor interaction. Hence the tensor part has a log $ft \simeq 5$. Zerianova (1956) deduces that the cancellation is even more complete, i.e., $S \sim 0.2\%\ S_{1T}$, implying that the log ft for the tensor part is ~4. Log ft values as low as 5 are found only for highly favored first forbidden transitions which occur near closed shells (cf. Wu 1955). Thus there is difficulty in accounting for the transition probability as well as for the spectrum shape with the Rose and Osborn pseudoscalar theory.

There is lack of agreement regarding the validity of the Rose and Osborn theory for pseudoscalar interaction. A modification has been proposed by Alaga, Sips, and Tadic (1957(*a*)), who introduce a term into the Hamiltonian

for the β-interaction to take account of the influence of nuclear forces. In this way they derive new formulae for S_{1P} and S_{1PT}. This gives an additional parameter Γ as well as C_P/C_T. So far they have only attempted to fit Laubitz' experimental shape factor. Their fit with $C_P/C_T \sim 10$–15 requires a Γ of ~ 30–40. These parameter values imply that the pseudoscalar contribution dominates the tensor contribution, $S_P > S_T$, whereas in the approximate fits obtained using Rose's formulation the reverse is true, i.e., $S_P < S_T$.

If one questions the method followed by Rose and Osborn in evaluating the nuclear moment $\int \beta\gamma_5$ on which the pseudoscalar coupling acts one may return to the earlier treatment of Konopinski and Uhlenbeck (1941). This gives the following formulae for T and P shape factors (cf. Konopinski 1955).

$$S_{1P} = (|C_P|^2 + |C_P'|^2)\left|\int \beta\gamma_5\right|^2 L_0, \tag{7}$$

$$S_{1TP} = 2\mathrm{Re}(C_T C_P^* + C_T' C_P'^*) i\left(\int \beta\boldsymbol{\sigma} \cdot \mathbf{r}\right)\left(\int \beta\boldsymbol{\sigma} \cdot \mathbf{r}\right)^* \{N_0 + \tfrac{1}{3} q L_0\}, \tag{8}$$

$$S_{1T} = (|C_T|^2 + |C_T'|^2)\left|\int \beta\boldsymbol{\sigma} \cdot \mathbf{r}\right|^2 \{M_0 + \tfrac{2}{3} q N_0 + \tfrac{1}{5} q^2 L_0\}. \tag{9}$$

In order to fit our experimental data with these factors we require a dominating contribution of pseudoscalar interaction which has the allowed (L_0) shape. Because of the uncertainty regarding the relative magnitudes of the two nuclear matrix elements it is difficult to derive good limits on the C_P/C_T coupling constant ratio. If $|\int \beta\gamma_5| \sim |\int \beta\boldsymbol{\sigma} \cdot \mathbf{r}|$ our data requires $|C_P/C_T| > 10$. In the light of Rose and Osborn's arguments it seems more probable that $|\int \beta\gamma_5| \ll |\int \beta\boldsymbol{\sigma} \cdot \mathbf{r}|$ which would require that $|C_P/C_T| \gg 10$ in order to account for our experimental data on the Konopinski Uhlenbeck formulation. In this event, however, one should also take into account the contributions from the smaller terms considered by Rose and Osborn. The present uncertainties regarding nuclear wave functions preclude a unique choice of the formulation for the pseudoscalar theory.

This uncertainty in treatment of our data in terms of PT admixtures is in marked contrast to its simple explanation in terms of pure axial vector interaction.

VII. CONCLUSIONS

The agreement between the experimental shape factor of a $0-$ to $0+$ β-spectrum and the theoretical shape for axial vector interaction is not peculiar to Pr^{144}. The available experimental evidence favors a $0-$ assignment for the Tl^{206} ground state. The Tl^{206} β-ray spectrum ($0-$ to $0+$) is unmasked by low energy components and has an allowed shape (Alburger and Friedlander 1951) consistent with axial vector predictions. The $0-$ assignment for the ground state of 27-hour Ho^{166} has been established in the same experimental manner as described in this paper for Pr^{144} (Graham, Wolfson, and Clark 1955). The 1854 kev $0-$ to $0+$ ground state β-spectrum from Ho^{166} is masked by an almost equally intense $(48 \pm 4)\%$ 1771 kev component which has a first forbidden "unique" B_{ij} shape. The shape of the 1854 kev spectrum is not

consistent with pure tensor interaction, but is, within the rather large errors, consistent with an axial vector shape (Wolfson and Graham 1955). The agreement in spectrum shape of these experimental examples is more satisfactorily explained by pure axial vector interaction than by invoking interfering TP admixtures which are very sensitive to the pseudoscalar coupling constant and which, in any case, only give qualitative fits.

This evidence from spectrum shapes for axial vector interaction in Gamow Teller decay is consistent with other recent experiments on the nature of the β-decay interaction. The electron recoil angular correlation results on the positron emitters A^{35} and Ne^{19} reported by Herrmannsfeldt *et al.* (1957) are most simply accounted for by a VA combination of interactions. The circular polarization and resonant scattering results of Goldhaber *et al.* (1957) on the γ-rays from Sm^{152} following K capture in Eu^{152} indicate a negative helicity for the neutrinos emitted in this decay. On the assumption that this neutrino helicity is the same as that for positron emission they conclude that this Gamow Teller decay is axial vector. The evidence to date for negatron emitters, excluding the He^6 study, comes from studies of the neutron decay.* The electron recoil results of Robson (1955 and 1958) on the neutron decay are consistent with the combination ST or VA but not with SA or VT. The measurements of Burgy *et al.* (1958) on the β and proton recoil asymmetries in the decay of polarized neutrons favor the vector–axial vector combination for this decay.

The β 2293–γ 691 directional correlation results and the coincidence spectrum shape of the β 2293 component strongly favor a 0− spin assignment for the Pr^{144} ground state. The experimental shape of the 0− to 0+ Pr^{144} β-spectrum is in disagreement with that for the tensor interaction and with those for pseudoscalar and pseudoscalar tensor admixtures on the Rose and Osborn (1954) pseudoscalar theory. The axial vector interaction provides the only satisfactory explanation for this 0− to 0+ β-spectrum shape. This conclusion is independent of assumptions regarding the presence or absence of the interference terms in the shape factor expressions.

ACKNOWLEDGMENTS

We would like to thank Dr. G. E. Lee-Whiting and Dr. M. E. Rose for their assistance and advice on the theoretical aspects of the shape factor analysis. We are indebted to Dr. G. T. Ewan, Messrs. D. A. Markle, H. Niemann, R. B. Walker, and D. Werner for help in the experimental aspects of this work. Dr. D. R. MacKenzie kindly prepared the P^{32} sources used. The continued advice and encouragement of Dr. L. G. Elliott is gratefully acknowledged.

**Note added in proof:*
Herrmannsfeldt *et al.* (preprint 1958) have recently measured the ion recoil spectrum following He^6 beta decay. Their results "clearly indicate that the axial vector interaction is dominant."

REFERENCES

ALAGA, G., SIPS, L., and TADIC, D. 1957*a*. Glasnik Matematicko Fizicki i Astronomski **12**, 207.

——— 1957*b*. To be published.

ALBURGER, D. E. and FRIEDLANDER, G. 1951. Phys. Rev. **82**, 977.

ALBURGER, D. E. and KRAUSHAAR, J. J. 1952. Phys. Rev. **87**, 448.

BELL, P. R. 1955. *Cf.* K. Siegbahn, Beta and gamma-ray spectroscopy (North-Holland Publishing Company, Amsterdam), p. 155.

BELL, R. E., GRAHAM, R. L., and PETCH, H. E. 1952. Can. J. Phys. **30**, 35.

BIEDENHARN, L. C. and ROSE, M. E. 1953. Revs. Modern Phys. **25**, 729.

BURGY, M. T., KROHN, V. E., NOVEY, T. B., RINGO, G. R., and TELEGDI, V. A. 1958. Preprint.

CHOPPIN, G. R. and SILVA, R. S. 1956. J. Inorg. & Nuclear Chem. **3**, 153.

CORK, J. M., BRICE, M. K., and SCHMID, L. C. 1954. Phys. Rev. **96**, 1295.

DIAMOND, R. M., STREET, K., Jr., and SEABORG, G. T. 1954. J. Am. Chem. Soc. **76**, 1461.

DZELEPOV, B. S. and ZERIANOVA, L. N. 1956. Vlianie Electrocheskoga Polia Atoma na Beta Raspad. Izdetelstvo Akademii Nauk S.S.S.R. Moscow-Leningrad.

ELLIOTT, L. G., PRESTON, M. A., and WOLFSON, J. L. 1954. Can. J. Phys. **32**, 153.

EMMERICH, W. S., AUTH, W. J., and KURBATOV, J.D. 1954. Phys. Rev. **94**, 110.

EWAN, G. T., KNOWLES, J. W., and MACKENZIE, D. R. 1957. Phys. Rev. **108**, 1308.

GOLDHABER, M., GRODZINS, L., and SUNYGAR, A. W. 1957. Phys. Rev. **106**, 826.

GRAHAM, R. L., WOLFSON, J. L., and BELL, R. E. 1952. Can. J. Phys. **30**, 459.

GRAHAM, R. L., WOLFSON, J. L., and CLARK, M. A. 1955. Phys. Rev. **98**, 1173.

HERRMANNSFELDT, W. B., MAXSON, D. R., STÄHELIN, P., and ALLEN, J. S. 1957. Phys. Rev. **107**, 641.

KONOPINSKI, E. J. 1955. *Cf.* K. Siegbahn, Beta and gamma-ray spectroscopy (North-Holland Publishing Company, Amsterdam), p. 302.

KONOPINSKI, E. J. and UHLENBECK, G. E. 1941. Phys. Rev. **60**, 308.

KREGER, W. E. and COOK, C. S. 1954. Phys. Rev. **96**, 1276.

LAUBITZ, M. J. 1956. Proc. Phys. Soc. A **69**, 789.

LAWSON, J. S. and FRAUENFELDER, H. 1953. Phys. Rev. **91**, 649.

LEE-WHITING, G. E. 1957. Private communication.

PEARSON, J. M. 1958. Private communication.

PORTER, F. T. and COOK, C. S. 1952. Phys. Rev. **87**, 464.

PORTER, F. T., FREEDMAN, M. S., NOVEY, T. B., and WAGNER, F. 1956. Phys. Rev. **103**, 921.

PORTER, F. T., WAGNER, F., and FREEDMAN, M. S. 1957. Phys. Rev. **107**, 135.

PULLMAN, I. and AXEL, P. 1956. Phys. Rev. **102**, 1366.

ROBSON, J. M. 1955. Phys. Rev. **100**, 933.

——— 1958. Private communication.

ROSE, M. E. 1955. *Cf.* K. Siegbahn, Beta and gamma-ray spectroscopy (North-Holland Publishing Company, Amsterdam), Appendix IV.

ROSE, M. E. and OSBORN, R. K. 1954. Phys. Rev. **93**, 1315.

ROSE, M. E., PERRY, C. L., and DISMUKE, N. M. 1953. Oak Ridge National Laboratory, 1459.

RUSTAD, B. M. and RUBY, S. L. 1955. Phys. Rev. **97**, 991.

RUSTAD, B. M. 1958. Post deadline paper at New York meeting, American Physical Society, Jan. 29–Feb. 1.

SCHARFF-GOLDHABER, G. 1953. Report of the Indiana Conference on Nuclear Spectroscopy and the Shell Model, Indiana University, Bloomington, Indiana.

SIEGBAHN, K. and GERHOLM, T. R. 1955. *Cf.* K. Siegbahn, Beta and gamma-ray spectroscopy (North-Holland Publishing Company, Amsterdam), p. 920.

SLIV, L. A. and BAND, I. M. 1956. Coefficients of internal conversion of gamma radiation, Part I, Academy of Sciences USSR Moscow-Leningrad. Issued in the U.S.A. as Report 57 ICC K1, Physics Department, University of Illinois, Urbana, Illinois.

STEFFEN, R. M. 1954. Phys. Rev. **95**, 614.

WOLFSON, J. L. and GRAHAM, R. L. 1955. Unpublished.

WU, C. S. 1955. *Cf.* K. Siegbahn, Beta and gamma-ray spectroscopy (North-Holland Publishing Company, Amsterdam), p. 335.

WU, C. S., AMBLER, E., HAYWARD, R. W., DOPPES, D. D., and HUDSON, R. P. 1957. Phys. Rev. **105**, 1413.

ZERIANOVA, L. N. 1956. Cern Physicheskaya, Izvest. Akad. Nauk S.S.S.R. **10**, 1399.

THE FORWARD-SCATTERED RADIO SIGNAL FROM AN OVERDENSE METEOR TRAIL[1]

P. A. FORSYTH

ABSTRACT

A recently presented expression for the forward-scattered signal from an overdense meteor trail is tested by applying it to the signals scattered from a single meteor trail. The particular trail was selected carefully in order to permit the derivation of each of its parameters in several different ways. The internal consistency of the derived information is taken as a measure of the validity of the theoretical expression. In particular, the electron line density at each of two reflection points is derived by three different methods, of which two depend upon the new expression, and the other depends only upon well-established theory. The resulting agreement is within the experimental error and suggests that the new expression is an adequate working relation for use in experimental investigations.

I. INTRODUCTION

The reflection of radio waves by an ionized meteor trail is, admittedly, a complex process. However, in its study, a remarkable degree of success has been achieved by applying theoretical expressions derived by consideration of only two relatively simple models. The two mechanisms concerned should apply separately to trails of very low and very high ionization density. The first process, which applies to weakly ionized trails, involves the free penetration of the trail by the radio waves and independent scattering of the radiation by the individual electrons. The second process applies when the ionization density within the trail is sufficiently great to prevent the radio waves from passing through the trail; in such circumstances it is customary to treat the trail as if it were a conducting metal cylinder. The formulation of the theoretical expressions appropriate to observations made by means of radar equipment (the back-scatter case) has been summarized by Kaiser (1953) and by Eshleman (1955), and the history of the various treatments has been outlined in a recent paper (Hines and Forsyth 1957).

In observational work it has been customary to assign each meteor trail to one of two classes according to the time-variation of amplitude in the reflected signal. If, over most of the lifetime of the trail, the low-density expression is appropriate then the trail is said to be "underdense" whereas if the high-density expression applies the trail is termed "overdense." In fact, since the ionization of the trail is confined initially within a small radius, all but the most weakly ionized trails must behave as high-density trails for a short time after formation. On the other hand, because of the diffusive spread of the ionization, every trail eventually must become sufficiently diffuse to permit the free passage of the radio waves and hence must behave as a low-density trail near the end of its lifetime.

[1]Manuscript received March 12, 1958.
*Contribution from the Radio Physics Laboratory of the Defence Research Board, Ottawa. The work was performed under project PCC No. D48-28-35-05.

In spite of the obvious limitations of the two separate models and of the rather arbitrary bridging which was used frequently to join the two sets of expressions in the transition region, the early back-scatter experiments achieved a surprising degree of success in the determination of various physical properties of the meteor trails and of the upper atmosphere (see, for example, the review by Lovell and Clegg 1952, and the more recent work by Lovell 1954). Later, it was shown by Eshleman (1952) that a more exact treatment leads to very similar results but by this time a large body of evidence had been accumulated which, by its internal consistency, attested to the validity of the expressions.

In recent years, studies of meteor trails have been carried out using radio systems in which the transmitter and receiver are separated by several hundreds of kilometers (see, for example, Eshleman and Manning 1954; Forsyth and Vogan 1955, 1956; McKinley and McNamara 1956; Hines and Vogan 1957). Under these conditions, the reflection process is described as forward-scattering in contrast to the back-scatter or radar case. In forward-scattering additional complications arise; however, a straightforward extension of the simple low-density formulae to include forward-scattering has been given by Eshleman (1952). Recently, a similar extension of the high-density formulae has been presented by Hines and Forsyth (1957), who also point out that, while the approach is oversimplified, it does not seem likely that a more exact treatment will lead to a simple result that is suitable for direct comparison with observation.

It has been suggested that since neither of the models is likely to apply exactly to a given meteor trail, the resulting expressions should be expected to have only a statistical validity, describing adequately the average behavior of the signals scattered by a large number of trails. The first attempts to study statistically the duration of forward-scattered signals have revealed some small discrepancies (Forsyth and Vogan 1956; McKinley and McNamara 1956) but it is not clear that these are due to a real failure of the theoretical expressions since the sampling procedures may have included some observational selection. Another approach is to test the formulae by the detailed study of the signals scattered from individual trails. In this paper an attempt is made to derive as much information as possible from the recordings of signals scattered from a single meteor trail. The internal consistency of this information is taken as a measure of the validity of the formulae.

II. THE EXPERIMENTAL ARRANGEMENT AND SIGNAL SELECTION

During March, 1956, recordings were made of the meteor signals received simultaneously at two stations in the Ottawa area, separated by about six kilometers. The transmitter was located at Greenwood, Nova Scotia, 860 km from Ottawa, and was operated at a frequency of 39.22 Mc/sec with an output power of 100 watts. The details of this circuit have been published previously by Vogan and Campbell (1957). The disposition of the receiving stations is shown in Fig. 1. Station 1 was located at the Radio Physics Laboratory and Station 2 was located at a remote site near the south shore of the Ottawa river.

The signals received at the remote station (2) were transmitted to the Radio Physics Laboratory (1) by means of a land line and were recorded on the same chart as were those received locally. The recordings were made with a chart speed of 10 mm/sec. The response of the recording system was such that the deflection of the recorded trace was very nearly proportional to the amplitude of the received signal.

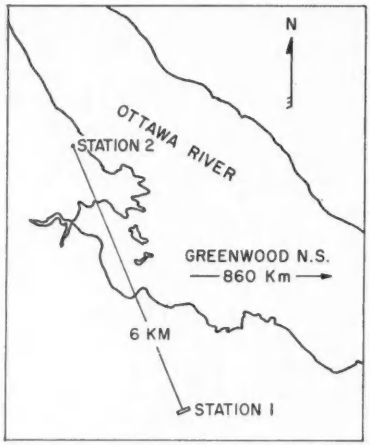

FIG. 1. Showing the disposition of the two receiving stations relative to the direction to the transmitter.

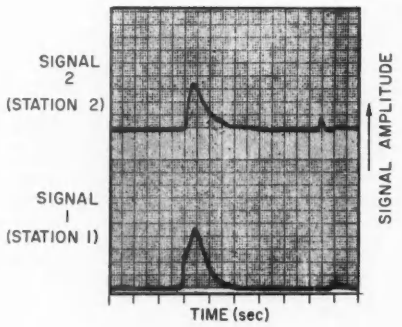

FIG. 2. The signals recorded at the two receiving stations at 1415 hours local time, 16 March, 1956.

In order to carry out the full analysis it was necessary to look for a pair of signals produced by a meteor that had fairly well-defined characteristics. In order to remove one of the ambiguities which enter the analysis it was necessary that the meteor trail lie in a plane inclined at an angle to the vertical of about 45 degrees. This plane is more completely specified later. It was necessary

also that the signals received at both stations be of reasonably large amplitude and free from any significant fading. Finally, it was necessary that both signals exhibit clearly those characteristics which indicate that the parent meteor trail was intermediate in electron density between the typical "underdense" and "overdense" trails, that is, that the signals show a rounding-off of the peak of the amplitude and have, also, an exponential decay. In spite of these stringent criteria a suitable event was found in the records after only a few hours of recording. The original recording of the signal pair is reproduced in Fig. 2. The signals were recorded at approximately 1415 hours local time on 16 March, 1956.

III. DISCUSSION OF THE THEORY

The method to be used is based upon a fairly simple concept of the way in which the signal arises from an overdense meteor trail. This concept may be explained with reference to Fig. 3 where an idealized signal is drawn for the purpose of illustration. In this diagram the ordinate is the *logarithm* of the

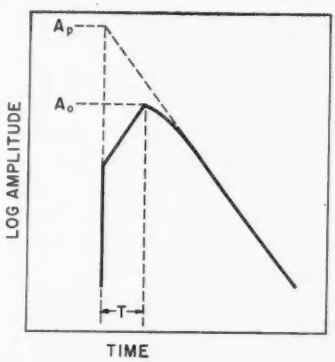

FIG. 3. Idealized signal amplitude variation for a meteor trail which has an electron line density slightly above the "transition" value.

signal amplitude and the abscissa is time. The initial sharp rise of the signal occurs as the meteor trail, in forming, bridges a principal Fresnel zone of the transmitter–receiver system. At formation, the electron density of the trail is too great to permit penetration by the radio waves, which are reflected at some critical radius. As this radius increases under the action of ambipolar diffusion the signal amplitude increases to a maximum value of A_0 at time T after the formation of the trail. Thereafter, as a result of further diffusion, the critical radius collapses to zero and the radio waves pass freely through the volume of the trail. From this point onward the individual electrons scatter independently and the signal amplitude decreases exponentially with time as the scattering volume increases and coherence of the scattered radiation is lost. By extending this decay rate backward in time (as indicated by the broken line in Fig. 3) to the initiation time of the signal it is possible to de-

termine a hypothetical amplitude A_p which would apply if all the electrons in the principal Fresnel zone could scatter independently and coherently.

The expressions appropriate to forward-scattering from an underdense meteor trail as given in the earlier paper (Hines and Forsyth 1957) are:

$$(1) \qquad P_R = \left[\frac{P_T G_T G_R \lambda^3 \sin^2\alpha}{16\pi^4 R_T R_R (R_T+R_R)(1-\cos^2\beta \sin^2\varphi)}\right]\left[\frac{\mu_0 e^2}{4m}\right]^2 q^2$$

and

$$(2) \qquad \tau = \frac{\lambda^2 \sec^2\varphi}{16\pi^2 D},$$

and for the overdense meteor trail:*

$$(3) \qquad P_R = \left[\frac{P_T G_T G_R \lambda^3 \sin^2\alpha}{16\pi^4 R_T R_R (R_T+R_R)(1-\cos^2\beta \sin^2\phi)}\right]\left[\frac{\pi}{4\epsilon}\frac{\mu_0 e^2}{4m}\right]^{\frac{1}{2}} q^{\frac{1}{2}}$$

and

$$(4) \qquad \tau' = \frac{\mu_0 e^2}{4m}\frac{q\lambda^2 \sec^2\varphi}{4\pi^3 D},$$

where

P_R = maximum received power,
P_T = transmitted power,
G_T, G_R = transmitting and receiving antenna gains (relative to an isotropic radiator),
λ = radio wavelength,
R_T, R_R = distances from meteor trail to transmitter and receiver,
α = angle between incident electric vector and the scattered ray,
β = angle between axis of the meteor trail and the plane that contains the transmitter, reflection point, and receiver,
φ = one half the interior angle formed by the lines along R_T and R_R,
μ_0 = $4\pi \times 10^{-7}$ henry/meter,
e = electronic charge,
m = electronic mass,
q = line density of free electrons in the meteor trail,
τ = time constant of the exponential decay of signal amplitude,
τ' = total duration of "overdense" signal,
D = ambipolar diffusion coefficient,
ϵ = base of the natural logarithms.

In the case of the overdense trail the maximum signal is received at a time $T = \tau'/\epsilon$ after the initiation of the signal.

The geometric factors that enter the expressions (1) and (2) now seem to be generally accepted. However, the reasoning that leads to similar factors

*The expression (3) is equation (18) of the earlier paper. It should be noted that equation (17) of that paper should have a bracket at the end of the first line and another at the beginning of the second line.

in (3) and (4) has not yet gained such support. Manning (1957) has suggested that, in particular, the factor, $\sec^2\varphi$, that appears in (4) is quite inappropriate.

For a signal from a "transition" meteor of the type represented by Fig. 3 it is possible to measure τ and $\tau' = T\epsilon$. Eliminating D between (2) and (4),

$$q = \frac{\tau'}{\tau}\frac{\pi m}{\mu_0 e^2} = \frac{T\pi m\epsilon}{\tau\mu_0 e^2} = 2.41\times10^{14}\frac{T}{\tau}, \tag{5}$$

which will provide a correct estimate of the line density only if the same geometric factor is used correctly in both (2) and (4).

A similar situation exists with respect to the amplitudes predicted by (1) and (3). Again referring to Fig. 3, it is clear that for a given signal of this type, A_p should correspond to the amplitude indicated by (1) and A_0 to that indicated by (3). Combining these two,

$$\frac{A_p}{A_0} = \left[\frac{\mu_0 e^2}{4m}\right]^{3/4} q^{3/4}\left[\frac{4\epsilon}{\pi}\right]^{1/4}$$

or

$$q = q_0\left(\frac{A_p}{A_0}\right)^{1.33}, \tag{6}$$

where q_0 is the transition density obtained by equating (1) and (3), and is equal to 0.75×10^{14} electrons/meter. This expression will yield the correct value of density only if the geometric factors in (1) are also applicable to (3). However, in this case, the ratio of the geometric factors in (1) and (3), if not equal to unity, would enter (6) raised only to the power 0.66.

The two expressions (5) and (6) provide independent methods for obtaining the line density of the parent meteor trail and, if expressions (1) and (2) are accepted, then the accuracy of (3) and (4) can be tested. For this purpose, it is desirable to have a third method of analysis that is independent of (3) and (4). Such a method is available provided all the quantities necessary for a numerical solution of (1) can be determined. This approach is followed in the succeeding section where it will be seen that in the course of the analysis it is necessary to derive several other parameters of the trail in addition to the electron density.

IV. ANALYSIS

In Fig. 4 the signal pair under consideration is shown replotted on a logarithmic amplitude scale. The similarity between each of these signals and the idealized signal of Fig. 3 is apparent. In the case of signal 2 (recorded at Station 2) there is a slight deviation from the exponential decay law toward the end of the signal. This deviation probably is due to a slight distortion of the trail in the neighborhood of the corresponding reflection point, but it does not adversely affect the analysis. The significant features of each signal are easily identified and measured.

The two signals may be associated with different points on the meteor trail. Before proceeding with the electron density analysis it is of interest to derive some preliminary information about the trail and the location of

the two reflection points. If the meteor trail is projected into a plane that is perpendicular to the transmitter–receiver axis, then the condition of specular

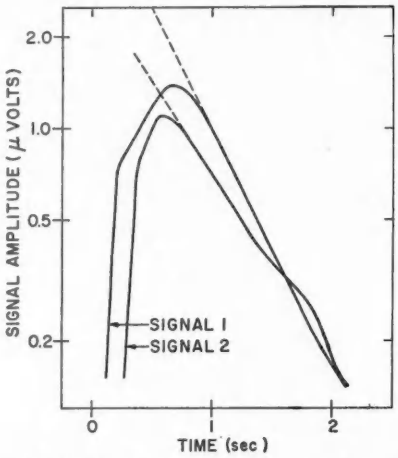

FIG. 4. The signals of Fig. 2 replotted against a logarithmic scale.

reflection requires that the point in the projected trail that corresponds to the reflection point be the point of tangency with a circle drawn about the transmitter–receiver axis. If it is assumed, as is reasonable in the present case, that the meteor trail was not formed near the transmitter or near the receiver but rather in the general vicinity of the mid-plane between the two (the region of validity of the cylindrical approximation of Hines (1955)), then the diagram of Fig. 5 (*a*) may be taken as a representation of the situation as projected into the plane that is perpendicular to the axis midway between the two transmitter–receiver axes. By reference to Fig. 5(*b*) it will be seen that

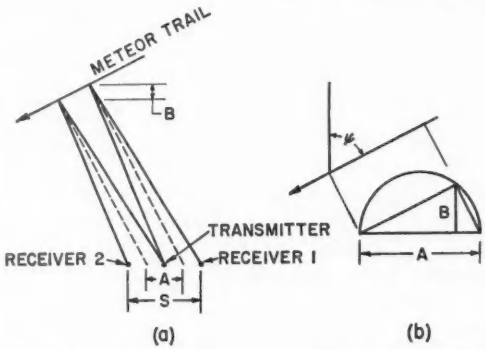

FIG. 5. The geometry of the transmission paths illustrating (*a*) the projection of the paths into a vertical north–south plane, and (*b*) the derivation of relation (7).

ψ, the angle between the vertical and the meteor trail as projected into this plane, is given by

$$\sin 2\psi = 2B/A. \tag{7}$$

There is an ambiguity in this expression, except when $\psi = 45°$, and it is for this reason that the angular restriction was included in the meteor selection criteria. For the present case, the value of B may be deduced from the decay rates measured for the two signals. The time taken for the amplitude of signal 1 to fall by a factor ϵ is

$$\tau_1 = 0.54 \text{ second},$$

and for signal 2

$$\tau_2 = 0.70 \text{ second},$$

and the ratio

$$\tau_1/\tau_2 = 0.77.$$

The height difference that corresponds to this ratio of diffusion times may be estimated from the slope of the curve of logarithm of diffusion coefficient against height, given by Greenhow and Neufeld (1955). From their results, the difference in height of the two reflection points is found to be about 1.7 km. Estimating $A = S/2 = 3$ km it is found from (7) above that:

$$\psi \doteq 45°$$

as required by the first selection criterion. It should be noted that the validity of this deduction depends upon the assumption that the value of A is approximately $S/2$; that the meteor trail was near the mid-plane between the transmitter and the receivers. Since the maxima of the radiation patterns of the antennas intersect near this mid-plane, this assumption seems reasonable. The possibility that the meteor trail was near the transmitter would appear to be ruled out entirely, since, for any smaller value of A, the right hand side of (7) would be much greater than unity. The fact that, for the value chosen, the right hand side of (7) is slightly greater than unity may indicate a slight displacement of the trail from the mid-plane toward the receivers, but the accuracy of measurement is not sufficient to support any such deduction.

Turning now to the calculation of electron density, and using the subscripts 1 and 2 to indicate the electron densities at the reflection points that correspond to the signals 1 and 2, from (5)

$$q_1 = 2.41\times10^{14}\,\frac{T_1}{\tau_1} = 2.41\times10^{14}\left(\frac{0.48}{0.54}\right) = 2.14\times10^{14}/\text{meter}$$

and

$$q_2 = 2.41\times10^{14}\left(\frac{0.25}{0.70}\right) = 0.86\times10^{14}/\text{meter}.$$

In practice there is some doubt concerning the initiation time of the signals, from which T should be measured. The finite rise time of the signal corresponds presumably to the time taken by the meteor to traverse the principal Fresnel

zone. In this analysis the initiation time of each signal is chosen at a point on the record near the top of the initial sharp rise.

From equation (6) another pair of estimates of electron density may be made. By projecting the decay curves backward in time to the initiation time of the signal as indicated above, values of A_p are found which lead to

$$q_1 = q_0\left(\frac{A_p}{A_0}\right)^{1.33} = 0.75\times10^{14}\left(\frac{4.18}{1.40}\right)^{1.33} = 3.22\times10^{14}/\text{meter}$$

and

$$q_2 = 0.75\times10^{14}\left(\frac{1.72}{1.13}\right)^{1.33} = 1.31\times10^{14}/\text{meter}.$$

The final method of estimating the electron density makes use of equation (1), for which it is necessary to deduce the appropriate values for α, β, and φ. A meteor with $\psi = 45°$ must occur approximately 100 km off to the side of the transmitter–receiver axis in order to satisfy the condition of specular reflection. Under the assumptions used earlier this leads to the approximate values $\alpha = 65°$ and $\varphi = 70°$. In an exact treatment, equation (1) should be corrected also for the polarization of the receiving antenna. In the present instance this correction is small.

The estimate of β is obtained by consideration of the meteor velocity. The difference in height of the two reflection points has been estimated at 1.7 km. The difference in initiation times for the two signals was 0.16 second, which leads to a vertical component of velocity of about 11 km/sec. The component of velocity in the plane which is perpendicular to the transmitter–receiver axis was, therefore, about 15 km/sec. The results of radar studies of meteor velocities (see, for example, Lovell 1954) indicate that in the neighborhood of the earth meteors travel with heliocentric velocities close to the parabolic limit of 42.1 km/sec. The velocity of the earth in its orbit is 29.8 km/sec so that with respect to an observer on the earth the meteor velocity is a simple function of the angle between the radiant point of the meteor and the apex of the earth's way, and it has a maximum value of about 72 km/sec when this angle is zero.

In the present circumstances the time of observation (1415 hours local time), the time of year (16 March), the direction of the path (nearly east–west), the latitude of the path (45° N), and the value of ψ (45°) serve to fix the angular relationship between the half-plane that contains the possible directions of the meteor trail (i.e., the half-plane in which β is measured) and the apex of the earth's way. Since each direction in this half-plane makes a definite angle with the apex direction, it is possible to determine the meteor velocity as a function of β. In the present case these computations are greatly simplified because the plane in which β is measured is parallel to the equatorial plane of the earth. The velocities deduced in this way must also be corrected for the gravitational pull of the earth. Finally, it is necessary to determine which of the permitted combinations of velocity and angle β could produce the observed component of velocity when projected into the direction $\beta = 90°$. These com-

putations have been carried out using graphical methods and they result in the following solutions:

$\beta = 16.5°$, $V = 53$ km/sec (meteor travelling toward transmitter);

$\beta = 55°$, $V = 17.5$ km/sec (meteor travelling toward receiver).

In order to choose between the two solutions given in the last paragraph it is necessary to consider the height at which the trail was formed. The results of an experimental determination of the variation of height of maximum ionization with velocity have been presented by Kaiser (1953). From Fig. 16 of Kaiser's paper it may be deduced that the height of maximum ionization for a meteor velocity of 53 km/sec is about 99.5 km and that for 17.5 km/sec is about 86 km. According to Greenhow and Neufeld (1955) the diffusion coefficients for the two heights are respectively 8.9 and 1.25 m²/sec. Taking the previously deduced value of φ (70°), the observed decay rate for signal 1 corresponds to a diffusion coefficient of 5.8 m²/sec or a height of about 96 km. The relative amplitudes of the two recorded signals suggest that the point of maximum ionization on the trail was above, rather than below the reflection points, which leads to a consistent picture only if the higher value of velocity is accepted. It is concluded therefore that the appropriate value of β is 16.5°.

The remaining numerical quantities required for a solution of equation (1) are:

$$\lambda = 7.65 \text{ m},$$

$$\frac{\mu_0 e^2}{4m} = 0.885\times10^{-14} \text{ m},$$

$$R_1 = R_2 = 4.5\times10^5 \text{ m},$$

$$P_T = 100 \text{ w},$$

$G_T = G_R = 12$ (this is the numerical antenna gain in the appropriate direction reduced by the amount of the cable losses),

$P_R = A_p^2/50$ (where A_p is expressed in volts and P_R is in watts),

$A_p = 4.18\times10^{-6}$ v for signal 1 and 1.72×10^{-6} v for signal 2,

hence

$$q_1 = 2.2\times10^{14}/\text{meter},$$

$$q_2 = 0.89\times10^{14}/\text{meter}.$$

The results of the three methods of determining the electron density are summarized in Table I.

TABLE I

ELECTRON LINE DENSITY AT TWO POINTS ON THE TRAIL AS DETERMINED BY VARIOUS METHODS

Determination method	Equation (1)	Equation (5)	Equation (6)
q_1(electrons/meter$\times10^{-14}$)	2.2	2.1	3.2
q_2(electrons/meter$\times10^{-14}$)	0.89	0.86	1.3
Ratio q_1/q_2	2.5	2.5	2.5

V. DISCUSSION OF RESULTS

The degree to which the results presented in Table I can be said to support the theoretical expressions quoted in Section III is, of course, dependent upon the nature of the modifications to these expressions that are contemplated. In what follows it is assumed that the validity of equations (1) and (2) is not in doubt, or more generally it might be said that the theoretical limitations of these expressions are assumed to produce errors that, in the present instance, are much smaller than the errors of measurement. An examination of Figs. 2, 3, and 4 suggests that the accuracy of the measured quantities cannot be better than a few per cent. On the other hand, it is doubtful that there are any very large errors of measurement in view of the remarkable agreement among the ratios listed in the last line of Table I. In addition, there are the errors that result both from the extrapolation of measured values and from the uncertainty about the correct initiation time in deriving the values for A_p and T. Together, these errors probably lead to a total uncertainty of the order of 50% in the derived values of q.

Table I indicates that equation (5) produces substantially the same values of electron density as does equation (1). Equation (5) is derived from equations (2) and (4), each of which contain the geometric factor, $\sec^2\varphi$. The appearance of this factor in equation (2) is not in question but its appearance in (4) has been questioned most recently by Manning, who has suggested that, if a factor that involves $\sec\varphi$ is to be included, then the exponent should be no greater than about 0.5. In the present instance this would lead to an increase by a factor of 5 in the values of q deduced from (5). It does not seem likely that the experimental uncertainties would permit so large a change.

The values of q in the last column of Table I were derived from equation (6) which in turn was derived from equations (1) and (3). Once again, the geometric factors that appear in (1) are not in doubt. The ratio of the geometric factors that appear in (3) and (1) would appear in (6) raised to the power 0.66. If it is assumed that in the overdense case there is no forward enhancement of the signal and that the geometric factor should be unity, then the values of q should be about one-third of those given in the last column of Table I. Here again it is not likely that so large a modification is acceptable, but an angular dependence which is somewhat more moderate than that of (3) cannot be precluded on the basis of the present measurements. Any change in the geometric factors of (3) would lead to a new value of q_0, the "transition" density. The value used is the same as that which applies in the case of back-scatter and the present results suggest that no great error is introduced thereby.

A final check on the consistency of the results is provided by the ratio of the electron densities found for the two reflection points. The theory of the variation of electron density along the trail as a function of height has been reviewed by Kaiser (1953). A suitable value for the scale height, H, at meteoric levels is 7 km. From the earlier analysis, the two reflection points are located below the maximum of ionization and are separated by $0.25H$. From Kaiser's treatment, for two points with this separation a ratio of 2.5 in electron density occurs only when the two points are located about $0.5H$ and $0.75H$

below the height of maximum ionization (displacement of these points by $0.1H$ in either direction leads to a variation of more than 0.5 in the electron density ratio). It has been deduced already that the reflection point for signal 1 was located at a height of about 96 km. By this argument the height of maximum ionization is found to be about 99.5 km. As indicated earlier, the appropriate height of maximum ionization for the deduced velocity of 53 km/sec is also about 99.5 km. The agreement is most satisfactory and serves to verify the argument which led to the angular values in the analysis.

VI. CONCLUDING REMARKS

The application of theoretical formulae to the signals scattered from a single meteor trail cannot positively verify those formulae; however, a quantitative description of the meteor trail has been built up through the use of the equations. This description shows a significant degree of internal consistency and also is in good agreement with the known properties of meteor trails. The manner in which each of the various expressions has been used to derive the properties of a particular trail is similar to the way in which these same expressions would be applied separately in statistical studies. In presenting the formula for the forward-scattered signal from an overdense trail (Hines and Forsyth 1957) it was pointed out that the expression could hardly be exact, but might prove useful as a working relation in the prediction and interpretation of forward-scatter data. The success of the present analysis would appear to justify this hope. Certainly, no similar simple relation which would provide a better basis for the analysis of the present data appears to be available.

In closing it may be appropriate to point out another limitation of the present analysis. It is now well known that after formation a meteor trail tends to be distorted sinuously by the action of large-scale turbulence in the upper atmosphere. After this distortion has proceeded for some time the scattered radio energy is no longer concentrated in well-defined directions and the amplitude of the signal, as received at a fixed point, fluctuates. This fading is characteristic of the signals received from distorted trails and such trails were excluded specifically from the analysis of this paper. For those statistical studies that do not exclude the fading signals, it is necessary to consider a further treatment to take account of the distorted trails. While fading occurs both in back-scattered and in forward-scattered signals, some forward-scattered signals last longer than do the corresponding back-scattered signals, so that distortion has a proportionately greater chance of becoming effective. The fact that distortion sometimes modifies the reflecting properties of the meteor trails does not invalidate the present analysis, but it does indicate that further analysis would be necessary in any comprehensive treatment of the statistical problem.

ACKNOWLEDGMENTS

The author is indebted to Messrs. C. Collins and W. Rolfe, who assisted with the recording of the signals. The transmitting equipment was supervised by the personnel of RCAF Station, Greenwood, N.S.

REFERENCES

ESHLEMAN, V. R. 1952. Tech. Rept. No. 49, Electronic Research Lab., Stanford University, Stanford, Calif.
——— 1955. Tech. Rept. No. 44, Radio Propagation Lab., Stanford University, Stanford, Calif.
ESHLEMAN, V. R. and MANNING, L. A. 1954. Proc. Inst. Radio Engrs. **42**, 530.
FORSYTH, P. A. and VOGAN, E. L. 1955. Can. J. Phys. **33**, 176.
——— 1956. Can. J. Phys. **34**, 535.
GREENHOW, J. S. and NEUFELD, E. L. 1955. J. Atmospheric and Terrest. Phys. **6**, 133.
HINES, C. O. 1955. Can. J. Phys. **33**, 493.
HINES, C. O. and FORSYTH, P. A. 1957. Can. J. Phys. **35**, 1033.
HINES, C. O. and VOGAN, E. L. 1957. Can. J. Phys. **35**, 703.
KAISER, T. R. 1953. Research Revs., Phil. Mag. Suppl. **2**, 495.
LOVELL, A. C. B. 1954. Meteor astronomy (The Clarendon Press, Oxford).
LOVELL, A. C. B. and CLEGG, J. A. 1952. Radio astronomy (Chapman and Hall, Ltd., London).
MANNING, L. A. 1957. XIIth General Assembly of URSI Boulder, Colorado, Commission V, Paper 266.
MCKINLEY, D. W. R. and MCNAMARA, A. G. 1956. Can. J. Phys. **34**, 625.
VOGAN, E. L. and CAMPBELL, L. L. 1957. Can. J. Phys. **35**, 1176.

LETTERS TO THE EDITOR

Under this heading brief reports of important discoveries in physics may be published. These reports should not exceed 600 words and, for any issue, should be submitted not later than six weeks previous to the first day of the month of issue. No proof will be sent to the authors.

The Kinematic Viscosity of Liquid Helium II

Previous studies with a rotating cylinder viscometer in liquid helium II (Heikkila and Hallett 1955; Woods and Hallett 1958) have been concerned with the measurement of the steady deflections of the inner cylinder while the outer rotated at constant angular velocity; such studies yield values of the dynamic viscosity, η, of the liquid.

Also of interest are the transient motions of the inner cylinder which occur when the rotation of the outer cylinder is started or stopped, because the time, constant for the decay of such transients, depends on the kinematic viscosity, $\nu = \eta/\rho$, of the liquid. Since in liquid helium II, ν might be determined either by ρ, the total density of the liquid (as suggested by Donnelly 1958), or by ρ_n, the density of the normal component, such studies are of considerable interest.

The apparatus used differed from that described by Woods and Hallett (1958) in two respects. A new outer cylinder was made giving a gap width, d, of 2.5 mm, thereby giving transient times of convenient duration. Also the R.F. system detecting the motion of the inner cylinder was replaced by the standard lamp, scale, and mirror system using windows constructed in the dewar walls.

Experimentally the deflection, $\phi(t)$, of the inner cylinder was measured as a function of time, t, from the starting and stopping of the outer cylinder. The appropriate transient solution of the Navier–Stokes equation gives the theoretical variation of ϕ with νt rather than t. Comparison between the experimental and theoretical transients can be made most easily if, for selected values of $\phi(t)/\phi(\infty)$ ($\phi(\infty)$ being the steady state deflection), the corresponding experimental times, t, and theoretical values, νt, are plotted against each other. The resulting curve should be a straight line whose slope gives the effective value of ν. A typical curve obtained in this way at 2.16° K (1955 L scale) where $\rho_n \simeq \rho$, is shown in Fig. 1 and has the form of the expected straight line. From the slope of this line $\nu = 1.6 \times 10^{-4}$ stokes in good agreement with $\eta/\rho = 1.67 \times 10^{-4}$ stokes. Thus the theoretical analysis fits the experimental observations reasonably well. The Reynolds number of the motion, $R = vd/\nu$, where v is the linear velocity of the outer cylinder, was 340 in this case.

At 0.925° K, however, the transient times, both for starting and for stopping, were much

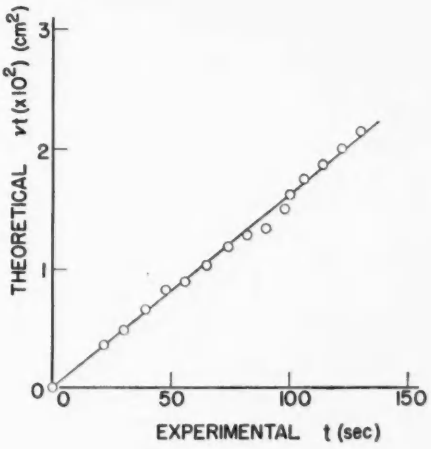

FIG. 1.

less than 16.4 seconds, the free period of oscillation of the inner cylinder. Since at this temperature $\eta = 55 \pm 2$ micropoise, it would be expected that the time required for $\phi(t)/\phi(\infty)$ to reach 0.5 would be about 25 seconds if $\nu = \eta/\rho$, or about 0.1 second if $\nu = \eta/\rho_n$. Thus it can be seen that the effective density determining ν is much less than ρ and is possibly ρ_n. These experiments were carried out at Reynolds numbers < 230, the critical value for this apparatus.

Between 0.925° K and 2.16° K the viscosity of helium II is much smaller and, in order to obtain measurable deflections, it was necessary to exceed the critical velocity and use Reynolds numbers of the order of 900. The results showed that the transient times for starting were much less than 16 seconds suggesting a very small value for the effective density; the transient times for stopping were, however, longer and easily measured, but $\phi(t)/\phi(\infty)$ varied with time in a manner different from that predicted theoretically. It is possible that these stopping transients could be described by assuming that the effective density determining ν increases from a value of the order of ρ_n to a value approaching ρ as the Reynolds number increases. Such behavior at high Reynolds numbers would then be in agreement with Donnelly's result that $\nu = \eta/\rho$.

The authors gratefully acknowledge the financial assistance of the National Research Council and the Ontario Research Foundation whose grants in aid of research have made this work possible.

DONNELLY, R. J. 1958. Phys. Rev. **109**, 1461.
HEIKKILA, W. J. and HOLLIS HALLETT, A. C. 1955. Can. J. Phys. **33**, 420.
WOODS, A. D. B. and HOLLIS HALLETT, A. C. 1958. Can. J. Phys. **36**, 253.

RECEIVED JUNE 16, 1958.
DEPARTMENT OF PHYSICS,
UNIVERSITY OF TORONTO,
TORONTO, ONTARIO.

A. D. B. WOODS
A. C. HOLLIS HALLETT

THE PHYSICAL SOCIETY

MEMBERSHIP of the Society is open to all who are interested in Physics.

FELLOWS pay an Entrance fee of £1 1*s*. ($3.00) and an Annual Subscription of £2 2*s*. ($6.00).

STUDENTS: A candidate for Studentship must be between the ages of 18 and 26, and pays an Annual Subscription of 5*s*. ($0.75).

MEETINGS: Fellows and Students may attend all Meetings of the Society including the annual Exhibition of Scientific Instruments and Apparatus.

PUBLICATIONS include the *Proceedings of the Physical Society*, published monthly, and *Reports on Progress in Physics*, published annually. Volume XX, 1957, is now available (price £3 3*s*. ($9.00)). Members are entitled to receive any of the Publications at a reduced rate.

Further information can be obtained from:

THE PHYSICAL SOCIETY
1, LOWTHER GARDENS, PRINCE CONSORT ROAD
LONDON, S.W.7, ENGLAND

CANADIAN JOURNAL OF PHYSICS

Notes to Contributors

Manuscripts

(i) General. Manuscripts, in English or French, should be typewritten, double spaced, on paper 8½×11 in. **The original and one copy are to be submitted.** Tables and captions for the figures should be placed at the end of the manuscript. Every sheet of the manuscript should be numbered.

Style, arrangement, spelling, and abbreviations should conform to the usage of recent numbers of this journal. Names of all simple compounds, rather than their formulas, should be used in the text. Greek letters or unusual signs should be written plainly or explained by marginal notes. Superscripts and subscripts must be legible and carefully placed.

Manuscripts and illustrations should be carefully checked before they are submitted. Authors will be charged for unnecessary deviations from the usual format and for changes made in the proof that are considered excessive or unnecessary.

(ii) Abstract. An abstract of not more than about 200 words, indicating the scope of the work and the principal findings, is required, except in Notes.

(iii) References. References should be listed **alphabetically by authors' names,** unnumbered, and typed after the text. The form of the citations should be that used in current issues of this journal; in references to papers in periodicals, titles should not be given and only initial page numbers are required. The names of periodicals should be abbreviated in the form given in the most recent *List of Periodicals Abstracted by Chemical Abstracts.* All citations should be checked with the original articles and each one referred to in the text by the authors' names and the year.

(iv) Tables. Tables should be numbered in roman numerals and each table referred to in the text. Titles should always be given but should be brief; column headings should be brief and descriptive matter in the tables confined to a minimum. Vertical rules should not be used. Numerous small tables should be avoided.

Illustrations

(i) General. All figures (including each figure of the plates) should be numbered consecutively from 1 up, in arabic numerals, and each figure referred to in the text. The author's name, title of the paper, and figure number should be written in the lower left corner of the sheets on which the illustrations appear. Captions should not be written on the illustrations (see Manuscripts (i)).

(ii) Line Drawings. Drawings should be carefully made with India ink on white drawing paper, blue tracing linen, or co-ordinate paper ruled in blue only; any co-ordinate lines that are to appear in the reproduction should be ruled in black ink. Paper ruled in green, yellow, or red should not be used. All lines should be of sufficient thickness to reproduce well. Decimal points, periods, and stippled dots should be solid black circles large enough to be reduced if necessary. Letters and numerals should be neatly made, preferably with a stencil (**do NOT use typewriting**) and be of such size that the smallest lettering will be not less than 1 mm high when reproduced in a cut 3 in wide.

Many drawings are made too large; originals should not be more than 2 or 3 times the size of the desired reproduction. Whenever possible two or more drawings should be grouped to reduce the number of cuts required. In such groups of drawings, or in large drawings, full use of the space available should be made; the ratio of height to width should conform to that of a journal page (4¾×7½ in), but allowance must be made for the captions.

The original drawings and one set of clear copies (e.g. small photographs) are to be submitted.

(iii) Photographs. Prints should be made on glossy paper, with strong contrasts. They should be trimmed so that essential features only are shown and mounted carefully, with rubber cement, on white cardboard, with no space between them. In mounting, full use of the space available should be made to reduce the number of cuts required (see Illustrations (ii)). Photographs or groups of photographs should not be more than 2 or 3 times the size of the desired reproduction.

Photographs are to be submitted in duplicate; if they are to be reproduced in groups one set should be mounted, the duplicate set unmounted.

Reprints

A total of 50 reprints of each paper, without covers, are supplied free. Additional reprints, with or without covers, may be purchased at the time of publication.

Charges for reprints are based on the number of printed pages, which may be calculated approximately by multiplying by 0.6 the number of manuscript pages (double-spaced typewritten sheets, 8½×11 in) and including the space occupied by illustrations. An additional charge is made for illustrations that appear as coated inserts. Prices and instructions for ordinary reprints are sent out with the galley proof.

Any reprints required in addition to those requested on the author's reprint requisition form must be ordered officially as soon as the paper has been accepted for publication.

Contents

M. J. Cabell—The thermal neutron capture cross section and the resonance absorption integral of Th^{230} (ionium) - - - - - - - - - - - 989

J. M. Daniels, J. L. G. Lamarche, and M. A. R. Le Blanc—Nuclear orientation experiments with Pr^{142} and Yb^{175} nuclei - - - - - - - - - - - 997

Gaston Fischer and W. B. Pearson—The electrical conductivity of manganese arsenide and antimonide - - - - - - - - - - - - - - - 1010

Z. S. Basinski and W. B. Pearson—The non-martensitic diffusionless transition in manganese arsenide at about 40° C - - - - - - - - - 1017

M. F. Crawford and R. E. MacDonald—Field-induced absorption in hydrogen 1022

A. G. W. Cameron—Nuclear level spacings - - - - - - - - - - 1040

R. A. Hurd—Scattering from a small anisotropic ellipsoid - - - - - 1058

R. A. Hurd—The magnetic fields of a ferrite ellipsoid - - - - - - 1072

R. L. Graham, J. S. Geiger, and T. A. Eastwood—Experimental evidence for axial vector interaction in the disintegration of Pr^{144} - - - - - 1084

P. A. Forsyth—The forward-scattered radio signal from an overdense meteor trail - 1112

Letters to the Editor:

A. D. B. Woods and A. C. Hollis Hallett—The kinematic viscosity of liquid helium II - 1125

Printed in Canada *by* University of Toronto Press